

Cosmic Infrared Background and Early Galaxy Evolution

A. Kashlinsky

Laboratory for Astronomy and Solar Physics, Goddard Space Flight Center, Greenbelt, MD 20771, and
SSAI
e-mail address: kashlinsky@stars.gsfc.nasa.gov

ABSTRACT

The Cosmic Infrared Background (CIB) reflects the sum total of galactic luminosities integrated over the entire age of the universe. From its measurement the red-shifted starlight and dust-absorbed and re-radiated starlight of the CIB can be used to determine (or constrain) the rates of star formation and metal production as a function of time and deduce information about objects at epochs currently inaccessible to telescopic studies. This review discusses the state of current CIB measurements and the (mostly space-based) instruments with which these measurements have been made, the obstacles (the various foreground emissions) and the physics behind the CIB and its structure. Theoretical discussion of the CIB levels can now be normalized to the standard cosmological model narrowing down theoretical uncertainties. We review the information behind and theoretical modeling of both the mean (isotropic) levels of the CIB and their fluctuations. The CIB is divided into three broad bands: near-IR, mid-IR and far-IR. For each of the bands we review the main contributors to the CIB flux and the epochs at which the bulk of the flux originates. We also discuss the data on the various quantities relevant for correct interpretation of the CIB levels: the star-formation history, the present-day luminosity function measurements, resolving the various galaxy contributors to the CIB, etc. The integrated light of all galaxies in the deepest near-IR galaxy counts to date fails to match the observed mean level of the CIB, probably indicating a significant high-redshift contribution to the CIB. Additionally, Population III stars should have left a strong and measurable signature via their contribution to the cosmic infrared background (CIB) anisotropies for a wide range of their formation scenarios, and measuring the excess CIB anisotropies coming from high z would provide direct information on the epoch of the first stars.

Subject headings: cosmology: diffuse radiation – galaxies: clusters: general – galaxies: high-redshift – surveys

Table of contents

Abstract

1. Introduction

2. Miscellaneous: definitions, units, magnitudes, etc

3. Theoretical preliminaries

3.1 Mean level

3.2 CIB anisotropies

3.2.1 *CIB anisotropies from galaxy clustering*

3.2.2 *Shot noise CIB fluctuations from galaxies*

3.2.3 *Cosmic variance*

3.2.4 *CIB dipole component*

3.3 Structure formation: cosmological paradigms

3.4 From cosmological paradigm to galaxies

4. Obstacles to measurement: confusion and foregrounds

4.1 Atmospheric emission

4.2 Galactic stars

4.3 Zodiacal emission

4.4 Galactic cirrus

4.5 Cosmic microwave background

5. Current CIB measurements

5.1 COBE/DIRBE

5.2 COBE/FIRAS

5.3 IRTS

5.4 ISO

5.5 2MASS

5.6 Results:

5.6.1 *Near-IR*

5.6.2 *Mid-IR*

5.6.3 *Far-IR*

5.6.4 *Bolometric CIB flux*

6. 'Ordinary' contributors to CIB

6.1 IMF and star formation history: from UV to far-IR

6.2 Normal stellar populations

6.3 Dust emission from galaxies: mid-IR to sub-mm

6.4 Contribution from quasars/AGNs

6.5 Present-day luminosity density

6.6 Deep galaxy counts

6.6.1 Near-IR

6.6.2 Mid-IR

6.6.3 Far-IR and sub-mm

6.7 CIB fluctuations from clustering of ordinary galaxies

6.9 Cumulative flux from galaxy counts vs CIB measurements

8. Population III

8.1 What were the first stars?

8.2 Isotropic component of CIB

8.3 Contribution to anisotropies in CIB

8.4 Can CIB anisotropies from Population III be measured?

9. Snapshot of the future

10. Concluding remarks

1. Introduction

Diffuse backgrounds contain important information about the history of the early Universe, when discrete objects either did not exist or are not accessible to telescopic studies. The cosmic infrared background (CIB) arises from accumulated emissions from early galaxy populations spanning a large range of redshifts. The earliest epoch for the production of this background occurred when star formation first began, and contributions to the CIB continued through the present epoch. The CIB is thus an integrated summary of the collective star forming events, star-burst activity and other luminous events in cosmic history to the present time. As photons move to observer they lose energy to cosmic expansion and any stellar emission from high redshift populations will now be seen in the infrared (mostly near-IR with $\lambda \lesssim$ a few μm , unless it comes from very cold stars at very high z). Emission from galactic dust will be shifted to still longer IR wavelengths. CIB thus probes the physics in the Universe between the present epoch and the last scattering surface and is complementary to its more famous cousin, the cosmic microwave background radiation (CMB) which probes mainly the physics at the last scattering.

Considerable effort has now gone into studying the luminosity sources during the most recent history of the universe ($z < 2 - 3$), but the period from recombination to the redshift of the Hubble Deep Field (HDF) remains largely an unexplored era because of the difficulty of detecting many distant galaxies over large areas of the sky. Significant progress in finding high redshift galaxies has been achieved using the Lyman dropout technique (Steidel et al 1996), but uncovering substantial populations of galaxies at $z \gtrsim 5$ is extremely difficult and the total sample is still very small. It is there that the CIB measurements can provide critical information about the early history of the Universe largely inaccessible to telescopic studies. At more recent epochs galaxy evolution is also constrained by the measurements of the visible part of the extragalactic background light or EBL (Bernstein et al 2002a,b; cf. Mattila 2003).

Chronologically, the importance of the CIB and early predictions about its levels (Partridge & Peebles 1968) followed the discovery of the CMB which observationally established the Big Bang model for the origin and evolution of the Universe. Because of the Earth's atmosphere it was clear from the start that the measurement of the CIB must be done from space and even there the Solar system and Galactic foregrounds presented a formidable challenge. It took a while for technology to reach the required sensitivity and, when the first rocket and space based CIB measurements were conducted, the results were inconclusive (Matsumoto, Akiba & Murakami 1988, Noda et al 1992). Following its launch in 1983 the IRAS satellite was the first to conduct all-sky infrared measurements of point sources between 12 and 100 μm (Soifer, Neugebauer & Houck 1987). It revealed that galaxies were efficient infrared emitters, but its design was not optimized for diffuse background measurements. The COBE DIRBE instrument, launched in 1990, operated between 1.25 and 240 μm and was the first to be devoted specifically to CIB measurements (Hauser & Dwek 2001). It led to the first reliable measurements of and limits on the CIB over a wide range of infrared bands and literally began the observational CIB era.

The status of the CIB measurements in the immediate post-DIRBE era has been reviewed extensively by Hauser & Dwek (2001) and a slightly earlier review by Leinert et al (1998) has provided a detailed discussion of the issues involved in measuring the extragalactic background light (EBL) levels. Since then several important developments happened, most notably the establishment, through CMB measurements, of the standard cosmological model for the overall evolution of the Universe, particularly the existence of the so-called dark energy, and of the standard paradigm (Λ CDM) for structure formation. CMB polarization measurements have identified the epoch of re-ionization, presumably due to first collapsed objects in the Universe. This now allows narrowing of CIB predictions and puts refined searches for the CIB on a much firmer basis. Also, in the CIB context, several new measurements have now been accomplished and several old ones are now more firmly confirmed. Scientific exploration is never static and the very recently (August 2003) launched NASA Spitzer satellite already led to several important findings for CIB and many more are expected to follow as Spitzer observational programs get implemented. New space instruments in the IR and sub-mm bands are planned by NASA and ESA which will shed new light on the early Universe and the interconnection between the CIB and early luminous systems. This thus seems like an opportune moment for a new attempt to review the CIB measurements and their interpretation.

Indeed, following the WMAP and balloon experiments we now know that the Universe is flat and dominated by the vacuum energy (cosmological constant) and/or even more exotic quintessence field. The recent WMAP results (Bennett et al 2003, Spergel et al 2003) imply that the Universe had a large optical depth since last scattering ($\tau \sim 0.2$) indicating unexpectedly early star formation ($z \sim 20$). Direct deep studies of the universe at $z > 2-3$ show that much of the luminosity of the universe at that time was probably involved in the process of galaxy formation, and the birth of the first generations of stars. Many systems, such as elliptical galaxies, already seem well-formed by the epoch of the HDF, and the metallicities for many systems are already near solar. Somewhere between $z \sim 20 - 30$ and $z \sim 6$ reside the systems made up of the first population of stars, the so-called zero-metallicity Population III, about which little is known observationally. All these galaxies should have left their imprint in the CIB and its structure.

Observationally, the CIB is difficult to distinguish from the generally brighter foregrounds contributed by the local matter within the solar system, and the stars and ISM of the Galaxy. A number of investigations have attempted to extract the isotropic component (mean level) of the CIB from ground- and satellite-based data as described below. This has in nearly all instances been a complicated task due to a lack of detailed knowledge of the absolute brightness levels and spatial variations across the sky for the many foregrounds that overlay the CIB signal. It is thus very important to understand and estimate to high accuracy the various foreground emissions which need to be subtracted or removed before uncovering the CIB.

The outline of this review is as follows: in Sec. 2 we start with a summary of the units, the various relevant astronomical magnitude systems and the list of frequent abbreviations used throughout the review. Sec. 3 discusses theoretical basis for CIB and its structure and how these

are related to information on the early galaxies and stellar systems. Sec. 4 reviews the foregrounds that inhibit the CIB measurements and Sec. 5 reviews the status of the current CIB measurements. In Sec. 6 we discuss the topics related to CIB measurements and their interpretation such as the contribution from ordinary galaxies composed of Population I and II stars, the role of star formation, dust, the current status of the present day galaxy luminosity density measurements, and the deep galaxy counts from near-IR to far-IR. Sec. 7 is devoted to the signature of Population III in the CIB and its structure and the almost unique role CIB plays in uncovering the Population III era. We end up with a review of the currently planned instruments and space missions that will or can have direct bearing on the CIB in Sec. 8 followed by a summary section.

2. Miscellaneous: definitions, units, magnitudes, abbreviations, etc.

We start with definitions. The surface brightness of the CIB per unit wavelength will be denoted as I_λ , per unit frequency as I_ν , and per logarithmic wavelength interval $F = \lambda I_\lambda = \nu I_\nu$, and we call them all “flux.” Throughout the paper B_ν will denote the Planck black-body function per unit frequency.

Fluxes of astronomical sources are often measured in narrow band filters. The flux units commonly used in astronomy for I_ν are $\text{Jy} = 10^{-26} \text{ W/m}^2/\text{Hz}$. The surface brightness of the CIB is usually given in units of either MJy/sr or $\text{nW m}^{-2} \text{sr}^{-1}$. The conversion between the two is:

$$1 \frac{\text{nW}}{\text{m}^2 \text{sr}} = \frac{3000}{\lambda(\mu\text{m})} \frac{\text{MJy}}{\text{sr}} \quad (1)$$

The range of wavelengths used in this review is divided into the following groups: near-infrared (NIR) covers $1 \mu\text{m} \lesssim \lambda \lesssim 5\text{--}10 \mu\text{m}$. Mid-infrared (MIR) is defined to lie in $5\text{--}10 \mu\text{m} \lesssim \lambda \lesssim 50\text{--}100 \mu\text{m}$ range. We call the Far-infrared (FIR) the region corresponding to $50\text{--}100 \mu\text{m} \lesssim \lambda \lesssim 500 \mu\text{m}$, and beyond that will be sometimes referred to as sub-mm. These definitions are neither exact nor unique and, although the band ranges cover (largely) different physical processes, this division is used for convenience only.

Throughout the review both Vega magnitudes and AB magnitudes are used. By definition, Vega’s magnitudes are zero in all filters. However, because of uncertainties in the absolute flux calibration of Vega, magnitudes of this star have been slightly corrected over time. The zero point of AB magnitude system is constant flux of 3631 Jy for apparent brightness (Oke & Gunn 1983).

Table 1. Magnitude system conversion

Filter	J	H	K	IRAC-1	IRAC-2	IRAC-3	IRAC-4
$\lambda (\mu\text{m})$	1.25	1.65	2.2	3.6	4.5	5.8	8
$m_{\text{AB}} - m_{\text{Vega}}$	0.90	1.37	1.84	2.79	3.26	3.73	4.40

Thus in AB magnitude system an object with $I_\nu = \text{constant}$ (flat energy distribution) has the same magnitude in all bands, and all colors are zero. For the wavelengths used frequently in the paper the conversion is given in Table 1. The numbers were adopted in the J,H,K photometric bands from the 2MASS Explanatory Supplement ¹ and in the four Spitzer IRAC channels from the Spitzer Observer's Manual ².

Table 2 lists the abbreviations and acronyms that will appear below.

3. Theoretical preliminaries

The near-IR CIB arises mainly from the stellar component of galaxies and probes evolution of stellar component of galaxies at early times. The mid- and far-IR CIB originates from dusty galaxies reprocessing stellar light and other energetic output. As will be discussed in Sec. 5, the recent mutually consistent detections of the near-IR CIB from the COBE/DIRBE and Japan's IRTS datasets (see Hauser & Dwek 2001 for review) indicated a surprisingly high amplitude of both the CIB fluctuations (Kashlinsky & Odenwald 2000a, Matsumoto et al 2000, 2002) and mean levels (Dwek & Arendt 1998, Gorjian & Wright 2000, Wright & Reese 2000, Cambresy et al 2001). In the mid-IR firm upper limits on the CIB have been found by various indirect methods, but because foreground emission is so high no direct detection has been possible. In the far-IR there are mutually consistent detections of the CIB from the DIRBE (Schlegel et al 1998, Hauser et al 1998) and FIRAS (Puget et al 1996, Fixsen et al 1998) datasets.

In this section we provide a general mathematical and observational basis for the underlying parameters and physics that determine the CIB and its structure. Specific cosmological and galaxy evolution models are mentioned only briefly (Sec. 3.4) and we attempt to make the discussion as general as possible.

3.1. Mean level

In the Friedman-Robertson-Walker Universe with flat geometry and the Robertson-Walker metric, $ds^2 = c^2 dt^2 - (1+z)^{-2}[dx^2 + x^2(d\theta^2 + \sin^2 \theta d\phi^2)]$, the comoving volume occupied by a unit solid angle in the redshift interval dz is $dV/dz = (1+z)^{-1}d_L^2(z)c dt/dz$, where $d_L \equiv x(z)/(1+z)$ is the luminosity distance. Thus the flux density in band λ from each galaxy with absolute bolometric luminosity L at redshift z is $\frac{L}{4\pi d_L^2(1+z)}f_\lambda(\frac{\lambda}{1+z}; z)$. Here $f_\lambda d\lambda$ is the fraction of the total light emitted in the wavelength interval $[\lambda; \lambda + d\lambda]$ and the extra factor of $(1+z)$ in the denominator accounts for the fact that the flux received in band λ comes from a redshifted galaxy. The contribution to

¹<http://www.ipac.caltech.edu/2mass/releases/allsky/doc/expsup.html>

²<http://ssc.spitzer.caltech.edu/documents>

Table 2. Summary of frequently used acronyms and abbreviations.

2dF	2 degree Field
2MASS	2 Micron All Sky Survey
AGN	Active Galactic Nucleus
CDM	Cold Dark Matter
CIB	Cosmic Infrared Background
CMB	Cosmic Microwave Background
COBE	COsmic Background Explorer
DIRBE	Diffuse InfraRed Background Experiment
EBL	Extragalactic Background Light
ELAIS	European Large Area ISO Survey
ESA	European Space Agency
FIR	Far IR
FIRAS	Far InfraRed Absolute Spectrometer
FOV	Field-Of-View
FSM	Faint Source Model
HDF	Hubble Deep Field
IGM	InterGalactic Medium
IMF	Initial Mass Function
IN	Instrument Noise
IPD	InterPlanetary Dust
IR	InfraRed
IRAC	InfraRed Array Camera
IRAS	InfraRed Astronomical Satellite
IRTS	InfraRed Telescope in Space
ISM	InterStellar Matter
ISO	Infrared Space Observatory
JWST	James Webb Space Telescope
MIPS	Multiband Imaging Photometer System for Spitzer
MIR	Mid IR
NASA	National Aeronautics & Space Agency
NGP/SGP	North/South Galactic Pole
NEP/SEP	North/South Ecliptic Pole
NIR	Near IR
NSF	National Science Foundation
PAH	Polycyclic Aromatic Hydrocarbon
RMS	Root Mean Square
SCUBA	Sub-mm Common-User Bolometer Array
SDSS	Sloan Digital Sky Survey
SED	Spectral Energy Distribution
SFR	Star Formation Rate
SNAP	SuperNovae Acceleration Probe
UDF	Ultra Deep Field
WMAP	Wilkinson Microwave Anisotropy Probe
ZL	Zodiacal Light

the total CIB flux from the redshift interval dz is given by

$$\frac{dF}{dz} = \frac{R_H}{4\pi} \frac{1}{(1+z)^2} \frac{d(H_0 t)}{dz} \sum_i \mathcal{L}_i(z) [\lambda f_{\lambda,i}(\frac{\lambda}{1+z}; z)], \quad (2)$$

where the sum is taken over all galaxy populations contributing flux in the observer rest-frame band at λ , and f_{λ} characterizes the spectral energy distribution (SED) of galaxy population i . Here $R_H = cH_0^{-1}$ and the (present-day) luminosity density is given by:

$$\mathcal{L}_{\nu}(0) = \sum_i \int \Phi_{0,i}(L_{\nu}) L_{\nu} dL_{\nu} \quad (3)$$

where $\Phi_{0,i}$ is the (present-day) luminosity function or the number density of galaxies of morphological type i in the dL_{ν} interval at frequency band ν .

It is illustrative to study the redshift dependence of the flux production rate, Eq. (2). At small redshifts the factor $(1+z)^{-2}dt/dz$ varies little with z , and the flux production rate, dF/dz , is governed by the comoving bolometric luminosity density $\mathcal{L}(z)$ and the SED of the galaxy emission f_{λ} . If the luminosity evolution at these redshifts is small, the flux production rate is governed by the SED shape. If $f_{\lambda}(\lambda)$ increases toward shorter wavelengths then dF/dz increases with z . For $\lambda f_{\lambda} = \text{const}$, and no luminosity evolution, the rate is roughly constant with small z . At sufficiently high redshifts, modest luminosity evolution in Eq. (2) would be offset by the factor $(1+z)^{-2}dt/dz$, so that the flux production rate would be cut off at sufficiently large z . This factor is responsible for resolving Olbers' paradox even for a flat SED.

There are three broad parameters that determine the possible modes of galaxy evolution at higher redshifts: 1) how bright individual galaxies shine (luminosity evolution), 2) their spectral energy distribution (SED) which determines how much of the luminosity was emitted at the rest frame of the galaxy (K-correction), and 3) how numerous the galaxies were (number density evolution). Consequently, one can separate the z -dependence in $\mathcal{L}_{\nu}(z)$ into terms due to K-correction (\mathcal{K}_{ν}), pure luminosity evolution (\mathcal{E}_{ν}) and pure number density evolution (\mathcal{N}_{ν}) (e.g. Yoshii & Takahara 1988), i.e.

$$\mathcal{L}_{\nu}(z) = 10^{-0.4[\mathcal{K}_{\nu}(z) + \mathcal{E}_{\nu}(z) + \mathcal{N}_{\nu}(z)]} \mathcal{L}_{\nu}(0) \quad (4)$$

Then the total CIB flux emitted by evolving galaxy populations becomes:

$$F_{\text{total}} = \sum_i \frac{\mathcal{L}_{\nu,i}(0) R_H}{4\pi} \int \frac{1}{(1+z)^2} \frac{d(H_0 t)}{dz} 10^{-0.4(\mathcal{K}_{\nu,i} + \mathcal{E}_{\nu,i} + \mathcal{N}_{\nu,i})} dz \quad (5)$$

where dt/dz is given by eq. 20 with the expansion factor $R \equiv (1+z)^{-1}$.

The details of galaxy spectral energy distributions (SED) will be discussed later, but a simple analysis can already be made using eq. (2). The SED at rest-frame wavelengths $\lambda \lesssim 10 \mu\text{m}$ is dominated by stellar emission, with a peak at visible wavelengths and a decrease for $\lambda > 0.7 \mu\text{m}$. Consequently, assuming no-evolution would mean that most of the predicted J band CIB comes

from redshifts $z \sim 0.3 - 1$, which shifts the visible emission of normal stellar populations to $\sim 1 \mu\text{m}$. In the M band at $5 \mu\text{m}$, most of the predicted CIB comes from $z > 1 - 2$. Evolution will likely push these redshift ranges toward earlier times. At $10 \mu\text{m} \lesssim \lambda \lesssim 200 \mu\text{m}$, the emission is dominated by galactic dust and the situation is reversed, so f_λ increases with wavelength roughly as λ^α with $\alpha \sim 1.5$. Hence, the dusty star-burst galaxies observed by IRAS at low redshifts should make the dominant contribution to the $10 \mu\text{m}$ CIB. In the far-IR, the K-correction is strongly negative (Sec. 6.3) and the measured CIB found can have large contributions from high redshifts.

It is useful to make a simple estimate of the expected CIB flux. Measurements of the galaxy luminosity function in both optical (Loveday et al 1992; Blanton et al 2001) and near-IR (Gardner et al 1997; Kochanek et al 2003,; Cole et al 2003) indicate approximately that the density of bright galaxies is $\Phi_* \sim 10^{-2} h^3 \text{Mpc}^{-3}$. Each of these galaxies emits in the rough neighborhood of $L_* \sim 10^{37} \text{ W}$. The flux-dimensional quantity composed of Φ_* , L_* and the Hubble constant is $F \sim \frac{1}{4\pi} \Phi_* L_* c H_0^{-1} \simeq 25 \text{ nWm}^{-2} \text{sr}^{-1}$. This is a crude estimate, but it already shows that in order to measure reliably the mean levels of the CIB, foregrounds must be eliminated to well below $\sim 10 \text{ nWm}^{-2} \text{sr}^{-1}$ levels. Section 4 shows how difficult a task that is in the infrared bands.

3.2. CIB anisotropies

Because of the difficulty of accurately accounting for the contributions of bright foregrounds such as Galactic stars, interplanetary and interstellar dust, which must be subtracted from the observed sky background (Arendt et al, 1998, Kelsall et al, 1998), Kashlinsky, Mather, Odenwald & Hauser (1996) have proposed to measure the structure of the CIB or its fluctuations spectrum. For a relatively conservative set of assumptions about clustering of distant galaxies, fluctuations in the brightness of the CIB have a distinct spectral and spatial signal, and these signals can be more readily discerned than the actual mean level of the CIB. The most common source of luminosity in the universe arises in galaxies, whose clustering properties at the present times are fairly well known and are consistent with the Λ CDM model predictions (Efstathiou, Sutherland & Maddox 1990, Percival et al 2002, Tegmark et al 2004). The CIB, being produced by clustered matter, must have fluctuations that reflect the clustered nature of the underlying sources of luminosity. This signature will have an angular correlation function (or angular power spectrum) that distinguishes it from local sources of background emission such as zodiacal light emission, and foreground stars in the Milky Way. Moreover, distant contributions of CIB will have a different redshift, and therefore spectral color, than nearby galaxies and sources of local emission. From galaxy evolution and cluster evolution models it is possible to match the predicted slopes for the power spectrum of the CIB against the power spectrum of the data.

On the largest angular scales (the dipole component), there would be an additional source of anisotropy due to our peculiar motion with respect to the inertial frame of the Universe. This component may be measurable over a certain range of wavelengths and is discussed after the more canonical source of CIB anisotropies, the galaxy clustering.

3.2.1. CIB anisotropies from galaxy clustering

Whenever CIB studies encompass relatively small parts of the sky (angular scales $\theta < 1$ sr) one can use Cartesian formulation of the Fourier analysis. The fluctuation in the CIB surface brightness can be defined as $\delta F(\boldsymbol{\theta}) = F(\boldsymbol{\theta}) - \langle F \rangle$, where $F = \lambda I_\lambda$, $\boldsymbol{\theta}$ is the two dimensional coordinate on the sky and $\langle F \rangle$ is the ensemble average. The two-dimensional Fourier transform is $\delta F(\boldsymbol{\theta}) = (2\pi)^{-2} \int \delta F_q \exp(-i\boldsymbol{q} \cdot \boldsymbol{\theta}) d^2\boldsymbol{q}$.

If the fluctuation field, $\delta F(\boldsymbol{x})$, is a random variable, then it can be described by the moments of its probability distribution function. The first non-trivial moment is the projected 2-dimensional correlation function $C(\theta) = \langle \delta F(\boldsymbol{x} + \theta) \delta F(\boldsymbol{x}) \rangle$. The 2-dimensional power spectrum is $P_2(q) \equiv \langle |\delta F_q|^2 \rangle$, where the average is performed over all phases. The correlation function and the power spectrum are a pair of 2-dimensional Fourier transforms and for an isotropically distributed signal are related by

$$C(\theta) = \frac{1}{2\pi} \int_0^\infty P_2(q) J_0(q\theta) q dq, \quad (6)$$

$$P_2(q) = 2\pi \int_0^\infty C(\theta) J_0(q\theta) \theta d\theta, \quad (7)$$

where $J_n(x)$ is the n -th order cylindrical Bessel function. If the phases are random, then the distribution of the brightness is Gaussian and the correlation function (or its Fourier transform, the power spectrum) uniquely describes its statistics. In measurements with a finite beam, the intrinsic power spectrum is multiplied by the window function W of the instrument. Conversely, for the known beam window function, the power spectrum can be de-convolved by dividing the measured power spectrum by the beam window function.

Another useful and related quantity is the mean square fluctuation within a finite beam of angular radius ϑ , or zero-lag correlation signal, which is related to the power spectrum by

$$\begin{aligned} C(0) &= \langle (\delta F)^2 \rangle_\vartheta = \frac{1}{2\pi} \int_0^\infty P_2(q) W_{TH}(q\vartheta) q dq \\ &\sim \frac{1}{2\pi} q^2 P_2(q) \Big|_{q \sim \pi/2\vartheta}. \end{aligned} \quad (8)$$

For a top-hat beam the window function is $W_{TH} = [2J_1(x)/x]^2 = 0.5$ at $x \simeq \pi/2$ where $x = q\vartheta$, and hence the values of q^{-1} correspond to fluctuations on angular scales of diameter $\simeq \pi/q$.

At small angles < 1 sr, the CIB power spectrum is related to the CIB flux production rate, dF/dz , and the evolving 3-D power spectrum of galaxy clustering, $P_3(k)$ via the Limber equation. In the power spectrum formulation it can be written as (e.g. Kashlinsky & Odenwald 2000):

$$P_2(q) = \int \left(\frac{dF}{dz} \right)^2 \frac{1}{c \frac{dt}{dz} d_A^2(z)} P_3(qd_A^{-1}; z) dz \quad (9)$$

where $d_A(z)$ is the angular diameter distance and the integration is over the epoch of the sources

contributing to the CIB. Eq. 9 can be rewritten as:

$$P_2(q) = \frac{1}{c} \int \left(\frac{dI_{\nu'}}{dt} \right)^2 \frac{P_3(qd_A^{-1}; z)}{d_A^2} dt \quad (10)$$

This is equivalent to:

$$\frac{q^2 P_2(q)}{2\pi} = \pi t_0 \int \left(\frac{dI_{\nu'}}{dt} \right)^2 \Delta^2(qd_A^{-1}; z) dt \quad (11)$$

where t_0 is the time-length of the period over which the CIB is produced and

$$\Delta^2(k) = \frac{1}{2\pi^2} \frac{k^2 P_3(k)}{ct_0} \quad (12)$$

is the fluctuation in number of sources within a volume $k^{-2}ct_0$. ³

To within a factor of order unity, the square of the fractional fluctuation of the CIB on angular scale $\simeq \pi/q$ is $\delta_{\text{CIB}}^2 = \langle (\delta I_{\nu})^2 \rangle / I_{\nu}^2 \simeq I_{\nu}^{-2} q^2 P_2(q) / 2\pi$. The meaning of eq. 11 becomes obvious if we assume $dI_{\nu'}/dt = \text{constant}$ during the lifetime of the emitters t_0 . In this case the fractional fluctuation due to clustering of early galaxies becomes:

$$\delta_{\text{CIB}}^2 = \frac{\pi}{t_0} \int \Delta^2(qd_A^{-1}; z) dt \quad (13)$$

In other words, the fractional fluctuation on angular scale π/q in the CIB is given by the average value of the r.m.s. fluctuation from spatial clustering over a cylinder of length ct_0 and diameter $\sim k^{-1}$.

The Cartesian formulation is equivalent to the spherical sky representation used in the cosmic microwave background (CMB) studies on small scales. It was used in some CIB analyses (Haiman & Knox 2000, Cooray et al 2003). In that case one expands the flux into spherical harmonics: $F(\theta, \phi) = \nu I_{\nu} = \sum_{l=0}^{\infty} \sum_{m=-l}^l a_{lm} Y_{lm}(\theta, \phi)$. The correlation function of the CIB, $C(\theta) = \langle \delta F(\mathbf{x}) \cdot \delta F(\mathbf{x} + \theta) \rangle$, is then $C(\theta) = \sum \frac{(2l+1)}{4\pi} \mathcal{C}_l \mathcal{P}_l(\cos \theta)$ with $\mathcal{C}_l = \langle |a_l|^2 \rangle \equiv (2l+1)^{-1} \sum_{m=-l}^l |a_{lm}|^2$ and \mathcal{P}_l denoting the Legendre polynomials (e.g. Peebles 1980). The angular power spectrum, $P_2(q)$, is the two-dimensional Fourier transform of $C(\theta)$ and for $l \gg 1$ is related to the multipoles via $\mathcal{C}_l = P_2(l + \frac{1}{2})$. This follows because at $l \gg 1$ the Legendre polynomials can be approximated as Bessel functions, $\mathcal{P}_l(\cos \theta) \simeq J_0((l + 1/2)\theta)$. The magnitude of the CIB fluctuation on scale π/l radian for large l is then $\sim \sqrt{l^2 \mathcal{C}_l / 2\pi}$. In the limit of small angles ($l \gg 1$) the values of \mathcal{C}_l 's are related to the power spectrum of galaxy clustering and the CIB flux production rate via:

$$\mathcal{C}_l = \frac{1}{c} \int \left(\frac{dI_{\nu'}}{dt} \right)^2 \frac{1}{d_A^2(z)} P_3 \left(\frac{l + \frac{1}{2}}{d_A(z)}; z \right) dt \quad (14)$$

³The $\Delta(k)$ defined by eq. 12 and used throughout the review should not be confused with another quantity - $\sqrt{k^3 P(k) / 2\pi}$ - sometimes encountered in the literature under the same symbol.

In surveys with arcsec angular resolution it is possible to identify and remove galaxies brighter than some limiting magnitude, m_{lim} . Because on average fainter galaxies are at higher z , by improving sensitivity and angular resolution, one can isolate contributions to the CIB fluctuations from progressively earlier epochs (Kashlinsky et al 2002). The luminosity density, $\mathcal{L} = \int_0^{L(m_{\text{lim}})} \Phi(L) dL$, is then peaked at some particular redshift - at lower z the (brighter than apparent magnitude m_{lim}) galaxies are removed and at larger redshifts the luminosity density gets dominated by the bright end of the luminosity function with a sharp drop-off in the galaxy number density. The following toy model is useful in estimating the effect: in the visible to near-IR bands the present day galaxy luminosity function is of the Schechter (1976) form $\Phi = \Phi_* L_*^{-1} (L/L_*)^{-\alpha} \exp(-L/L_*)$. Measurements of the galaxy luminosity function from B to K bands indicate that within the statistical uncertainties $\alpha \simeq 1$ (Loveday et al 1992, Gardner et al 1997), leading to $\mathcal{L} = \Phi_* L_* (1 - \exp[-L(m_{\text{lim}})/L_*])$. This then defines the redshift window in eqs. 10,4 which contributes most to the power spectrum of the CIB. Contribution from low z galaxies, for which $L(m_{\text{lim}}) < L_*$ is $\mathcal{L} \simeq \Phi_* L(m_{\text{lim}}) \propto d_L^2(z)$. In practice the typical redshift at which most of the contribution arises can be estimated as $L(m_{\text{lim}}) \sim L_*$. If one can further remove galaxies lying in narrow bins, Δm , around progressively fainter apparent magnitude m_{lim} , one can hope to isolate contributions to the CIB by epoch (Kashlinsky 1992, Kashlinsky et al 2002).

3.2.2. Shot noise fluctuations from individual galaxies

In addition to fluctuations from galaxy clustering there would also be a shot-noise component arising from discrete galaxies occasionally entering the beam. The relative amplitude of these shot noise fluctuations will be $\sim N_{\text{beam}}^{-1/2}$ where N_{beam} is the average number of galaxies in the beam. This component is important in surveys with good angular resolution where $N_{\text{beam}} \lesssim$ a few.

If galaxies are removed down to some magnitude m , the shot noise contribution from the remaining sources to the flux variance, $C(0)$, in measurements with beam of the area ω_{beam} steradian is given by:

$$\sigma_{\text{sn}}^2 = \frac{1}{\omega_{\text{beam}}} \int_m^\infty F^2(m) \frac{dN_{\text{gal}}}{dm} dm \quad (15)$$

Here $F(m) \equiv F_0 10^{-0.4m}$ is the flux from galaxy of magnitude m and dN_{gal}/dm is the number of galaxies per steradian in the magnitude bin dm .

Fourier amplitudes of the shot noise are scale-independent and equation 8 implies that the shot noise contribution to the power spectrum of the CIB would be given by:

$$P_{\text{sn}} = \int_m^\infty F^2(m) \frac{dN_{\text{gal}}}{dm} dm \quad (16)$$

Because galaxy clustering has power spectrum that increases towards large scales, the shot noise component becomes progressively more important at smaller angular scales.

3.2.3. Cosmic variance for CIB anisotropies

Any measurement of the angular power spectrum will be affected by the sample or cosmic variance in much the same way as the cosmic microwave background measurement (Abbot & Wise 1984). This results from the fact that in the best of situations we can only observe 4π steradian leading to poor sampling of the long wavelength modes. If the power spectrum is determined from fraction f_{sky} of the sky by sampling in concentric rings of width Δq in angular wavenumber space, the relative uncertainty on $P_2(q)$ will be $N_q^{-1/2}$, where $N_q \propto q\Delta q$ is the number of ring elements in $[q; q + \Delta q]$ interval. Therefore, the relative uncertainty from cosmic variance in the measured power spectrum on scale $\theta \simeq \pi/\theta$ will be:

$$\frac{\sigma_{P_2}^{\text{CV}}}{P_2}|_{\text{cosmic variance}} \simeq \frac{1}{2\pi} \frac{\theta}{180^\circ} \sqrt{\frac{q}{\Delta q}} f_{\text{sky}}^{-1/2} \quad (17)$$

In order to get reliable and independent measurements at a given scale, it is useful to have narrow band $\Delta q/q \sim 0.05 - 0.1$. Therefore, for reliable measurements on scales up to θ , one has to cover an area a few times larger.

3.2.4. CIB dipole component

The dipole anisotropy of the CIB arises from our local motion with respect to the inertial frame of the Universe, rather than galaxy clustering. It carries important cosmological information and its amplitude and wavelength dependence can be predicted in a model-independent way and may one day be measurable.

If all of the dipole anisotropy of the CMB is produced by peculiar motion of the Sun and the Local Group with respect to the inertial frame provided by a distant observer (the last scattering surface in the case of the CMB or early epochs, high z , in the case of the CIB), the CIB should have dipole anisotropy of the corresponding amplitude and in the same direction. The amplitude of the dipole anisotropy can be characterized by the first term, \mathcal{C}_1 in expanding the sky in spherical harmonics. Since I_ν/ν^3 is an optical constant along the ray's trajectory, the motion of the terrestrial observer at speed v_{pec} with respect to the observed background will produce dipole fluctuation of the amplitude $\delta I_\nu/\langle I_\nu \rangle = (3 - \alpha_\nu)(v_{\text{pec}}/c) \cos \theta = \mathcal{C}_1 \cos \theta$ (e.g. Peebles & Wilkinson 1968). Here θ is the angle between the line-of-sight and the direction of motion and $\alpha_\nu \equiv \partial \ln I_\nu / \partial \ln \nu$ is the spectral index of the radiation.

For CMB measurements in the Rayleigh-Jeans part of the CMB spectrum the index is $\alpha_{\text{CMB}} \simeq 2$. Hence, the CIB dipole is related to that of the CMB via $\mathcal{C}_{1,\text{CIB}} = (3 - \alpha_\nu) \mathcal{C}_{1,\text{CMB}} / T_{\text{CMB}} F_{\text{CIB}}$. The CMB dipole is known very accurately to be $\mathcal{C}_{1,\text{CMB}} = 3.346 \pm 0.017$ mK (Bennett et al 2003). Hence the CIB dipole amplitude is expected to be

$$\delta F_{\text{CIB,dipole}} \simeq 1.2 \times 10^{-3} (3 - \alpha_\nu) F_{\text{CIB}} \quad (18)$$

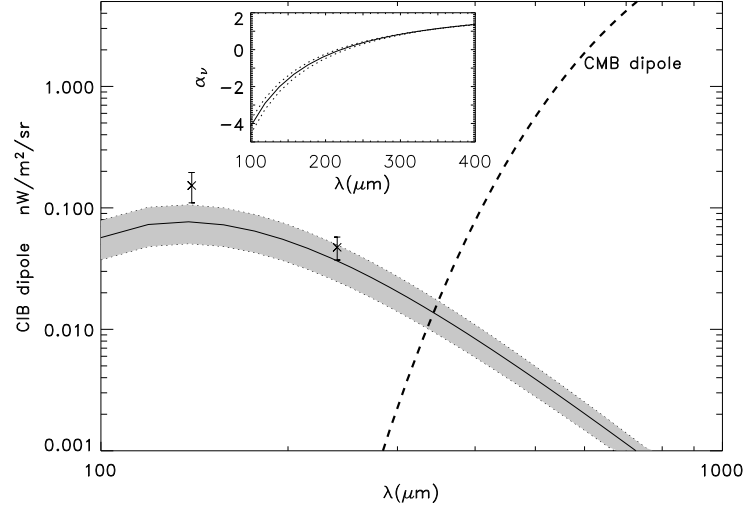


Fig. 1.— The insert shows the mean spectral index of the far-IR CIB according to eq. 24 (solid line) with its approximate uncertainty (dotted lines). Main figure shows the expected amplitude of the CIB dipole anisotropy normalized to the CMB dipole. The mean CIB dipole according to eq. 24 is shown with solid line and the shaded area denotes its approximate uncertainty. Crosses with errors show the dipole expected for the DIRBE measured levels of the CIB at 140 and 240 μm (Hauser et al 1998), which are also plotted with crosses in Fig. 9. Thick dashed line shows the latest measurements of the CMB dipole (Bennett et al 2003).

The current measurements of the CIB are discussed at length in Sec. 5. In the far-IR they show that the energy spectrum of the CIB has a 'window' where α_ν is strongly negative (see Fig. 9 and eq. 24). Fig. 1 shows the spectral index of the CIB derived from the FIRAS based measurements of the CIB, eq. 24, (Puget et al 1996, Fixsen et al 1998) and the resultant CIB dipole amplitude normalized to the observed CMB dipole. This component may be measurable at wavelengths where the CIB has a strongly negative α_ν and a sufficiently high flux level. The measurements show that α_ν is strongly negative for $\lambda < 200\mu\text{m}$ reaching the levels of $\alpha_\nu \sim -2$ to -4 there. Around $\sim 100\mu\text{m}$ the CIB spectrum has $\alpha_\nu \simeq -4$ and the CIB dipole should be $\simeq 7$ times more sensitive than the CMB dipole. The CIB flux at these wavelengths is $\sim 10 - 20\text{ nW m}^{-2}\text{sr}^{-1}$ and the CIB dipole at this range of wavelengths should have a non-negligible amplitude of $\sim 0.1 - 0.2\text{ nW m}^{-2}\text{sr}^{-1}$ and may be detectable in some future measurements. At longer wavelengths the CIB dipole will be difficult to measure due to steep increase in the residual uncertainty from the CMB dipole which is also shown in the Figure.

The CIB dipole anisotropy could be additionally enhanced because the over-density that provides our peculiar acceleration also presumably has excess IR luminosity. Indeed, there are persistent claims of large bulk flows on scales of $\sim 150 - 200h^{-1}\text{Mpc}$, whose direction roughly coincides with that of the CMB dipole (see Willick 2000 and references cited therein). Furthermore, the dipole of the distribution of rich (Abell) clusters does not converge out to $\sim 200h^{-1}\text{Mpc}$, while its direction roughly coincides with the CMB dipole (Scaramella et al. 1991).

The measurement of the CIB dipole anisotropy should be possible in the wavelength range 100–300 μm and will be important to provide additional information on the peculiar motions in the local part of the Universe and will serve as additional, and perhaps ultimate, test of the cosmological nature of any CIB detection at that wavelength.

3.3. Cosmological paradigms

CIB levels and structure depend on the history of energy production in the post-recombination Universe. The energy production is driven mainly by nucleosynthesis which is related to the history of the baryonic component of the Universe. Ultimately, it is the gravity that drives baryon evolution and the latter is determined by the evolution of the density inhomogeneities, the nature of dark matter and the cosmological parameters.

With the WMAP (Bennett et al 2003) measurements the structure of the last scattering surface has been mapped and a firm cosmological model has now emerged: the Universe is flat, dominated by the vacuum energy or an exotic quintessence field and is consistent with the inflationary paradigm and a cold-dark-matter (CDM) model. In this paper, we adopt the ΛCDM model (Efstathiou et al 1990) with cosmological parameters from the WMAP and other observations: $\Omega_{\text{baryon}} = 0.044, h = 0.71, \Omega_m = 0.3, \Omega_\Lambda = 0.7, \sigma_8 = 0.84$. Following the last scattering at $z \sim 1000$, the Universe entered an era known as the "Dark Ages", which ended with the star formation which produced Population III stars. The WMAP polarization results (Kogut et al 2003) show that the Universe had an optical depth since last scattering of $\tau \sim 0.2$, indicating an unexpectedly early epoch of the first star formation ($z_* \sim 20$). From the opposite direction in z , optical and IR telescopes are now making progress into understanding the luminosity history during the most recent epoch of the universe ($z < 5$), but the period from recombination to the redshift of the galaxies in the Hubble Deep Field (HDF) remains largely an unexplored era. CIB offers an alternative and powerful tool to probe those epochs.

The evolution of dark halos, destined to convert baryons into stars, is fixed by the power spectrum of the (dark) matter inhomogeneities. The latter are believed to have been imprinted during inflationary era and COBE DMR and WMAP observations confirm that it started out with the scale invariant spectrum of the Harrison-Zeldovich slope. Within the CDM framework the later evolution of the density fluctuations is fairly well understood: during radiation-dominated era fluctuations inside the horizon remain frozen, whereas super-horizon modes grow self-similarly. When the Universe became matter dominated, all modes grew at equal rate. The epoch of the matter radiation equality thus determines the overall shape of the power spectrum with the horizon scale at that time ($\propto \Omega_{\text{matter}} h^2$) being the only scale imprinted. The initial power spectrum is modified by the so-called transfer function and, in linear approximation, depends only on the cosmological parameters. Various approximations exist for its shape; we chose the approximation from Sugiyama (1995) with normalization to the COBE and WMAP CMB anisotropies for the numbers that follow.

The amplitude of matter density fluctuations on a given scale π/k is $\simeq \sqrt{k^3 P(k)/2\pi^2}$, where $P(k)$ is the power spectrum of density perturbations. Fourier modes evolution in the post-recombination Universe is determined by the cosmological parameters and the equation of state, $p = w\rho$. Cosmological constant, or vacuum energy, would lead to $w = -1$; various quintessence models generally require $-1 < w < -1/3$ and the "normal" matter dominated Universe requires $w = 0$. The growth of fluctuations, $\Psi \equiv \delta(z)/\delta(0)$ is governed by the differential equation:

$$\ddot{\Psi} + 2\frac{\dot{R}}{R}\dot{\Psi} - 4\pi G\bar{\rho}_{\text{matter}}\Psi = 0 \quad (19)$$

where $R = (1+z)^{-1}$ is the expansion factor. This is coupled with the cosmic time – redshift relation, or Friedman equation, which for the flat Universe becomes:

$$\dot{R}^2 = H_0^2 \left(\frac{\Omega_m}{R} + \frac{1-\Omega_m}{R^{1+3w}} \right) \quad (20)$$

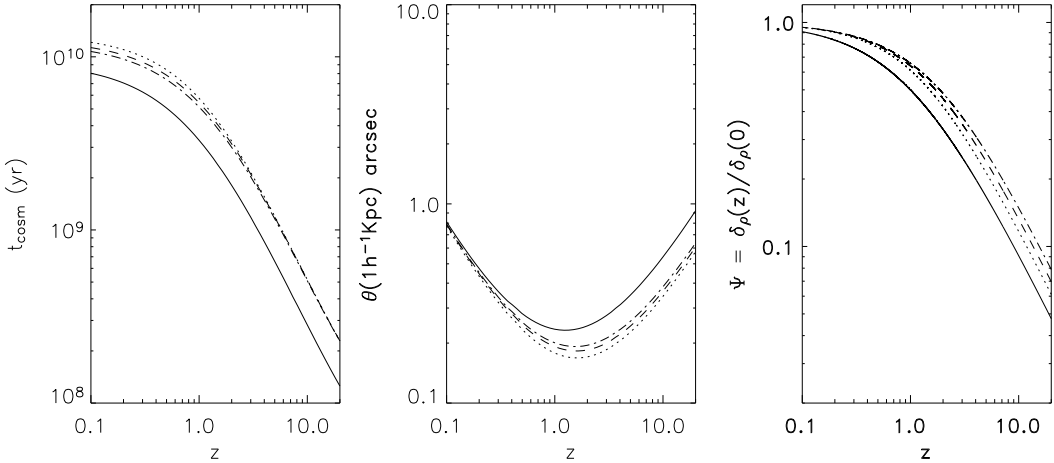


Fig. 2.— **Left:** cosmic time as function of redshift. **Middle** angular scale subtended by the physical scale $1h^{-1}\text{Kpc}$ vs z ; and **Right** the growth factor for linear density fluctuations. Solid lines in all panels correspond to $\Omega_m = 1$ with $w = 0$ and sets of broken lines to flat Universe with $\Omega_m = 0.3$ and equation of state $P = w\rho c^2$ with $w = -1, -2/3, -1/2$.

Fig. 2 shows the various parameters out to $z = 20$, the redshift of the first star formation indicated by the WMAP polarization measurements at large angular scales, which will be useful throughout the review: left panel shows the cosmic time from the Big Bang to the given redshift z (WMAP analysis suggests the present age is $\simeq 14$ Gyr), middle panel shows the angular scale subtended by physical scale $1h^{-1}\text{Kpc}$, and the right panels shows the growth evolution of density fluctuations, $\Psi(z)$. The middle panel also shows the necessity of the CIB studies: e.g. the candidate $z \sim 7$ galaxy (Kneib et al 2004) is estimated to have the total extent of $\lesssim 1$ Kpc and is likely to be among the largest systems at those epochs. Even if one resolves such compact systems, one would have to compromise on simultaneously observing a sufficiently large part of sky to gather robust statistics about the abundance and large-scale distribution of (very) high redshift galaxies. Thus the bulk of stellar material at high redshifts may be inaccessible to current and even future direct studies unless such work is complemented by the measurements of the CIB and its structure.

3.4. From cosmological paradigm to galaxies.

Eq. 19 applies only in the linear regime, where the density contrast $\delta_\rho \equiv \delta\rho/\rho \ll 1$. As time goes on density fluctuations grow until they become non-linear, turn around, separate from the general expansion frame and collapse to form compact objects. For CDM models the typical density contrast increases toward smaller scales, so the small scale objects collapse earlier. At present epoch the RMS fluctuation in the counts of galaxies is close to unity at $r_8 = 8h^{-1}\text{Mpc}$ (Davis & Peebles 1983) and the power spectrum of galaxy clustering has been accurately measured on scales up to $\sim 100h^{-1}\text{Mpc}$ from the 2dF (Percival et al 2002) and SDSS (Tegmark et al 2004) surveys and found in good agreement with the Λ CDM model (Efstathiou et al 1990). The power spectrum should be normalized to reproduce at present ($z = 0$) the RMS fluctuations of $\sigma_8 = 0.84$ over a sphere of radius r_8 . On non-linear scales gravitational effects would modify the shape and amplitude of the mass power spectrum. We modeled its evolution with z using the Peacock & Dodds (1996) approximation. Fig. 3 shows the evolution of the mass power spectrum, or the RMS density contrast $\delta_{\text{RMS}} \simeq \sqrt{k^3 P_3(k)/2\pi^2}$, for Λ CDM model normalized to WMAP cosmological parameters as function of scale. Non-linear scales correspond to $\sqrt{k^3 P_3(k)/2\pi^2} \gtrsim 1$ and in the Harrison-Zeldovich regime $\sqrt{k^3 P_3(k)/2\pi^2} \propto k^2$. The total mass contained in a given scale is $M \simeq 1.25 \times 10^{12} (r/1h^{-1}\text{Mpc})^3 \Omega h^{-1} M_\odot$; the baryonic mass would be smaller by $\Omega_{\text{baryon}}/\Omega_{\text{matter}}$. Adopting spherical model for the evolution and collapse of density fluctuations would give that any mass that, in linear approximation, reached the density contrast of $\delta_{\text{col}} = 1.68$ could collapse. Therefore $\eta = \delta_{\text{RMS}}/\delta_{\text{col}}$ gives the number of standard deviations a given object had to be in order to collapse at the given z . CDM and most inflation inspired models predict that the primordial density was Gaussian, so the probability that a given mass has collapsed at redshift z is given by $P_M = \text{erfc}(\eta(z)/\sqrt{2})$.

Once the fluctuation on a given scale turns around and collapses, gaseous processes will be critically important in determining how, when and which compact objects will form. Hoyle (1953) was the first to point out the importance of cooling in determining the galaxy masses, Rees & Ostriker (1977) have set it in the cosmological context. Galaxy morphology (roughly speaking, ellipticals vs disk galaxies) may be related to either dissipative collapse and fragmentation with angular momentum determining the efficiency of fragmentation and star formation (Kashlinsky 1982) or mergers (Toomre & Toomre 1972).

A further complication is that the distribution of luminous systems may not trace that of the mass, or the so-called biasing. This is likely to be important at early times when stars formed in rare regions with fluctuations of the necessary amplitude. Biasing amplifies the 2-point correlation function in locations traced by the objects (Kaiser 1984). Various biasing schemes exist (e.g. Politzer & Wise 1986, Jensen & Szalay 1986, Kashlinsky 1987, 1991, 1998) which may (or may not) at least be good approximations to real situations.

The era of metal-rich stellar populations composed of Population I and II stars, which we term 'ordinary', was likely preceded by a (possibly brief) period of the first zero metallicity stars, the

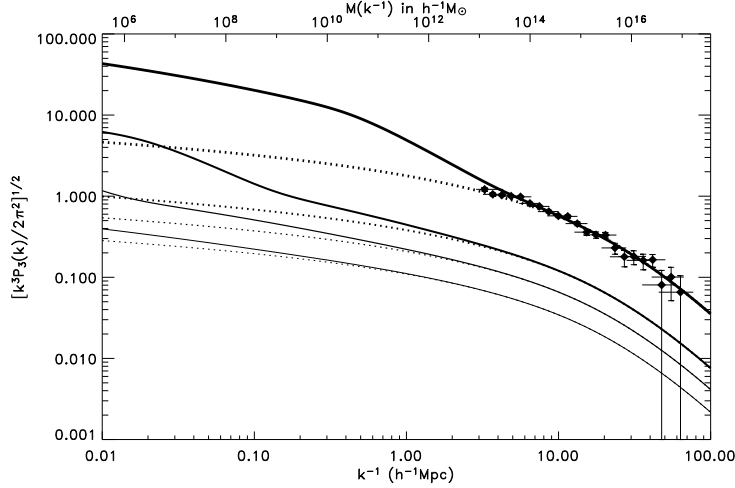


Fig. 3.— Λ CDM density field at $z = 20, 10, 5$ and 0 (thin to thickest) using the Peacock & Dodds (1996) approximation for non-linear evolution. Dotted lines corresponds to linear density field and solid lines include non-linear evolution. Filled diamonds with errors show the measurements of the present-day power spectrum of galaxy clustering from SDSS survey (Tegmark et al 2004); assuming no biasing it would coincide with the power spectrum of mass fluctuations. The top axis shows the mass in $h^{-1}M_\odot$ contained within a comoving radius of $1/k$ for $\Omega = 0.3$.

so-called Population III. Theoretically this is a special case, much less rooted in observational data, but also very important for understanding the later formation and evolution of ordinary galaxy populations. These populations and their imprint on the CIB are discussed in a separate sec. 7.

In order to interpret the measurements of the CIB, one needs to understand or model the details related to individual galaxy formation and evolution. Partridge & Peebles (1967) were the first to discuss the levels of the CIB expected from galaxy formation in the Big Bang model. Tinsley (1976, 1980) pioneered the studies of evolution of stellar populations, their SEDs and metallicity. Bond, Carr & Hogan (1980) have discussed a wide range of scenarios under which a measurable CIB can be produced, from contribution by primeval galaxies to those of decaying elementary particles; they also provided early estimates of the angular power spectrum of the expected CIB anisotropies. Later works continued the empirical approach or using a combined N-body and analytical machinery. The number of papers relevant to this brief theoretical section by far exceeds the limit of this review and in what follows we concentrate on only a few representative works to illustrate the tools used and the results obtained.

- *Backward and forward evolution:* Lonsdale (1996) divided empirical modeling of CIB into the forward and backward evolution classes. In the backward evolution approach one uses the measurements of the CIB, galaxy luminosity function, their assumed or modeled SEDs, observed galaxy counts, etc to translate galaxy evolution back in time. The forward evolution approach takes the opposite route, starting with galaxies at some initial epoch and evolving their properties to the present time. Very often, both approaches are needed.

Galaxy modeling generally consists of the following stages: 1) One specifies galaxy morphology

and morphological evolution with cosmic time; 2) One then needs to specify the stellar IMF, which may depend on cosmic time and vary among the various galaxy types; 3) Star formation rate must be assumed for each morphological type and z ; 4) Stellar evolution tracks must be distributed according to the IMF and SED for each morphological type reconstructed at each cosmic time; 5) Stellar emissions depend on the cosmic abundances and chemical evolution of the ISM must be accounted for and dust formation treatment is critically important at mid- to far-IR; 6) The various parameters described above may vary among galaxies of different mass or luminosity and this must be specified also; 7) For CIB fluctuations one must assume the model for the power spectrum of galaxy clustering, biasing and their time evolution. Additionally, these parameters depend on the total age of the Universe, the redshift of galaxy formation z_f , which may vary for different galaxies, etc. The models must be normalized to reproduce as many observational data as possible and are constrained by the data on galaxy morphology, metallicity Z (including at high z), observations of galaxy counts at various wavelengths, colors, etc. Despite the many parameters (and uncertainties) involved in the above construction, one can arrive at meaningful and fairly accurate limits on galaxy formation and evolution from the CIB.

Yoshii & Takahara (1988) used the stellar evolution models from Arimoto & Yoshii (1987) in order to compute the near-IR CIB (and the EBL) as function of the galaxy formation epoch and the deceleration parameter. The evolving galaxies were divided into five morphological types and their colors and counts were computed for the various cosmological and evolutionary parameters. They found that at visible bands most contribution to the EBL comes from late types (Sa to Sd), whereas at the NIR bands early types (E/S0) and late types give comparable contributions. Totani et al (1997) have extended the Yoshii & Takahara modeling for various morphological types to model the observed evolution of the luminosity density from UV to 1 μm (Lilly et al 1996). They noted that if the proportion of galaxy mixes remains constant from $z \sim 1$, then a flat Universe dominated by a cosmological constant is preferred by the data.

Franceschini et al (1991) made an early detailed study with predictions of future extragalactic surveys from near- to far-IR. They modeled chemical evolution of early and late-type galaxies normalized to K galaxy counts and allowed for various evolutionary modes of AGNs. Mid- to far-IR emission from dust was modeled with data from IRAS galaxies allowing for realistic distribution of dust grain sizes and temperatures and included emission from PAHs. They presented estimates of confusion limits from both Galactic stars and high- z galaxies.

Fall, Charlot & Pei (1996) presented an original way to relate the CIB to other observed parameters. They assumed that the dust at each redshift, having the same spatial distribution as stars, is traced by the neutral hydrogen. In turn, the neutral hydrogen column density can be normalized to reproduce the observed comoving density of HI in damped Ly- α systems out to $z \simeq 4$. They assumed a Salpeter type IMF for all galaxies and solved for chemical evolution under various approximations. The resultant CIB at long wavelengths was in good agreement with the detection from FIRAS data (Puget et al 1996). In the near-IR the predicted CIB is produced by stars, and they discuss how warm dust can produce substantial levels of mid-IR CIB without

significantly affecting the far-IR part of the CIB spectrum, which was argued to come from the $z \lesssim 4$ galaxies responsible for the damped Ly- α systems. They note that, for a wide range of the IMF, the agreement of the computed emissivities with estimates from the Canada-France Redshift Survey or CFRS (Lilly et al 1996) requires that the initial density parameter of material that went into stars and dust at $z \lesssim 4$ was between $10^{-3}h^{-1}$ and $8 \times 10^{-3}h^{-1}$.

Jimenez & Kashlinsky (1999) used synthetic models of stellar populations to analyze the contribution of normal galaxies to near-IR CIB and its fluctuations. The galaxies were assumed to form at fixed z_f and were divided into five morphological types from E to Sd/Irr. Stars in the disks were assumed to form with the Scalo IMF and in spheroids with the Salpeter IMF. Late type galaxies were modeled to follow the Schmidt law for star formation with the timescale which depended on the bulge-to-disk ratio. Ellipticals were assumed to form at the fixed high z_f in a single burst of star formation and passively evolve. Because early type galaxies contribute a significant fraction of the near-IR CIB one has to be careful in normalizing to the observed properties of these populations; hence the early-type galaxies were normalized to the present-day fundamental plane of elliptical galaxies assumed to mimic the metallicity variations along their luminosity sequence. They found that, despite their simplicity, the models gave good fits to the observed near-IR galaxy counts, the CFRS measurements of the luminosity density evolution (Lilly et al 1996), and gave good matches to the observed metallicities of the damped Ly- α systems (Pettini et al 1997) and galaxy colors. This then allowed to refine the range of predictions for the CIB and its fluctuations in the near-IR.

In the far-IR the bulk of the CIB comes from dust emission. Beichman & Helou (1991) constructed a model of dust emission, which coupled with the observed IRAS galaxy luminosity function and evolutionary assumptions for the various components of galaxy emission, allowed (pre-COBE) theoretical estimates of the far-IR CIB. Dwek et al (1998) normalized the mid- to far-IR emissions from galaxies to the mean SED of IRAS galaxies and reproduce the far-IR CIB by assuming a simple evolution of thereby constructed galaxies. Haiman & Knox (2000) computed the angular spectrum of the far-IR CIB fluctuations assuming that the dust temperature is determined by the UV radiation, i.e. that both the rate of dust production and its temperature are determined by the (measured) SFR (Star Formation Rate). They get that for a wide range of models the far-IR CIB fluctuations should be $\sim 10\%$ of the mean CIB levels on degree and sub-degree scales consistent with more general arguments of Kashlinsky et al (1996) and Kashlinsky & Odenwald (2000). Haiman and Loeb (1997) discussed the imprint in the CIB produced by smooth dust in IGM spread by remnants of the first stars. Knox et al (2001) have further expanded the analysis exploring the possibilities of measuring the FIR CIB anisotropies with the Planck space mission. Lagache et al (2003) considered a phenomenological model at far-IR to sub-mm wavelengths, constructing sample SEDs for starburst and normal galaxies and assuming only the luminosity function evolution with z . The model gave successful fits to the data on galaxy counts and redshift distribution, the far-IR CIB and they used it to give predictions for future observations with Herschel and Planck missions.

- *Semianalytical galaxy formation* modeling presents another track for theoretical insight and revolves around various numerical codes to generate dark matter evolution for a given hierarchical clustering model (usually CDM) and trace the merging history for present galaxy haloes. Prescriptions for galaxy formation inside the formed dark matter haloes are put in following gas dynamics and radiative processes and hydrodynamics with the choices constrained by data on e.g. Tully-Fisher (1977) relation, Lyman- α galaxies, galaxy colors, SFR history etc (e.g. Kauffmann, White & Guiderdoni 1993, Baugh et al 1998, Sommerville, Primack & Faber 1999). Guiderdoni et al (1998) used semi-analytic modeling, normalized to reproduce the observed far-IR/sub-mm part of the CIB, to study a plausible range of redshift distributions and faint galaxy counts at these wavelengths for the various evolutionary assumptions.

4. Obstacles to measurement: confusion and foregrounds

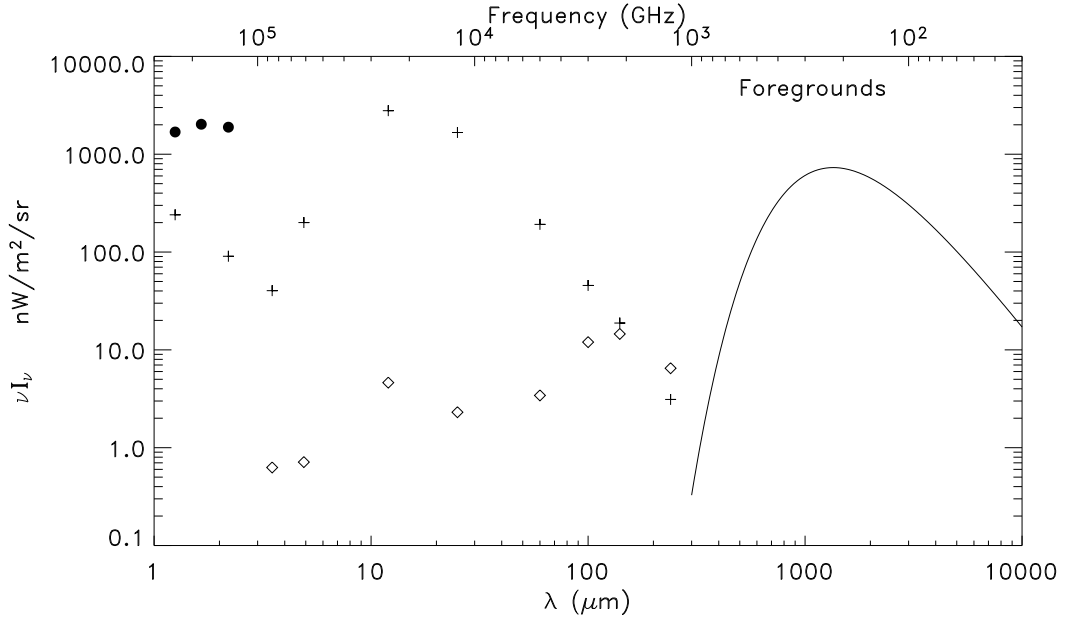


Fig. 4.— IR emission from the various foregrounds in CIB measurements: zodiacal light at high Ecliptic latitudes (crosses, Kelsall et al 1998), Galactic cirrus at high Galactic latitudes (diamonds, Arendt et al 1998), atmospheric emission fluctuations at $1''$ after $\simeq 8$ sec integration (filled circles, <http://pegasus.phast.umass.edu/adams/airglowpage.html>), and CMB (solid line)

CIB measurements are very difficult because while the CIB signal is relatively weak, the various foregrounds conspire to be fairly bright as one moves to the IR range of wavelengths. Fig. 4 summarizes the various foregrounds and the remainder of this section discusses them and their structure. The figure illustrates the difficulty of eliminating the foreground emission down to levels of $\sim 10 \text{ nWm}^{-2}\text{sr}^{-1}$ in the infrared. While some of the foregrounds may be small at certain wavelengths, their sum-total always conspires to be well above the required level of $\sim 10 \text{ nWm}^{-2}\text{sr}^{-1}$.

Foreground emission from the Galaxy and the solar system is the main problem in unveiling the expected CIB. At wavelengths less than $10 \mu\text{m}$, the dominant foreground after removing the zodiacal light model is emission from stars in our Galaxy. At sub-mm wavelengths cosmic microwave background (CMB) emission dominates everything else. In ground-based measurements atmospheric emission is important.

Intensity fluctuations of the Galactic foregrounds are perhaps the most difficult to distinguish from those of the CIB. Stellar emission may exhibit structure from binaries, clusters and associations, and from large scale tidal streams ripped from past and present dwarf galaxy satellites of the Milky Way. At long IR wavelengths, stellar emission is minimized by virtue of being far out on the Rayleigh–Jeans tail of the stellar spectrum (apart from certain rare classes of dusty stars). At near-IR wavelengths stellar emission is important, but with sufficient sensitivity and angular resolution most Galactic stellar emission, and related structure, can be resolved and removed.

4.1. Atmospheric emission

For ground-based observations, the largest contribution to the sky background comes from the atmosphere itself, which at K_s band amounts to 295 MJy/sr. At wavelengths longer than $\sim 2.5 \mu\text{m}$ the spectrum of the emission is characteristic of a black-body with a typical atmospheric temperature near 250 K. The emission at $1\text{--}2.5 \mu\text{m}$ range is dominated by many intrinsically narrow OH lines with some contribution from molecular hydrogen (at $1.27 \mu\text{m}$) and other species. The atmospheric seeing is typically $\sim 1''$. On sub-arcminute angular scales fluctuations in the atmospheric emission have white noise spectrum both in the spatial and time domains and hence scale $\propto \theta^{-1}t^{-1/2}$. On larger angular scales atmospheric gradients become important (<http://pegasus.phast.umass.edu/adams/airglowpage.html>). Solid circles in Fig. 4 show typical atmospheric fluctuations at $1''$ during nighttime observations by 2MASS survey after 7.8 sec of integration.

4.2. Galactic stars

For low resolution experiments (e.g. DIRBE) Galactic stars are a major contributor to foreground emission at wavelengths $\lesssim 3 \mu\text{m}$. In narrow beam observations beam observations they can be excised out to fairly faint magnitude. In larger beam measurements, one can use their statistical properties for removal of their cumulative emission. For purposes of measuring the CIB, regions of the sky within 20° – 30° of the Galactic plane can be ignored.

In the near-IR Galactic stars, have two useful properties: 1) at the Galactic poles star counts have a simple scaling with magnitude given by:

$$\frac{dN}{dm} \propto 10^{Bm} \quad (21)$$

and 2) outside the Galactic plane ($|b_{\text{Gal}}| \geq 20^\circ$) and away from the Galactic center ($90^\circ < \ell_{\text{Gal}} < 270^\circ$) the Galaxy can be approximated as plane-parallel. In a plane-parallel Galaxy in which the radial structure can be neglected, the differential counts in the direction $x = \text{cosec}|b|$ can be related to those at the Galactic pole by (Kashlinsky & Odenwald 2000)

$$\frac{dN}{dm}|_x = x^3 \frac{dN(m - 5 \log_{10} x)}{dm}|_{\text{Pole}}. \quad (22)$$

The right panel of Fig. 5 illustrates the degree of accuracy of the plane-parallel approximation for the Galaxy (eq. 22) using DIRBE data (Kashlinsky & Odenwald 2000). Using these approximations, once the counts at the Galactic pole are measured, one can evaluate the expected number counts in any direction b and then compute the flux and fluctuations in the flux they produce via:

$$F_{\text{stars}}(< m) \propto \int_m^\infty 10^{-0.4m} \frac{dN}{dm}|_x dm \quad ; \quad \sigma^2(x) \propto \int_m^\infty 10^{-0.8m} \frac{dN}{dm}|_x dm. \quad (23)$$

For $B < 0.4$ both are dominated by the brightest stars remaining in the field.

The left panel in Fig. 5 shows compilation of stars counts at 2.2 μm (K band) in the North Galactic Pole (NGP) region from various measurements. The data show that $B \simeq 0.3$; the value of $B = 0.6$ would correspond to homogeneous distribution of sources or stars coming from well within the scale height of the Galactic disk. The NGP star counts were observed directly by Elias (1978). We show his data at $K = 1, 2.5, 3.25$ and 8 with $N^{1/2}$ error bars and our binning of his data. Further NGP data were obtained by the 2MASS survey in K_s band, almost identical to the DIRBE Band 2, and were kindly provided to us by Tom Jarrett (1998, private communication) who created it using the 2MASS point source catalog, now available to the public. The cumulative counts from these measurements were shown in Fig. 1 of Beichman (1997) out to $K_s > 15$, who found that they follow $dN/dm \propto 10^{0.3m}$ (cf. his Table 4). Actual 2MASS star counts from a region of 5 square degrees centered on the NGP are plotted in Fig. 5. The agreement between the DIRBE counts, the Elias (1978) and Jarrett (1998, private communication) data, and the $B = 0.3$ extrapolation is excellent over 15 magnitudes, or six decades in flux. South Galactic Pole counts from Minezaki et al. (1998) are also shown. At $m_K < 1.5$, the counts tend to the slope of $B = 0.6$ coming from stars much closer than the scale height; if B were less than 0.6, the integrated star brightness would diverge at the bright end.

The star counts agree with model predictions. Both Beichman (1996) in his Fig. 1 and Minezaki et al. (1998) in their Fig. 1 show that the counts are fitted well by extensions of either the Bahcall & Soneira (1980) or Wainscoat et al. (1992) models. An eyeball fit to their data gives $B = 0.3 - 0.32$ at $K = 11$. The Wainscoat et al. model at $K = 11$ shown in Fig. 1 of Minezaki et al. (1998) gives $\log dN/dm \simeq 1.35$, whereas continuation of the solid line in the left panel of Fig. 5 to $K = 11$ gives $\log dN/dm = 1.3$ if $B = 0.3$ and 1.4 if $B = 0.33$. The agreement between the two slopes and normalizations is thus very good. Even the large-beam DIRBE instrument sees far beyond the scale height of the bright K band stars.

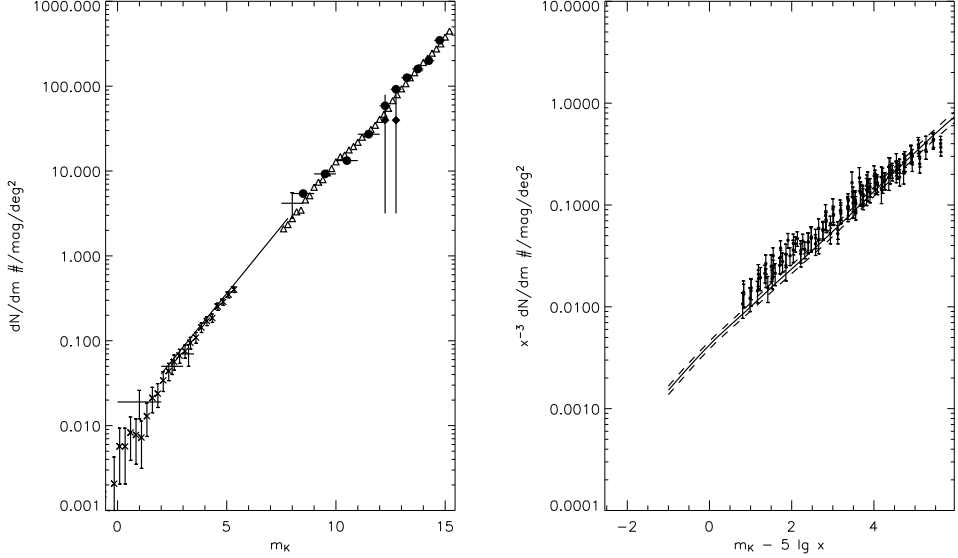


Fig. 5.— **Left** – Number counts measurements of Galactic stars in K band at the Galactic Poles. DIRBE based counts (crosses) are from Kashlinsky & Odenwald (2000) (at fainter magnitudes the DIRBE counts are affected by the confusion noise of the large DIRBE beam - see Fig. 7 in Kashlinsky & Odenwald 2000). Filled triangles are differential counts from Elias (1978) NGP measurements. Filled circles are differential NGP counts from 2MASS (Jarrett 1998). Open triangles are cumulative 2MASS counts from Beichman (1998) multiplied by $0.3 \ln 10$ to convert to differential counts for $dN/dm \propto 10^{0.3m}$. Filled diamonds with error bars are South Galactic Pole counts from Fig. 1 of Minezaki et al. (1998). Solid line shows the $B = 0.3$ fit.

Right – DIRBE star counts at $2.2 \mu\text{m}$ plotted in coordinates where a plane-parallel Galaxy would collapse on a single line; $x = \text{cosec}|b|$. Data are from the $\simeq 20^\circ \times 20^\circ$ DIRBE patches with $|b| \geq 20^\circ$ and $90^\circ < l < 270^\circ$, with Poisson errors shown. For the DIRBE beam the confusion noise affects counts at $K > 5.5$. Lines show the model Galaxy: solid is mean $x^{-3} dN/dm$ and dashes are the ± 1 -sigma spread.

4.3. Zodiacal emission

Zodiacal emission from interplanetary dust (IPD) is the brightest foreground at most IR wavelengths over most of the sky. There are some structures in this emission associated with particular asteroid families, comets and comet trails, and an earth-resonant ring, but these structures tend to be confined to low ecliptic latitudes or otherwise localized (Reach et al 1995). The main IPD cloud is inclined at $\sim 2^\circ$ with respect to the Ecliptic and is generally modeled with a smooth density distribution that also contains additional features of a circumsolar ring, a density enhancement in the Earth's wake and the dust bands at several AU (Kelsall et al 1998). Combining DIRBE and FIRAS observations, Fixsen & Dwek (2002) find a sharp break in the dust distribution at radius of $\sim 30 \mu\text{m}$ and that the zodiacal energy spectrum beyond $\sim 150 \mu\text{m}$ can be fitted with a single black-body with λ^{-2} emissivity and temperature of 240K. Observationally, intensity fluctuations of the main IPD cloud have been limited to $< 0.2\%$ at $25 \mu\text{m}$ (Ábrahám, Leinert, & Lemke 1997). Because the Earth is moving with respect to (orbiting within) the IPD cloud, the zodiacal light varies over time. Likewise, any zodiacal light fluctuations will not remain fixed in celestial coor-

dinates. Therefore repeated observations of a field on timescales of weeks to months should be able to distinguish and reject any zodiacal light fluctuations from the invariant Galactic and CIB fluctuations.

4.4. Galactic cirrus

IR emission from the ISM (cirrus) is intrinsically diffuse and cannot be resolved. Cirrus emission is known to extend to wavelengths as short as $3 \mu\text{m}$. Statistically, the structure of the cirrus emission can be modeled with power-law distributions, $P_2(q) \propto q^n$ (Gautier et al 1992), and has the power index $n \simeq -2, -2.5$ (Wright 2000, Kashlinsky & Odenwald 2000, Ingalls et al 2004). This power index lead to almost scale-independent fluctuations in cirrus emission which are typically $\lesssim 10^{-2}$ of the mean flux level. Using the mean cirrus spectrum, measurements made in the far-IR can be scaled to $3.5 \mu\text{m}$, providing estimates for the fluctuation contribution from cirrus. The extrapolation to shorter wavelengths is highly uncertain, because cirrus (diffuse ISM) emission has not been detected at these wavelengths, and the effects of extinction may become more significant than those of emission.

4.5. Cosmic microwave background

Ironically, the cosmic microwave background (CMB) has to be put in the category of “foregrounds” when searching for the CIB. CMB is a relic from the Big Bang and has a strict black-body energy spectrum correspond to $T_{\text{CMB}} = 2.725 \pm 0.001\text{K}$ with very small, if any, deviations from the black-body spectrum (Mather et al 1993; Fixsen et al 1996; Fixsen & Mather 2002). CMB is also very homogeneous with the largest fractional spatial deviation being $\sim 10^{-3}$ on dipole scales; the other angular moments are some two orders of magnitude smaller (Bennett et al 2003). Its brightness, shown with solid line in Fig. 4, overwhelms all other emissions at wavelengths longer than $\sim 500 \mu\text{m}$ and is even a non-negligible source of noise in many everyday electric appliances. Because its energy spectrum is known so accurately and its spatial structure is so small, the CMB can be subtracted down to levels $\ll 1 \text{nWm}^{-2}\text{sr}^{-1}$.

5. Current CIB measurements

This section discusses the current observational status of both the mean CIB levels and its structure (fluctuations).

Observationally, the CIB is difficult to distinguish from the generally brighter foregrounds contributed by the local matter within the Solar system, and the stars and ISM of the Galaxy. A number of investigations have attempted to extract the isotropic component (mean level) of the CIB

from ground- and satellite-based data. These analyses of the *COBE* data have revealed the CIB at far-IR wavelengths $\lambda > 100 \mu\text{m}$ (Hauser et al 1998), and probably at near-IR wavelengths from 1 - 3 μm (Dwek & Arendt 1998, Gorjian et al 2001, Cambresy et al 2001) with additional support from analysis of data from *IRTS* (Matsumoto et al 2000, 2003). However, it would probably be fair to say that none of the reported detections of the isotropic CIB are very robust (especially in the NIR), because all are dominated by the systematic uncertainties associated with the modeling and removal of the strong foreground emission of the zodiacal light and Galactic stars and ISM. Furthermore, the near-IR colors of the mean CIB do not differ greatly from those of the foregrounds, thus limiting the use of spectral information in distinguishing the true CIB from residual Galactic or solar system emission.

In order to avoid the difficulty of exactly accounting for the contributions of these bright foregrounds in direct CIB measurements, (and the difficulty in detecting *all* the contributing sources individually), Kashlinsky, Mather, Odenwald and Hauser (1996) have proposed measuring the structure or anisotropy of the CIB via its angular power spectrum. They noted that for a relatively conservative set of assumptions about clustering of distant galaxies, fluctuations in the brightness of the CIB have a distinct spectral and spatial signal, and these signals can be perhaps more readily discerned than the actual mean level of the CIB.

Figure 6 shows the filters and the IR wavelengths covered by the measurements from the instruments described below.

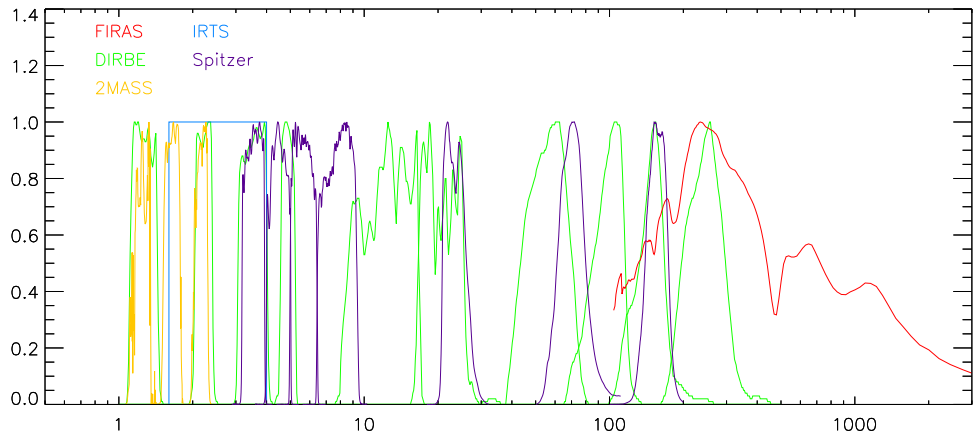


Fig. 6.— Filter responses for the various instruments discussed in the paper. The curves were normalized to a unity peak. DIRBE, FIRAS, 2MASS, IRTS, Spitzer (IRAC and MIPS) filters correspond to the colors shown in the upper left corner. The multiple ISO filters filters are not shown for clarity.

5.1. COBE DIRBE

The primary mission of the DIRBE instrument on board COBE satellite was to find, or set very strict limits on, the CIB contribution from near- to far-IR. The DIRBE was described by Boggess *et al.* (1992) and is a 10-band, photometer system covering the wavelength range from 1.25 to 240 μm with an angular resolution of 0.7° . The 1.25, 2.2 and 3.5 μm DIRBE bands are similar, although not identical, to the ground based J, K and L bands. It was designed to achieve stray light rejection of less than $1 \text{ nWm}^{-2}\text{sr}^{-1}$ and a low absolute brightness calibration uncertainty. Accurate beam profile and beam response maps were obtained in flight by observing multiple transits of bright point sources. All spectral channels simultaneously observed the same field-of-view on the sky. Its cryogenic stage lasted from November 1989 to September 1990 collecting 41 weeks of data.

Absolute photometry was obtained through frequent (32 Hz) chopping between the sky and an internal zero flux surface maintained at temperatures below 2 K. System response was monitored every 20 minutes throughout the 10 month mission by observing an internal thermal reference source. The DIRBE was designed to achieve a zero-point to the photometric scale with an uncertainty below $\nu I(\nu) = 10^{-9} \text{ Wm}^{-2}\text{sr}^{-1}$ at all wavelengths; tests conducted prior to launch and in flight indicate that this goal was indeed reached.

Absolute calibration of the DIRBE photometric scale, and long-term photometric consistency, was established by monitoring a network of stable celestial sources. The primary calibrator for the *J*, *K* and *L*-bands was the star Sirius. Although DIRBE is a broad-band instrument, the measured in-band intensities are reported as spectral intensities at the nominal effective wavelengths of each band. Sources that have an SED significantly different from a flat $\nu I(\nu)$ would require color corrections. In the *J*, *K* and *L*-bands, these color corrections are of the order of a few percent or less over the temperature range from 1500 to 20,000 K. Long-term stability of the instrumental photometric scale at each wavelength was better than 1%. The stability of the band-to-band intensity ratios, or colors, was 1.4%. The absolute photometric uncertainty in the DIRBE *J*, *K* and *L*-bands was $\approx 4\%$.

The calibrated DIRBE observations were binned into 20 arcmin pixels of approximately equal area for each of the forty one weeks and are available from (http://lambda/product/cobe/dirbe_overview.cfm). Each week covered about half the sky and four months of data gave one full sky coverage.

In a real tour d'force the background and foreground results of the combined 41 week maps of DIRBE sky observations have been analyzed by the DIRBE team (Hauser *et al* 1998, Arendt *et al* 1998, Kelsall *et al* 1998, Dwek *et al* 1998). From these maps, the *models* of contributions from the interplanetary dust (IPD) cloud and the Galaxy, both its interstellar dust and stellar components, were subtracted for each direction.

The DIRBE IPD model is described in Kelsall *et al* (1998). It represents the zodiacal sky brightness as the integral along the line of sight of the dust emissivity times the 3-D dust density distribution function. The emissivity arises from both thermal emission and scattering; the former

dominates at $\lambda \gtrsim 5\mu\text{m}$ and the latter at shorter wavelengths. The thermal emission at each location assumes a single dust temperature for all IPD cloud components and is assumed to drop as a power law of the distance to the Sun. The density model included contributions from a smooth cloud, three pairs of asteroidal dust bands and a circumsolar dust ring. Parameters of the analytical functions that enter the model were determined by matching the observed temporal brightness variations in various directions on the sky. Once the optimal set of model parameters was determined, the IPD model was integrated along the line of sight at the mean time of each week of observations. The calculated IPD brightness map was then subtracted from each week of the DIRBE weekly maps. Because of the brightness of the zodiacal emission, the residual sky maps are dominated by the uncertainties in the IPD model at between 12 and 60 μm .

The Galactic emission was modeled by Arendt et al (1998) as made up of emission of bright and faint Galactic stars and discrete sources and the interstellar medium, or cirrus cloud emission. It was removed from the combined the maps after the zodiacal component removal. Bright(er) sources above a wavelength dependent threshold were removed from the maps at all bands. The contribution to the integrated light from faint sources was removed using a statistical source count Faint Source Model (FSM - Arendt et al 1998) which is based upon Wainscoat et al (1992). Prior to subtracting the FSM, bright stars with flux greater than 15 Jy (corresponding to $K \simeq 4$) have been subtracted directly. Stellar contribution is negligible at mid- and far-IR DIRBE bands. The model for the ISM emission was taken to be a product of the standard spatial template times a single spectral factor at each wavelength. At 100 μm the spatial template was a map of HI emission constructed from three different 21 cm HI surveys (see Arendt et al 1998 and references cited therein); at other wavelengths the 100 μm data were used.

Hauser et al (1998) presented the limits on the CIB after removal of the zodiacal light model, the FSM and the Galactic cirrus contributions from the combined DIRBE maps. In the residual maps, they selected for the analysis "high-quality" regions that are located high Galactic and ecliptic latitudes, are free of foreground removal artifacts and cover at least 2% of the sky. The smallest and best region contains some 8,140 pixels in both northern and southern hemispheres allowing to test for isotropy of the residual signal. Their criteria for a CIB detection were that the residuals had to be in excess of 3σ , σ being *both* systematic and statistical uncertainty, and be isotropic in the high-quality region. They reported firm detections at 140 and 240 μm and upper limits at shorter wavelengths. The 100 μm residual they find at the level of $21.9 \pm 6.1 \text{ nW m}^{-2} \text{ sr}^{-1}$ also has high statistical significance, but is not isotropic. The dominant errors in the DIRBE CIB measurements are the systematic errors associated with the foreground subtraction. Dwek et al (1998) show in detail that the isotropic signal detected at 140 and 240 μm is unlikely to arise from some Solar system and Galactic sources. Adopting the DIRBE detections at 140 and 240 μm , Dwek et al (1998) claim a *lower* limit of $5 \text{ nW m}^{-2} \text{ sr}^{-1}$ at 100 μm assuming that the CIB emission arises from the coldest possible dust fitted to the 140, 240 μm detections.

Figure 7 shows the map of the 240 μm residual emission from Hauser et al (1998); it is plotted here in Galactic coordinates (cf. Arendt et al 1998). The produced map corresponds to the original

240 μm map from which the zodiacal light was removed along with a two-component ISM model, corresponding to a weighted subtraction of the DIRBE 140 and 100 μm maps. The bright sources near the Galactic plane are clearly visible as are the Small and Large Magellanic clouds. The remaining emission is isotropic and was identified with the CIB. The 140 μm map also passed the isotropy limits, although is significantly more anisotropic outside the high-quality region used for identifying the CIB.

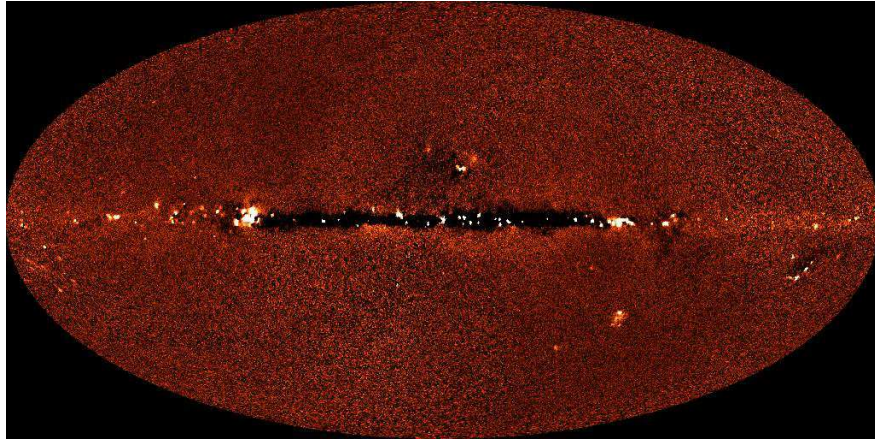


Fig. 7.— DIRBE map of the CIB at 240 μm shown in Galactic coordinates with the South Galactic Pole pointing toward the bottom of the figure.

Chronologically, the DIRBE discovery of the far-IR CIB was preceded by a few months by an independent analysis of Schlegel et al (1998), who have combined the well calibrated DIRBE data that has relatively poor resolution ($\sim 0.5^\circ$) with the IRAS data, which have much better angular resolution ($\sim 5'$) but poor absolute calibration. The combined maps at 100 μm provides a very accurate to-date template of the diffuse Galactic emission and dust distribution. To construct the map, they have removed 1) zodiacal emission from the DIRBE maps, 2) striping artifacts from the IRAS data, 3) confirmed point sources, and then combined the maps preserving the DIRBE calibration and IRAS resolution. The ratio of the 100 μm to 240 μm emission gave the dust temperature leading to estimate of column density of the radiating dust. The 25 μm channel data was used to model the zodiacal light emission from the interplanetary dust (IPD) cloud. Fitting black-body functions from 12 to 60 μm they find variations in the IPD temperature of less than 10 %. As the zodiacal light contributes ca. $300 \text{ nWm}^{-2}\text{sr}^{-1}$ at 100 μm the temperature variations of the cloud lead to absolute errors of $\sim 30 \text{ nWm}^{-2}\text{sr}^{-1}$ if the 25 μm template is used linearly in subtracting from the longer wavelength maps. After accounting for the (non-linear) corrections for the IPD temperature variations in subtracting the zodiacal light emission, the CIB was determined as the zero offset in cross-correlation between the residual "de-zodied" emission with the Galactic HI column density from the Leiden-Dwingeloo 21 cm survey (Hartmann & Burton 1997). The analysis has been applied to the 100, 140 and 240 μm maps restricted to lie outside the ecliptic plane leading to null-detection at 100 μm and robust CIB values at the two longer bands for $|\beta| \gtrsim 20^\circ$.

Finkbeiner, Schlegel & Davis (1998) extended the analysis to the DIRBE data at 60 and 100 μm . They applied two different methods to remove the zodiacal light component: The first of these methods used the North-South asymmetry with a 1 year period of the zodiacal component and concentrated on the data within 5° of the ecliptic poles, where effects dependent on solar elongation cancel out. The method further assumed that the zodiacal light North-South asymmetry is the same in all bands. Cirrus was taken from the 100 μm map produced in the Schlegel et al (1998) analysis. They decomposed each of the North and South datasets into time-dependent (zodi) and time-independent (cirrus, CIB etc) components and obtain robust solutions for the latter. In the second method they remove zodiacal component by using its dependence on the ecliptic latitude in each of the DIRBE's 41 weeks of data with solar elongation 90° . A statistic was then constructed that ratios the flux in the various diagonal directions to that toward the ecliptic poles and whose advantage is that it has a known dependence on the ecliptic latitude ($\propto \csc|\beta|$) with a negligible annual variation. The CIB flux was determined as a term at $\csc|\beta| = 0$. Both methods gave consistent and robust, if high compared to other measurements, levels of the CIB at 60 and 100 μm .

Because of the difficulty in measuring the isotropic component of the CIB, Kashlinsky, Mather, Odenwald & Hauser (1996) have proposed to probe the CIB structure instead. For a reasonable set of assumptions about the underlying distribution of emitters/galaxies, the fluctuations in the CIB can provide important information about the rate of production of the CIB and luminous activity in the early Universe. The method leads to particularly strong constraints at mid- to far-IR where the foregrounds are very smooth (Kashlinsky, Mather & Odenwald 1996). The analysis, however, could not have been applied to the DIRBE's longest channels (140 and 240 μm), which required the use of bolometers instead of the photoconductors, resulting in much larger noise than at shorter wavelengths.

Kashlinsky & Odenwald (2000) have applied the method to the final DIRBE data release leading to detection of the near-IR CIB anisotropies. They started with the final DIRBE sky maps from which the zodiacal model from Kelsall et al (1998) was subtracted. The sky was divided into (384) patches of 32 pixels ($\simeq 10^\circ$) on the side which were individually clipped of Galactic stars and other point sources by various procedures all of which led to the same final results. The RMS flux fluctuation, $\delta F_{\text{RMS}} \equiv \sqrt{C(0)}$, or fluctuation on the DIRBE beam scale ($\simeq 0.6^\circ$) was computed in each of the clipped patches. The residual fluctuation is the sum of contributions from the remaining Galactic stars, CIB, instrument noise, etc. When the data in the near-IR 1.25 to 5 μm were selected from high Galactic latitude ($|b_{\text{Gal}}| \geq 20^\circ$) and away from the Galactic center ($90^\circ \leq \ell_{\text{Gal}} \leq 270^\circ$), they showed a very tight correlation between $\text{cosec}(|b_{\text{Gal}}|)$ and $C(0)$. That NIR fluctuation was explained in terms of the *observed* Galactic star counts in the plane parallel Galaxy, such as given by eqs. 21,22, shifted by a constant (isotropic) component. The latter presumably arises from CIB fluctuations as well as instrumental noise. Extrapolation of the correlation to $\text{cosec}(|b_{\text{Gal}}|) = 0$, or zero contribution from Galactic stars, gave a robust value of the near-IR CIB anisotropies, which was demonstrated to be independent of the clipping methods, sky maps processing and other effects.

The instrument noise was evaluated in Kashlinsky et al (1996), Kashlinsky & Odenwald (2000) and Hauser et al (1998) and was shown to be significantly lower than the detected near-IR signal at wavelengths from 1.25 to 5 μm . At mid- and far-IR wavelengths the results of the analysis led to slightly tighter upper limits than in the previous analysis (Kashlinsky, Mather & Odenwald 1996) which used an intermediate zodiacal light model from the DIRBE team.

Dwek & Arendt (1998) have presented another original method to isolate the isotropic component of the near-IR CIB by using prior information of the flux in one of the bands. They noted that the observed galaxy contribution to the K band CIB pretty much saturates at $\simeq 9 \text{ nWm}^{-2}\text{sr}^{-1}$. They started with the DIRBE maps at 1.25, 2.2, 3.5 and 4.9 μm from which they subtracted the zodiacal light model from Kelsall et al (1998). From DIRBE near-IR maps the regions were selected with small errors in the subtraction of the foreground emission (Hauser et al 1998, Arendt et al 1998). Small cirrus emission at 3.5 and 4.9 μm was removed by scaling the average 100 μm intensity in DIRBE maps as in Arendt et al (1998). The 2.2 μm DIRBE map minus the assumed CIB at that band was taken as a template of the Galactic stellar emission. That template was then cross-correlated with the maps at the other wavelengths to give a positive and statistically significant residuals (zero intercepts) summarized in Table 3. This technique was pushed farther by Arendt & Dwek (2003) attaining a more isotropic removal of Galactic foregrounds, but at the expense of increased uncertainty in the absolute zero point.

In order to reduce the uncertainty in the Galactic stars contribution to the NIR DIRBE maps, Gorjian et al (2000) have imaged a high Galactic latitude region of the sky of 2° on the side in K and L bands with arcsec resolution to $K \simeq 9$ and $L \simeq 8$ magnitudes reducing the stellar contribution to confusion noise a factor of ~ 16 below that of DIRBE. They subtracted a modified zodiacal light model proposed by Wright (1997) which comes in two flavors: a "weak" zodi model which requires that the DIRBE high Galactic latitude sky at 25 μm be isotropic in addition to its non-ZL components remaining constant in time, and a "strong" zodi model which requires that the former component in addition is negligibly small. This reduced the residual 25 μm intensity by a factor of 7 compared to the DIRBE model (Kelsall et al 1998). They then selected 17 DIRBE pixels where overlap with star position is sufficient for robust statistics in subtracting the Galactic stellar component. The CIB was evaluated after subtracting the zodiacal components, the measured flux from the Galactic stars and the model flux from fainter and unobserved stars. Wright & Reese (2000) used the above ZL model subtraction and the Arendt et al (1998) method for removing the ISM contribution to the residual emission. They found a constant flux offset in the flux histograms at 2.2 and 3.5 μm compared to the Wainscoat et al (1992) model after testing the latter with 2MASS observations in several selected fields. The flux offset is identified as the CIB and is consistent with the Gorjian et al (2000) results. Wright (2000) used the 2MASS catalog stars in order to subtract Galactic star contribution to the DIRBE maps flux in selected regions near the Galactic poles. After the subtraction he finds a statistically significant flux excess at 2.2 μm that is in agreement with the Gorjian et al (2000) and Wright & Reese (2000) results.

Cambresy et al (2001) used the 1,400 deg^2 of the 2MASS data from standard exposures (7.8

sec) in J, H, K_s. They degraded the 2MASS maps (2'') to 5' resolution. After subtracting the zodiacal light from DIRBE weekly maps using the zodiacal subtracted mission average maps, the residual intensity maps were averaged together. The subset of the 2MASS that was used to account for Galactic contribution to the DIRBE intensities came from high Galactic latitude ($|b_{\text{Gal}}| \geq 40^\circ$) and high ecliptic latitude ($|\beta_{\text{ecl}}| \geq 40^\circ$) regions of low cirrus emission for which a complete 2MASS coverage existed in each DIRBE pixel. After removing bright stars, which contaminate more than one DIRBE pixel, the final area for analysis was 1,040 deg². The intensities in the DIRBE sky were cross correlated with the observed fluxes from 2MASS stars. The zero-intercept of this correlation minus the (small) contribution from faint stars, which was computed from Galaxy modeling, is the CIB flux.

Table 3 summarizes the results of the CIB measurements based on the DIRBE data.

5.2. COBE FIRAS

Far-Infrared Absolute Spectrometer (FIRAS) on board COBE was designed for measuring the energy spectrum of the CMB and the far-IR CIB. It is a four-port Michelson interferometer. At each port (Left and Right) a dichroic filter split the beam into Low (30-660 GHz) and High (600-2880 GHz) frequency beams producing spectra with a resolution of 4.2 GHz or 16.9 GHz. The FIRAS data have angular resolution of 7 degrees, with pixel size of 2.6 degrees. FIRAS is described in Boggess et al (1992) and Mather et al (1993). The FIRAS Pass 4 data consist of spectra between 104 μm and 5000 μm in each of 6,063 out of the 6,144 pixels of the sky (81 pixels that have no data are omitted). They were calibrated using the method described in Fixsen et al. (1994, 1996).

The Pass 4 FIRAS data have approximately half of the noise of the previous data releases (Pass 3). This is partly due to combining all FIRAS frequency bins and scan modes and partly due to improved understanding of the systematic errors. Particularly important was the reduction in the systematic errors since these have a complicated spectrum in the spatial domain. Since the fluctuations of the far-IR CIB may themselves look like noise with some a priori uncertain spatial power spectrum, finding a noise floor leaves one uncertain whether it is the fluctuations in the far-IR CIB or systematic effects in the instrument. The Pass 4 FIRAS data have many of the known systematics removed, which enables a direct and substantial lowering of the noise spectrum.

Puget et al (1996) made a first cut at detecting the far-IR CIB from the Pass 3 FIRAS data. They used the particular spatial and spectral distribution of the different far-IR components of the sky emission in subtracting them from the Pass 3 FIRAS maps. First, DIRBE maps were degraded to the FIRAS resolution in order to map and subtract the zodiacal emission. In the DIRBE 25 μm channel the emission is dominated by the zodiacal light and they noted the average brightness ratio $B_\nu(100\mu\text{m})/B_\nu(25\mu\text{m}) = 0.167$ and used the FIRAS observations of the spectral dependence of the zodiacal light, $B_{\nu,\text{zodi}} \propto \nu^3$ (Reach et al 1995), to model the zodiacal light emission along each line-of-sight as $0.167(\lambda/100\mu\text{m})^{-3}B_\nu(100\mu\text{m})$. The CMB along with its dipole

Table 3. SUMMARY OF DIRBE MEASUREMENTS (nWm⁻²sr⁻¹)

Ref	1.25 μm	2.2 μm	3.5 μm	4.9 μm	12 μm	25 μm	60 μm	100 μm	140 μm	240 μm
νI_ν										
1										
2	< 75	< 39	< 23	< 41	< 468	< 504	< 75	< 34	32 ± 13	17 ± 4
3	26.9 + 2.3 $F_{2.2\mu\text{m}}$ ± 20.9	—	9.9 + 0.3 $F_{2.2\mu\text{m}}$ ± 2.9	23.3 + 0.1 $F_{2.2\mu\text{m}}$ ± 6.4					25.0 ± 6.9	13.6 ± 2.5
4,\$							28.1 ± 1.8 ± 7	24.6 ± 2.5 ± 8		
5		22.4 ± 6	11.0 ± 0.3							
6		23.1 ± 5.9	12.4 ± 3.2							
7		20.2 ± 6.3								
8	54.0 ± 16.8	27.8 ± 6.7								
$\sqrt{C(0)}$										
9,10,*	15.5 ^{+3.7} _{-7.0}	5.9 ^{+1.6} _{-3.7}	2.4 ^{+0.5} _{-0.9}	2.0 ^{+0.25} _{-0.5}	≤ 1.	≤ 0.5	≤ 0.7	≤ 1	—	—

Note. — : Refs: ¹ Schlegel, Finkbeiner & Davis (1998), ² Hauser et al (1998), ³ Dwek & Arendt (1998) – $F_{2.2\mu\text{m}}$ is the flux at 2.2 μm in nWm⁻²sr⁻¹, ⁴ Finkbeiner, Davis & Schlegel (2000) – ^{\$} random and systematic errors shown, ^{5,6,7} Gorjian, Wright & Chary (2000), Wright & Reese (2000), Wright (2000), ⁸ Cambresy et al (2001), ^{9,10} Kashlinsky, Mather & Odenwald (1996), Kashlinsky & Odenwald (2000) – * 92% confidence level uncertainties are shown.

anisotropy was then subtracted from the raw FIRAS spectrum at each pixel. The Leiden-Dwingeloo HI survey (Hartmann & Burton 1997) degraded to the FIRAS resolution was used to subtract the Galactic interstellar dust emission which at far-IR correlates well with the neutral hydrogen emission (Boulanger et al 1996). At high Galactic latitude ($|b_{\text{Gal}}| > 20^\circ$) and low HI column density lines-of-sight the residual was positive, approximately isotropic, and homogeneous with amplitude of $\simeq 3.4(\lambda/400\mu\text{m})^{-3} \text{ nW m}^{-2} \text{ sr}^{-1}$ in the 400-1000 μm range.

Fixsen et al (1998) used Pass 4 FIRAS data with significantly lower noise and systematic errors. From the FIRAS data they subtracted the DIRBE zodiacal model (Kelsall et al 1998) extrapolated to FIRAS bands and the low-frequency FIRAS CMB model with dipole anisotropy. In order to separate the Galactic emission they used three independent methods: 1) They noted that after subtracting CMB and zodiacal model, the residual emission has approximately identical spectral energy distribution across the sky. This spectral template was to model emission of the Galaxy for further subtraction. Using all the FIRAS channels and assuming a non-negative prior for the CIB, they find a statistically significant residual. 2) HI (21 cm) and CII (158 μm) Galactic lines were used together with a quadratic fit to the Galactic HI map degraded to FIRAS resolution from the AT&T survey by Stark et al (1992) to subtract Galactic IR emission. After the subtraction, the darkest 1/3 of the sky, where the HI data was sufficiently accurate, showed a statistically significant CIB residual at longer wavelengths. 3) Finally, they constructed Galactic templates from the DIRBE 140 μm and 240 μm maps with zodiacal emission subtracted together with the levels of the CIB detected by DIRBE at these bands. The template was degraded to FIRAS resolution. The CIB was obtained by extrapolating the correlations with the DIRBE templates to the DIRBE measurements at 140 μm and 240 μm . All three methods gave consistent results.

An attempt to study far-IR CIB fluctuations has been undertaken by Burigana & Popa (1998) on the FIRAS Pass 3 data between 200 and 1,000 μm . From the data they subtracted CMB monopole and dipole components, a two-temperature dust model and a zodiacal light model using the DIRBE 25 μm channel and the ν^{-3} frequency scaling. The analysis resulted in upper limits on the CIB fluctuations on scales greater than the FIRAS beam ($\simeq 7^\circ$).

5.3. IRTS

Japan's InfraRed Telescope in Space (IRTS) was launched in March 1995. The Near InfraRed Spectrometer (NIRS) on board IRTS was designed to obtain spectrum of the diffuse background emissions (Noda et al 1994). It covers the wavelengths from 1.4 μm to 4 μm in 24 independent bands with spectral resolution of 0.13 μm . IRTS observations covered ca. 7% of the sky in 30 days (Murakami et al 1996). The resolution of IRTS is $\simeq 8'$, significantly better than DIRBE and allows better removal of faint stars.

The results from the IRTS CIB analysis have been presented in Matsumoto (2000, 2003). A narrow strip at high Galactic latitude was chosen for the CIB analysis in order to reduce the

contribution from Galactic stars. Contribution of Galactic stars not resolved by the IRTS beam was estimated from the point source sky model of the Galaxy by Cohen (1997). They used the DIRBE physical model of the interplanetary dust (Kelsall et al 1998) to remove the zodiacal component corresponding to the NIRS bands and the observed sky directions. There was a good correlation between the star-subtracted data and the modeled zodiacal component. The isotropic component was determined as the intercept of that correlation at zero modeled zodiacal brightness. The brightness of the isotropic emission found in this analysis was about 20 % of the sky brightness with an in-band energy of $\sim 30 \text{ nWm}^{-2}\text{sr}^{-1}$ and was estimated to be a factor of $\simeq 2.5$ greater than the integrated light of faint stars.

In order to determine the spatial spectrum of the fluctuations, Matsumoto et al (2000, 2003) have added the NIRS short wavelength bands (with smaller noise) from $1.43 \text{ } \mu\text{m}$ to $2.14 \text{ } \mu\text{m}$. They then calculated the correlation function of the emission, $C(\theta)$, which was converted into the power spectrum by Fourier transformation. The RMS fluctuations of the isotropic component was, after subtracting read-out noise and stellar fluctuations, consistent with the Kashlinsky & Odenwald (2000) results from the DIRBE sky analysis. The color of fluctuations was essentially the same as that of the isotropic component, consistent with both having the same origin.

5.4. ISO

Infrared Space Observatory (ISO) was operated by the European Space Agency between November 1995 and April 1998. Its infrared camera (ISOCAM) had a 32×32 pixel array and two IR channels with multiple filters: short wavelength channel operated between 2.5 and $5.2 \text{ } \mu\text{m}$ and the long wavelength operated between 4 and $17 \text{ } \mu\text{m}$. The other instrument relevant to CIB studies was ISOPHOT which covered the wavelength range from 2.5 to $200 \text{ } \mu\text{m}$ but had much smaller arrays. The ISO telescope had no shutter making absolute calibration difficult for studies of the isotropic component of the CIB.

There were several important findings concerning the mid- to far-IR CIB from the ISO surveys.

IR number counts indicate that the IR-luminous galaxies evolved more rapidly than their optical counterparts and make a substantial contribution to the star formation at higher z (Elbaz et al 1999) which in turn makes them the dominant contributors to the CIB at mid-IR bands. Elbaz et al (2002) computed the contribution from distant galaxies observed by deep ISOCAM extragalactic surveys at the central wavelengths of 6.75 and $15 \text{ } \mu\text{m}$ to the CIB. The $6.75 \text{ } \mu\text{m}$ sample was strongly contaminated by Galactic stars, whereas at $15 \text{ } \mu\text{m}$ the stars are readily separated from galaxies using optical-MIR color-color plots. They estimate that in this way they accounted for the CIB from dust in the starburst galaxies out to $z \sim 1.5$ and ISO measurements at 15 and $170 \text{ } \mu\text{m}$ reveal that the bulk of CIB at these wavelengths comes from galaxies at $z \lesssim 1.2$ (Dole et al 2001, Elbaz et al 2002). They find that galaxies above their completeness level of $50 \text{ } \mu\text{Jy}$ produce at least $2.4 \pm 0.5 \text{ nWm}^{-2}\text{sr}^{-1}$ contribution to the total CIB at $15 \text{ } \mu\text{m}$. (For comparison, the IRAS galaxies at 60

μm with completeness limit of 0.5 mJy contribute only $\sim 0.15 \text{ nW m}^{-2} \text{ sr}^{-1}$ to the CIB at $60 \mu\text{m}$.)

Lagache & Puget (2000) have analyzed a sub-field from the deep extragalactic FIRBACK survey with the ISOPHOT instrument at $170 \mu\text{m}$. The survey covered 4 deg^2 and they selected for analysis a subfield of low cirrus emission covering 0.25 deg^2 . 24 extragalactic sources were detected and subtracted up to the confusion limit of $3\sigma = 67 \text{ mJy}$. The pixel size of the maps was $\theta_p = 89.4''$ implying the Nyquist frequency of $k_{\text{Nyquist}} = (2\theta_p)^{-1} = 0.3 \text{ arcmin}^{-1}$. On scales corresponding to spatial frequencies below the Nyquist limit $k < 0.3 \text{ arcmin}^{-1}$ the results lead to upper limits on the CIB fluctuations at $170 \mu\text{m}$ that correspond to about $0.5 \text{ nW m}^{-2} \text{ sr}^{-1}$ at 0.5 arcmin .

5.5. 2MASS

The 2-Micron All Sky Survey (2MASS) uses two 1.3-m Cassegrain telescopes, one at Mt. Hopkins in the Northern Hemisphere, and one at CTIO in the Southern Hemisphere. Each telescope is equipped with a three-channel camera, capable of observing the sky simultaneously at J ($1.25 \mu\text{m}$), H ($1.65 \mu\text{m}$), and K_s ($2.17 \mu\text{m}$) at a scale of $2''$ per pixel. As the telescopes are scanned in declination, individual 1.3-second sky frames are imaged on an overlapping grid by stepping 1/6 the array. The frames are combined six at a time, to form the standard 2MASS Atlas images of size 512×1024 pixels with re-sampled $1''$ pixels, and an effective integration time of 7.8 seconds per pixel. Hereafter, we will use the term ‘image’ to refer to the calibrated 2MASS Atlas images which have been co-added to an effective integration time of 7.8 seconds. The 2MASS photometric stability is <0.02 mag in all bands. A detailed description of the calibration process can be found in the 2MASS Explanatory Supplement (Cutri et al 2003).

The standard 2MASS images are too shallow to be useful for CIB studies. But a limited number of standard stars had to be observed repeatedly each night, and for several months at a time, to establish the photometric zero-points for the data. The 2MASS standard stars were drawn from near infrared standard star catalogs (e.g. Persson et al. 1998, Casali and Hawarden 1992). Each calibration observation consisted of six independent scans of a calibration field. Each scan is a mosaic of 48 images, and the scans were made in alternating north-south directions, each displaced $5''$ in RA from the previous one to minimize systematic pixel effects. Repeated observations of calibration fields during a night at a variety of elevation angles were also used to develop long-term atmospheric extinction statistics. By collecting the calibration scan data, which spanned nearly 6 months of repeated observation, effective integration times exceeding one hour could be achieved for a small number of sky locations.

Kashlinsky et al (2002) and Odenwald et al (2003) used the long exposure 2MASS data for CIB analysis and reported the first detection of small angular scale fluctuations in the near-IR CIB. They have selected data from the 2MASS Second Incremental Data Release between 1998 March 19 and 1999 February 20, and used the 2MASS, on-line catalog of completed calibration fields in order

to identify fields that had the largest number of repeated measurements. One of these, 90565N, with a total exposure $\gtrsim 1$ hour was selected for further study. The field has Galactic and Ecliptic coordinates $(243^\circ, 27^\circ)$ and $(21^\circ, 35^\circ)$ respectively, around the star P565-C in the constellation Hercules, 5° north of the bright star λ Ophiuchus. The data analyzed by them consisted of 2080 calibrated $8.6' \times 15'$ frames covering an $8.6' \times 1'$ swath oriented north-south, obtained during observations at CTIO between Apr and Aug 1998. The images from individual exposures were co-added to produce a $8.6' \times 1'$ field from which resolved sources (both stars and distant galaxies) and other artifacts were removed by various methods to ensure consistency and robustness of the final results. After assembling the final image with a total exposure $> 3,700$ secs the data were calibrated and the field was divided into seven square patches $512''$ on the side. In each patch, individual sources (stars and galaxies) were removed by an iterative procedure where each pixel with surface brightness exceeding 3 standard deviations for the patch was excised along with 8 neighboring pixels. The 2MASS beam of $\sim 2''$ subtends comoving scale $\gtrsim 30h^{-1}\text{Kpc}$ at $z=1$ corresponding to a large galaxy so the sources near the the clipping threshold are unresolved. Because of the variation in background level and associated noise, the patches were clipped to different point source absolute flux levels. In K_s band these varied from 18.5 to 19 Vega magnitudes. The clipping left $> 90\%$ of the pixels in the patches, which provided a good basis for a Fourier analysis of the diffuse light. For the final images, the fluctuation spectrum of the residual diffuse emission was computed; its slope in the co-added images is consistent with that of galaxy clustering. They estimated the contributions to the power spectrum from atmospheric fluctuations, remaining Galactic stars and cirrus emission, zodiacal light, instrument noise and extinction. These components had different slopes and negligible amplitudes compared to the detected signal, suggesting that the diffuse component fluctuations in the final image are dominated by the CIB. Because in this type of analysis fairly faint galaxies ($K \lesssim 19$) have been removed, the resultant CIB provides a probe of still fainter sources which are presumably located at high redshifts, and allows to start isolating the contributions to the CIB from various cosmic epochs.

Fig. 8 shows one of the patches in K_s band after 7.8 sec integration (left panel - standard 2MASS product) and after the integration used in the analysis (middle panel). The right panel shows the final 3-color image (J, H and K_s) which was identified with the map of the near-IR CIB from galaxies fainter than $K_s \simeq +19$. An important step forward in this measurement is the removal of progressively fainter and more distant galaxies. This allows to begin to identify how much of the CIB comes from earlier times. Observations and theory both suggest that $K \gtrsim +19$ galaxies are typically located at $z \gtrsim 1$ (Cowie et al 1996, Kashlinsky et al 2002).

5.6. Results

The results on the mean CIB levels from the measurements described above are shown in Fig. 9. Only detections are shown; upper limits, in the absence of detections, are discussed below for each range of wavelengths. Hence the gap in the figure at the MIR wavelengths where

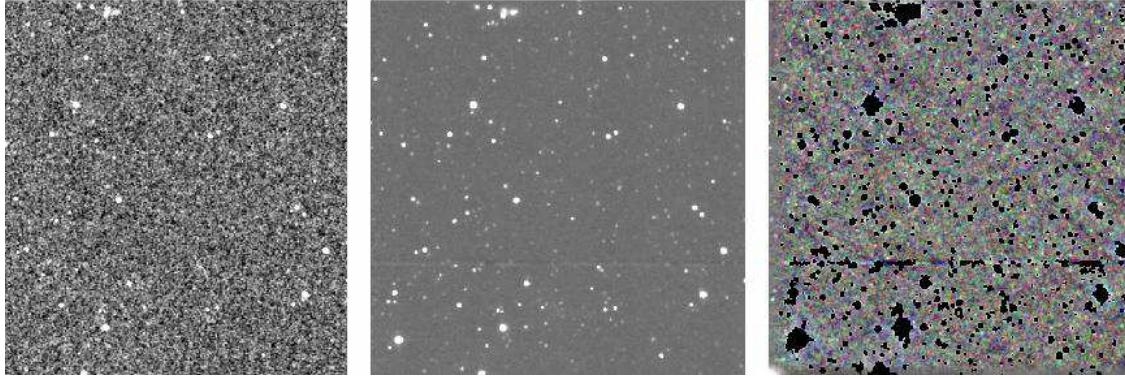


Fig. 8.— **Patch 3** of $512'' \times 512''$ in size from the deep 2MASS data analysis of Kashlinsky, Odenwald et al (2002) and Odenwald, Kashlinsky et al (2003). (**Left**) Individual 2MASS images for 7.8-second integration in K_s band. (**Middle**) Corresponding deep-integration co-added K_s band image for an effective integration time of 3,900 seconds. (**Right**) 3 color image of the patch after co-adding, clipping and de-striping in Fourier space. Red, green and blue correspond to J, H, K_s bands. The structure in the image is identified with near-IR CIB from galaxies fainter than $K_s \simeq 19$.

zodiacal foreground is brightest. Total fluxes from the observed galaxy population are also shown for comparison; they are discussed at length in Sec. 6.

Displaying measurements of CIB fluctuations is more complicated because of the extra spatial dependence and some of their measurements will be discussed for each wavelength range separately. Figure 10 shows the amplitude of CIB anisotropies at $\sim 0.5^\circ$ from the DIRBE data analysis of Kashlinsky & Odenwald (2000) and Fig. 11 shows the results for CIB fluctuations from the deep 2MASS data analysis described in Sec. 5.5.

Below we itemize the status of CIB measurements in three IR wavelength ranges: NIR, MIR and FIR.

5.6.1. Near-IR

In the near-IR there are detections of the mean isotropic part of the CIB based on analysis of DIRBE and IRTS data (Dwek & Arendt 2000; Matsumoto et al 2000, 2003, Gorjian et al 2000, Wright & Reese 2000, Cambresy et al 2001). The measurements agree with each other, although the methods of analysis and foreground removal differ substantially. They also agree with the measured amplitude of CIB fluctuations. The results seem to indicate fluxes significantly in excess of those from observed galaxy populations. Total fluxes from galaxies are shown with filled circles in Fig. 9; in near-IR they saturate and are a factor is $\sim 2 - 3$ below the detected CIB.

Detections of CIB fluctuations come from three independent experiments and are consistent with each other. At 0.5° Kashlinsky & Odenwald (2000) find a statistically significant CIB anisotropy in the DIRBE first 4 channels. Matsumoto et al (2000, 2003) measured a spectrum of CIB anisotropies on degree scales from IRTS data band-averaged to $\sim 2 \mu\text{m}$; their results are

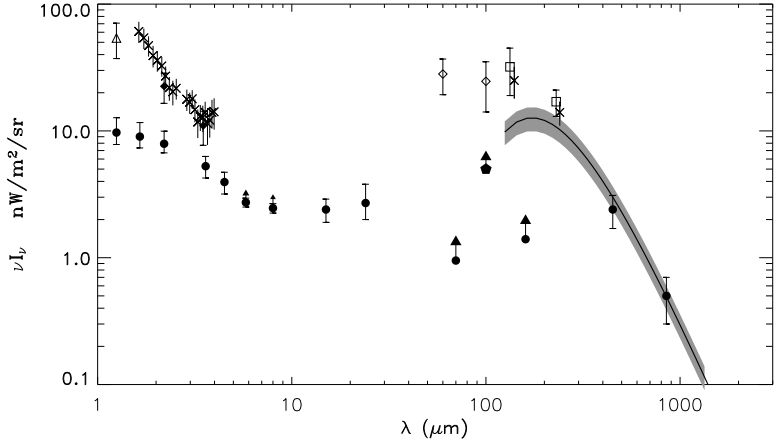


Fig. 9.— **NIR**: Mean levels of the near-IR CIB from the IRTS (crosses) from (Matsumoto et al 2000) and open symbols from COBE/DIRBE data. Open triangle shows the CIB results of the DIRBE J-band analysis ($1.65 \mu\text{m}$) from (Cambresy et al 2001) and filled diamonds at $2.2 \mu\text{m}$ from (Gorjian et al 2001), at $3.5 \mu\text{m}$ from (Dwek & Arendt 1998). **FIR**: Thick solid line with shade showing the results from COBE FIRAS data analysis from Puget et al (1996) and Fixsen et al (1998). DIRBE data detection at 140 and $240 \mu\text{m}$ is shown with crosses from Hauser et al (1998) and open squares from Schlegel et al (1998). Filled pentagon shows the lower limit on the CIB from the DIRBE data at $100 \mu\text{m}$ from Dwek et al (1998). Open diamonds correspond to results of DIRBE analysis by Finkbeiner et al (2000). Different results at the same wavelength are slightly shifted for clearer display. **Cumulative fluxes from observed deep galaxy counts** are shown with the filled circles from Table 5. The cases where the flux from progressively fainter galaxies does not saturate or the saturation is not as clear are marked with an upward arrow.

consistent with Kashlinsky & Odenwald (2000). Because the beam was large in both instruments, no galaxy removal was possible in the data and the CIB anisotropies arise from *all* galaxies, i.e. from $z = 0$ to the earliest times. Based on the amplitude of the present-day galaxy clustering, the NIR detections exceed the expectations from galaxies evolving with no or little evolution by a factor of $\sim 2 - 3$ and are consistent with the measured (high) mean CIB levels in the NIR.

Figure 11 summarizes the 2MASS-based results and compares them with the other measurements. Analysis of deep 2MASS data (Kashlinsky et al 2002, Odenwald et al 2003) has allowed to remove galaxies out to $K \simeq (18.5 - 19)$ and measure the spectrum of CIB anisotropies in J, H, and K 2MASS bands on sub-arcminute angular scales. These galaxies are typically located at cosmological times when the Universe was less than \sim half its present age and when extrapolated to the present-day the 2MASS based results are consistent with the DIRBE- and IRTS-based measurements. This indicates that the near-IR CIB excess, if real, must originate at still earlier times.

All NIR CIB results are mutually consistent, exceed the simple extrapolations from the observed galaxy populations with little evolution and, if true, probably imply significant energy-release activity at early cosmic times.

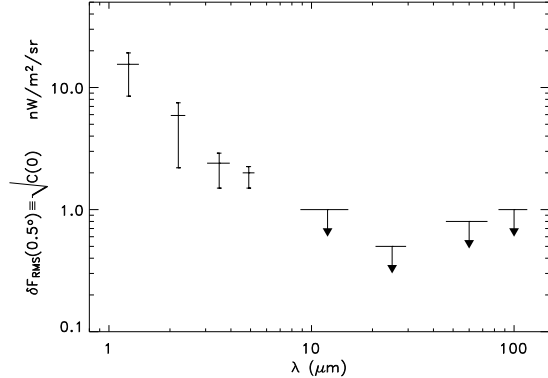


Fig. 10.— Detections of and upper limits on the RMS CIB fluctuation at 0.5° from the DIRBE data analysis by Kashlinsky & Odenwald (2000).

5.6.2. Mid-IR

Because the zodiacal light is so bright at these wavelengths there is no direct detection of the CIB between ~ 10 and ~ 50 μm . There are low upper limits though. Some come from the fluctuations analysis of the DIRBE data by Kashlinsky, Mather & Odenwald and use the fact that zodiacal light, while very bright, is also very smooth. Whereas light emitted by galaxies must be clustered with amplitude of about $\sim 10\%$ in flux fluctuations on the DIRBE beam scale. This leads to upper limits of about ~ 10 $\text{nW m}^{-2} \text{sr}^{-1}$ at these wavelengths.

Other upper limits come from scattering of γ -ray and CIB photons producing electron positron pairs if $E_\gamma E_{\text{CIB}} \geq 2(m_ec^2)^2$. For γ -rays the cross-section is peaked in the IR wavelength range, $\lambda_{\text{peak}} \simeq 2.5 \frac{E_\gamma}{1\text{TeV}} \mu\text{m}$ (Stecker et al 1992). If a drop in the spectrum of an extragalactic γ -ray source in TeV range can be observed this should lead to limits on the CIB in the corresponding wavelength range (Stecker & de Jager 1993). Dwek & Slavin (1994) applied this analysis to the γ -ray spectrum of Mrk 421. The best *upper* limits come from analysis of the 1997 γ -ray outburst of the blazar Mrk 501 and are $\simeq 5$ $\text{nW m}^{-2} \text{sr}^{-1}$ from 5 to 15 μm (Stanov & Franceschini 1998, Renault et al 2001).

The ISO and Spitzer deep counts provide important *lower* limits on the CIB at these wavelengths which are very close to the upper limits from γ -ray and fluctuations analyses. It would be thus very surprising if the MIR CIB is not inside this $2.5 \text{ nW m}^{-2} \text{sr}^{-1} \lesssim \nu I_\nu \lesssim 5 \text{ nW m}^{-2} \text{sr}^{-1}$ range.

5.6.3. Far-IR

Far-IR CIB measurements come from the COBE FIRAS (Puget et al 1996, Fixsen et al 1998) and COBE DIRBE (Schlegel et al 1998, Hauser et al 1998, Finkbeiner et al 2000) data analysis. They are broadly consistent although the COBE DIRBE detections at 140 and 240 μm give larger fluxes (at almost 2σ level) and the Finkbeiner et al (2000) analysis gives an even bigger

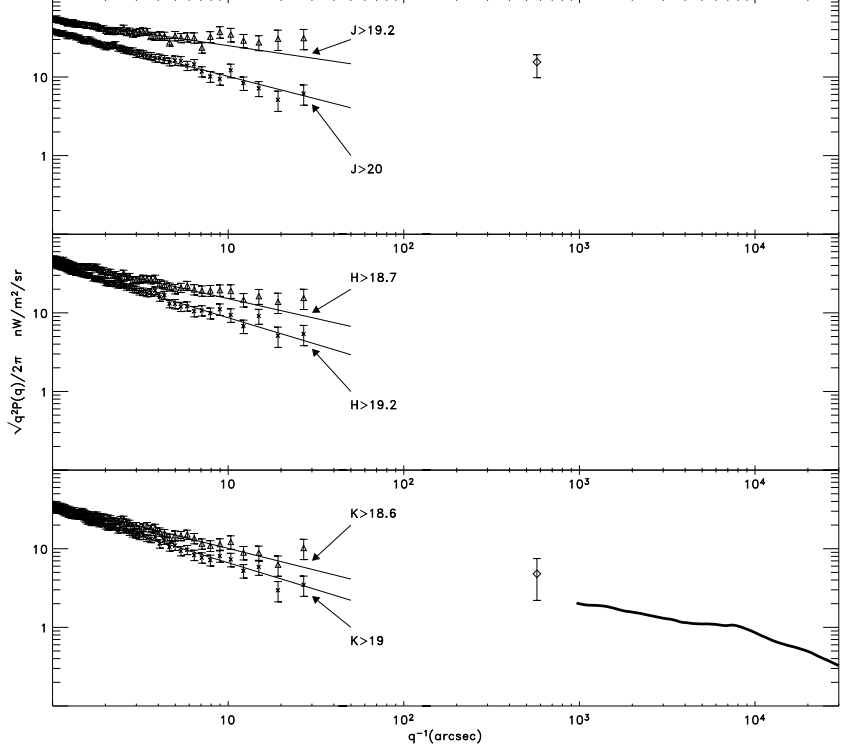


Fig. 11.— The angular spectrum of the CIB fluctuations from the 2MASS analysis by Kashlinsky, Odenwald et al (2002) and Odenwald, Kashlinsky et al (2003) at J, H and K bands. Triangles correspond to the results from the patch from which galaxies out to $K_S \lesssim 18.6$ have been removed and crosses to another $512'' \times 512''$ patches with galaxies removed out to $K_S \lesssim 19$. Open diamonds with 92% errors show the fluctuation on larger angular scale from Kashlinsky & Odenwald (2000) analysis of COBE DIRBE data. Thick solid line shows the CIB result from IRTS analysis (Matsumoto et al 2000, 2003). Both the DIRBE and IRTS analyses included all galaxies and are consistent with each other and the 2MASS data when account is made of the contribution from the removed (brighter) galaxies (Odenwald, Kashlinsky et al 2003).

discrepancy at $60 \mu\text{m}$ if the COBE FIRAS results are simply extrapolated to that wavelength. Hauser et al (1998) discuss these differences and point that the differences are probably due to different instrumental calibrations.

Fixsen et al (1998) suggest a simple fit to the CIB at $\lambda \gtrsim 100 \mu\text{m}$:

$$I_\nu = A \left(\frac{\nu}{\nu_0} \right)^\beta B_\nu(T) \quad (24)$$

where $A = (1.3 \pm 0.4) \times 10^{-5}$, $\beta = 0.64 \pm 0.12$, $T = 18.5 \pm 1.2 \text{ K}$, $\nu_0 = 100\text{cm}^{-1} = 3000 \text{ GHz}$ and B_ν is the Planck function. In eq. 24 the uncertainties are highly correlated with correlations +0.98 for A and β , -0.99 for A, T and -0.95 for β, T (Fixsen et al 1998).

The bulk (likely all) of the CIB at these wavelengths comes from dust in high- z and present-day galaxies and the SCUBA galaxy counts at $850 \mu\text{m}$ (Smail et al 1997) compare favorably with eq. 24.

5.6.4. Bolometric CIB flux

Table 4 shows the integrated IR fluxes over the three ranges of wavelengths where direct CIB measurements were possible to meaningfully integrate (hence, e.g. the gap between 4 and 10 μm). In the NIR out of 37 $\text{nWm}^{-2}\text{sr}^{-1}$ approximately 13 $\text{nWm}^{-2}\text{sr}^{-1}$ is contributed by the Cambresy et al (2001) measurement at the DIRBE’s J band; the remaining come from the IRTS data and other measurements out to $\simeq 4 \mu\text{m}$. In order to evaluate the contribution in the MIR region we assumed an upper limit between ~ 10 and 50 μm of $\nu I_\nu \lesssim 5\text{nWm}^{-2}\text{sr}^{-1}$ from the γ -ray absorption. (An upper limit from fluctuations analysis would be a little higher). In the far-IR we integrated the approximation eq. 24; including the other DIRBE detections will increase this number.

The table shows that CIB carries very substantial fluxes testifying to significant energy release throughout the evolution of the Universe. For comparison the total flux from the CMB is only \sim one order of magnitude higher. Table 5 and discussion in Section 6 show that normal stellar populations observed in deep galaxy counts surveys contribute about as much CIB flux in the near-IR as the total far-IR CIB in Table 4, meaning that approximately half the energy produced by stars has been absorbed and re-emitted in the far-IR by dust in (high- z) galaxies. The observed NIR galaxies in J,H,K bands contribute only $\simeq 5\text{nWm}^{-2}\text{sr}^{-1}$. The total fluxes from the deepest counts in Spitzer data are also shown although at 5.8 and 8 μm does not saturate as clearly as at 3.6 and 4.8 μm . If one integrates the flux from galaxies in J, H, K bands and the Spitzer 3.6 μm one gets 8.6 $\text{nWm}^{-2}\text{sr}^{-1}$. Extending the range of integration to the other Spitzer IRAC channel at 4.5 μm where the total flux from galaxies saturates (see Sec. 6) gives 9.7 $\text{nWm}^{-2}\text{sr}^{-1}$ and integrating over galaxies from 2MASS and all Spitzer IRAC channels gives total flux of $\simeq 11.4 \text{nWm}^{-2}\text{sr}^{-1}$ between 1 and 10 μm . The observed galaxy populations contribute only a small fraction of the observed flux.

This means a substantial excess of the total CIB measurements over that observed to come from total galaxies. It then appears likely that either 1) the total contributions from ordinary galaxies are significantly underestimated, or 2) the bulk of the CIB comes from still earlier epochs than probed by the systems accessible to current telescopic studies, e.g. from the Population III era, or 3) all the the NIR measurements contain systematic errors mistaken for CIB. The first of these possibilities is discussed in Sec. 6 and shown not very likely, the second is discussed in Sec. 7 and the third possibility should always be borne in mind when interpreting the very difficult measurements of the CIB.

Historically the excess CIB flux in the near-IR has been nearly simultaneously and independently detected for the isotropic part of the CIB by Dwek & Arendt (1998) and for fluctuations by

Table 4. Bolometric/integrated CIB flux ($\text{nWm}^{-2}\text{sr}^{-1}$)

NIR: $1 \mu\text{m} \lesssim \lambda \lesssim 4 \mu\text{m}$	MIR: $10 \mu\text{m} \lesssim \lambda \lesssim 50 \mu\text{m}$	FIR: $120 \mu\text{m} \lesssim \lambda \lesssim 1,000 \mu\text{m}$	Total: $1 \mu\text{m} \lesssim \lambda \lesssim 1 \text{ mm}$
37	$\lesssim 8$	13	$50 \lesssim F_{\text{total}} \lesssim 58$

Kashlinsky & Odenwald (2000). ⁴

6. 'Ordinary' contributors to CIB

In this review we use the term “ordinary” galaxy populations to refer to galaxies made of the observed normal *metal-enriched* stellar populations containing Population I and II stars and the dust produced by them. Observations from the Hubble Deep (and Ultra Deep) Field suggest that metal enrichment has happened fairly early on in the history of the Universe. Similarly, data on quasar emission and intrinsic absorption lines indicate that solar metallicities in the surrounding medium have already been reached at $z \gtrsim 4$ (Hammann & Ferland 1999). This is also suggested by the existence of the oldest Population II stars with non-zero metal abundances. Star formation processes in the metal enriched medium (metallicity $Z \gtrsim 10^{-3} - 10^{-2} Z_{\odot}$) should lead to formation of populations with stellar properties not radically different from those observed today. These populations must have been preceded by completely metal-free (first) stars, the so-called Population III that formed at very high redshifts, $z \gtrsim 10$. Population III stars likely form a completely different class of stellar objects, probably have a very different range of masses and also form in a different environment. Their case is special, necessarily more speculative, and their possible contribution to the CIB is discussed in the following section.

Before we proceed a simple “back-of-the-envelope” evaluation is in order for the amount of the near-IR CIB produced by ‘ordinary’ stellar populations. If such stars had Salpeter-type IMF most of the light would be produced by the high mass end of the stellar mass spectrum, i.e. by stars that produced the metal abundances ($Z \sim Z_{\odot}$) observed today. If galaxies whose stellar contents contribute $\Omega_* \simeq 3 \times 10^{-3} h^{-1}$ to the critical density (ρ_{cr}), then during their main sequence the stars would have produced energy density of $\epsilon \Omega_* \rho_{\text{cr}} c^2$, where ϵ is the radiative efficiency. For hydrogen burning $\epsilon = 0.007$ and this efficiency is reached for massive stars, $M \gtrsim 10 M_{\odot}$. For present-day stellar populations with a Salpeter IMF and a lower cutoff of $0.1 M_{\odot}$, the effective efficiency is only $\epsilon \simeq 0.001$ (Franceschini et al 2001) ⁵. A fraction $f(\lambda \geq \frac{1}{1+z} \mu\text{m})$ of the emitted energy will contribute to the near-IR CIB at wavelengths longer than $1 \mu\text{m}$, assuming it was not absorbed or re-processed. This would lead to the CIB flux of:

$$\nu I_{\nu} \sim \frac{c}{4\pi} \epsilon Z \Omega_* \rho_{\text{cr}} c^2 \left\langle \frac{f(\lambda \geq \frac{1}{1+z} \mu\text{m})}{1+z} \right\rangle = 8h \frac{Z}{10^{-2}} \frac{\epsilon}{0.007} \frac{\Omega_*}{3 \times 10^{-3} h^{-1}} \left\langle \frac{f(\lambda \geq \frac{1}{1+z} \mu\text{m})}{1+z} \right\rangle \frac{\text{nW}}{\text{m}^2 \text{sr}} \quad (25)$$

⁴The paper by Kashlinsky & Odenwald (2000) has been received by the Ap.J on April 30, 1998, but due to an editorial mishandling the manuscript was not sent to an independent referee for review until over a year later, in May 1999.

⁵Solar mass stars burn a core of about $\sim 10 - 15\%$ of their hydrogen mass during main-sequence stage. During their red giant stage the hydrogen burning core is $\simeq 0.5 M_{\odot}$ for $M \lesssim 2.5 M_{\odot}$ (Sweigart, Greggio & Renzini 1990). For the IMFs where the bulk of stellar mass is locked in the low end of the stellar mass-spectrum this results in effective ϵ considerably smaller than the canonical value of 0.007 (Sweigart, private communication)

The stars responsible for producing metals are predominantly hot stars with surface temperature $T_* \gtrsim (1 - 2) \times 10^4$ K. In this case $f(\lambda \geq \frac{1}{1+z}\mu\text{m})$ the CIB flux comes from the Rayleigh-Jeans part of the spectrum, where $f \propto T_*^{-3}(1+z)^3$ and the redshift-dependent term on the right-hand-side of eq. 25 increases toward high z because a larger part of the emitted spectrum is shifted into the IR today. With $T_* \simeq 10^4$ K and $z \sim 2 - 3$ one gets contribution to the CIB around a few $\text{nWm}^{-2}\text{sr}^{-1}$, but if there were very hot (massive) stars at very early times, their contribution may well exceed that of the 'normal' stellar populations.

Silk (1996) makes a similar argument to eq. 25 differentiating between the metals (iron) produced in early and late type galaxies and their respective mass-to-light ratios, and Hauser & Dwek (2001) normalize instead to helium production; both get similar numbers. Helium is produced by less massive (and longer living) stars, and they could produce an amount of CIB comparable to (or less) than eq. 25.

Comparison with the near-IR levels of CIB implies that, if the measurements are true, it is difficult to explain these high levels by left-over emissions from galaxy populations with IMF similar to that of today. The levels of the near-IR CIB can be increased in one (or all) of the following ways over eq. 25: 1) If there exists a population of stars that can emit significant amounts of light without producing metals (as happens e.g. in stars more massive than $\simeq 240M_\odot$, Heger 2003), one can have extensive period of energy production that would not violate the observed metallicities. 2) If emission comes from populations that contribute a larger fraction of $\Omega_{\text{baryon}} \simeq 0.044$ than the stellar populations of today which have $\Omega_* \ll \Omega_{\text{baryon}}$. Interestingly, most of the baryons today are in dark form (Fukugita, Hogan & Peebles 1998), the dark baryons possibly being in remnants of the Population III era. 3) And if there existed at high z a population of very hot stars, the bulk of their emission will today be shifted into the NIR bands. We discuss such possibility in the context of Population III stars contribution in the following section.

The remainder of this section discusses the various aspects necessary for estimating the contributions from ordinary (metal-rich) stellar populations in galaxies to the CIB from NIR to FIR.

6.1. IMF and star formation history

SFR indicators include UV and emission-line luminosities indicative of light from short-lived massive stars. Conversion to SFR depends on the assumed IMF, but once the IMF assumption is made, the relative SFR is less sensitive to IMF. The conversion of the UV luminosities into the SFR must also correct for the absorption of UV photons by dust which is generally associated with the same young stars.

In the first calculation of the stellar IMF, Salpeter (1953) approximated the Solar neighborhood measurements with IMF having a power law of slope -1.35 and it still is commonly used in modeling synthetic stellar populations. Scalo (1986), from measurements of the Solar neighborhood, gives an IMF with a mass fraction peak at $\simeq 0.5 - 1M_\odot$. While very useful and necessary in constructing

synthetic stellar population models, it is not clear whether the assumption of the *universal* IMF is valid in the real Universe. E.g. it cannot reproduce H α luminosities (Kennicutt et al 1994) or match mean galaxy colors (Madau et al 1998) because it has too few stars of $M \gtrsim 10M_\odot$.

In galaxies with on-going star formation, the composite UV spectrum is approximately flat. If this is combined with the Salpeter IMF between 0.1 and 100 M_\odot in stellar mass, one can relate the rest frame UV luminosity to SFR (Madau et al 1998) for galaxies with continuous star formation on timescales longer than $\gtrsim 0.1$ Gyr:

$$\text{SFR}(M_\odot/\text{yr}) = 1.4 \times 10^{-28} L_\nu(\text{erg/sec/Hz}) \quad (26)$$

Because in starburst galaxies a significant fraction of luminosity, which is dominated by young stars, is absorbed and re-emitted in the infrared by dust, the IR luminosity can also be used as tracer of SFR. Assuming that the bolometric luminosity is dominated by young stars, Kennicutt (1998) obtained in the optically thick limit (when IR luminosity measures the total bolometric luminosity) for continuous star bursts lasting at least 10 Myr, solar metal abundance and a Salpeter IMF:

$$\text{SFR}(M_\odot/\text{yr}) = 1.71 \times 10^{-10} L_{\text{IR}}(8 - 1000\mu\text{m})(L_{\odot,\text{bol}}) \quad (27)$$

so luminous IR galaxies with $L_{\text{IR}} > 10^{11} L_\odot$ form more than $20 M_\odot/\text{yr}$ in stars. Note that these calibrations depend on the IMF in star forming galaxies, since the integrated UV spectrum is dominated by massive stars and is assumed to lead to dust (re)emission in the mid- to far-IR.

Lilly et al (1996) used galaxies from the Canada-France Redshift Survey (CFRS) to construct the comoving luminosity, $\mathcal{L}_\nu(z)$, of the Universe out to $z \simeq 1$ at rest-frame wavelengths of 0.28, 0.44 and 1 μm . The sample included 730 I-band selected galaxies, with luminosities extrapolated to the above rest wavelengths using interpolations from the *BVIK* photometry with SEDs interpolated from synthetic spectra designed to match the observed colors. The present-day I-band corresponds to the blue-band for rest frame emission at $z \sim 1$. They found observational evidence for an increase of $\mathcal{L}_\nu(z)$ out to $z \simeq 1$ in the galaxy rest-frame UV to near-IR (1 μm) bands and argued that the data requires $\text{SFR} \propto (\Delta t)^{-2.5}$ where Δt is the time elapsed since the initial star formation.

With the Lyman-dropout technique (Steidel et al 1996), galaxies are now found to progressively higher redshifts (Giavalisco 2002). Flux amplification by gravitational lensing by known clusters of galaxies can lead to galaxy detections at even higher redshifts as amplifications of order $\sim 10 - 100$ can be achieved for distant galaxies lying on caustics of the cluster potential. Kneib et al (2004) measured optical and IR photometry of one such candidate galaxy at $z \sim 7$ and find that, while only $\lesssim 1$ Kpc in extent, it undergoes star formation at the rate of $\simeq 2.6 M_\odot/\text{yr}$. A claim was made recently of a galaxy at $z \simeq 10$ among the objects lensed by a known cluster A1835 (Pello et al 2004, but see Bremer et al 2004). Bouwens et al (2004) have applied the z_{850} dropout search to the Hubble Ultra Deep Field (UDF) data and detected four (and possibly five) potential $z \sim 7 - 8$ objects that are seen in J and H bands, but have no detection shortward of 8,500 Å (one of the candidates has a weak signal at 8,500 Å). The objects are strongly clustered covering a total area of 1 arcmin² and also appear very blue in their rest frame. Using VLA observations of the molecular

gas in the underlying galaxy of the current record-holder $z = 6.4$ quasar, Walter et al (2004) detect $\sim 5 \times 10^9 M_\odot$ in molecular gas extended to ~ 2.5 Kpc. The amount of gas is comparable to what is found in the nearby ULIRGs and its brightness temperature is about that of the nearby starburst centers. Clearly stars must have formed early on in the Universe’s history and at vigorous rates.

Madau et al (1996) have analyzed the Hubble Deep Field (HDF) observations reaching AB magnitudes $\gtrsim 28$ in four bands from 3000 Å to 8140 Å. They modeled the HI opacity and used stellar population synthesis models to separate low- and high- z galaxies using the Lyman continuum drop-out method (Steidel et al 1996). From the images they constructed a sample of star-forming galaxies from which the comoving UV luminosity density was estimated out to $z \sim 4$. Assuming that the UV luminosities give a complete view of star formation, the SFR density can be evaluated from the conversion factors for the Salpeter IMF (Madau et al 1998). The derived SFR, known as the Madau curve, was found to rise rapidly toward early times possibly peaking at $z \sim 2$. Estimating the comoving UV luminosity density from the high redshift galaxies found in the UDF data (Bouwens et al 2004) suggests a factor of $\gtrsim 3.5$ drop in SFR from $z = 3.8$ to $z \sim 7.5$ consistent with what is found at $z \sim 6$ (Dickinson et al 2004, Stanway et al 2004).

Guiderdoni et al (1997) argued that most galaxies are hidden by dust which leads to substantial underestimating of the high redshift SFR deduced from optical surveys. They constructed models of several galaxy populations to separately match the optical surveys’ data and the far-IR CIB deduced from the COBE/FIRAS data. The galaxy population responsible for the FIR CIB has a high SFR at early times, information on which will be missing from SFR deduced from optical bands. Indeed, if most of energy is (re)emitted at IR wavelengths, the SFR may be underestimated when deduced from surveys in the UV bands.

Rowan-Robinson et al (1997) analyzed ISOCAM observations of the HDF at 6.7 and 15 μm (Serjeant et al 1997), where thirteen HDF galaxies have been detected by ISO in the 12.5 hour exposure. In eleven of these, there was a substantial mid-IR emission excess, which they interpreted as dust emission from a strong star-burst. The SEDs were modeled from 0.3 to 15 μm using the available photometry from visible to NIR bands and the Bruzual-Charlot stellar evolution models with a Rayleigh-Jeans fall-off beyond 2.5 μm , and the conversion to SFR was done using starburst modeling with emission from dust and PAHs. If these star-forming galaxies are typical of the fainter HDF galaxies, then Rowan-Robinson et al argued that the true SFR remains flat at $z \gtrsim 1.5$ instead of falling off.

6.2. Normal stellar populations

Normal stellar populations are defined as those with Population I and II metallicities and the (locally) observed IMF, usually taken to be either of Salpeter or Scalo type.

Constructing realistic SEDs of galaxies is important for proper comparison of contributions of galaxies of various types, from various redshifts and at various wavelengths to the observed CIB.

In the near-IR such SEDs can be approximated with the spectrum and its evolution derived from synthetic stellar population models. This approach requires input of a universal IMF, assumptions about the rate of star formation, self-consistent treatment of stellar evolution, metal enrichment etc. The early studies have been pioneered by Tinsley (1976) with Bruzual (1983) developing the state-of-the art models that can be compared with detailed observations. The current versions of the synthetic stellar models e.g. by Bruzual-Charlot (1993) or PEGASE (Fioc & Rocca-Volmerange 1997) codes are available on the world-wide-web. The modeling has to be done carefully and many priors are required, since the SEDs in turn depend on many parameters: IMF, metallicities, galaxy ages, dependence of each of them on other, galaxy luminosity, SFR, etc. Still, such modeling gives a fair representation of reality and can certainly provide approximate answers.

For the purpose of calculations in this section we used the PEGASE⁶ code to construct SEDs of Early and Late type galaxy stellar populations as follows: Early type galaxy stellar populations were assumed to be all described by Salpeter IMF and form at some early time in a single short burst of star formation lasting 0.5 Gyr. Late type stellar populations in galaxies were assumed to form via an on-going star formation with Scalo IMF starting at some early epoch. The PEGASE models were run for a grid of galaxy ages and metallicities. The left panel in Fig. 12 shows the SED for the two types of populations for ages between 10 and 14 Gyr and metallicities $Z = 0, 10^{-3}, 2 \times 10^{-3}, 5 \times 10^{-3}, 10^{-2}$. The symbols show the value of the relative flux when averaged over SDSS and 2MASS filters to compare with data discussed below. (Plus signs correspond to early types and diamonds to late types.) The NIR luminosities are dominated by red giants in the old stellar populations and are directly related to the total stellar mass.

The right panel in Fig. 12 shows how the mass-to-light ratio varies with time for such populations. Basically the differences in the spectra reflect the ratio of young ($\lesssim 1$ Gyr) to old stars (Kennicutt 1998).

Shaded regions show the approximate range of the mass-to-light ratios of the two populations (e.g. Fukugita, Hogan & Peebles 1998) plotted for $t_{\text{cosm}} \leq 14$ Gyr, the age implied by - *inter alia* - WMAP measurements. They agree reasonably well with the plots especially if early populations are older than a few Gyrs, although there may not be one 'magical' value to plot for each of the galaxies (Faber & Gallagher 1979, Roberts & Haynes 1994).

In order to compare with CIB measurements, the synthetic SEDs must be averaged over the entire ensemble of galaxy populations. This includes averaging over all morphological types and, within each type, averaging over the luminosity function. The first is important because early-type galaxies contribute substantially to the near-IR EBL (Jimenez & Kashlinsky 1999). The second step is also important because, at least for early-type galaxies, the mass-to-light depends on galaxy mass or luminosity as suggested by the fundamental plane measurements for elliptical galaxies (Faber et al 1989, Djorgovski & Davis 1987). In the visible, the fundamental plane implies

⁶<http://www2.iap.fr/users/fioc/PEGASE.html>

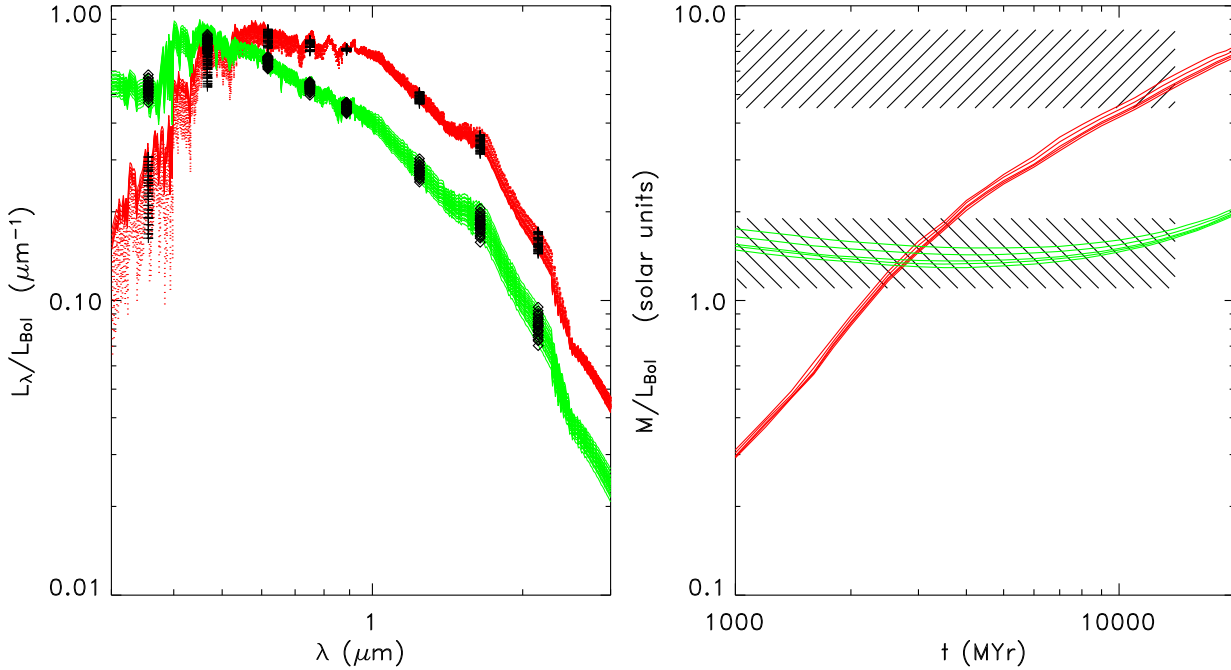


Fig. 12.— Runs of synthetic galaxy SED spectra using PEGASE. Green lines correspond to late types, red lines to early types stellar populations. **Left:** black symbols correspond to the SEDs integrated over the SDSS and 2MASS filters. The sets of lines are shown for five metallicities of $Z = 0, 0.001, 0.002, 0.005, 0.01$ and five ages between 10 and 14 Gyr. **Right:** Mass-to-(bolometric) light ratios in solar units for early and late stellar populations are plotted vs their age for $Z = 0, 0.001, 0.002, 0.005, 0.01$. Cross-shaded areas correspond to typical mass-to-light ratios observed locally at $z = 0$ in the early (top cross-shaded area) and late populations with uncertainties from Fukugita, Hogan & Peebles (1999); the observed variations in the mass-to-light ratios are larger.

$M/L_B \propto L_B^{\kappa_B}$ with $\kappa_B \simeq 0.25$. The slope varies systematically with wavelength from $0.35 \mu\text{m}$ through the K band (Pahre et al 1998). Also, measurements of cluster galaxies out to $z \sim 1$, or $\sim \frac{1}{2}$ look-back time, indicate that the fundamental plane preserves its logarithmic slope while the amplitude changes (Treu et al 2002, van Dokkum et al 2001, 2004, van der Wel et al 2004). The origin of this wavelength trend may lie in various quantities, like systematic variations in the IMF along the luminosity sequence (Pahre et al 1998), or with metallicity (Jimenez & Kashlinsky 1999).

6.3. Dust emission from galaxies: mid-IR to sub-mm

The near-IR CIB data provide information on the brightness and structure of largely unextincted starlight. The mid- and far-IR observations are necessary to complete the picture, by providing the corresponding information for starlight that has been absorbed by dust and thermally re-radiated. In many environments, even at early epochs, this re-radiated emission is a substantial or even dominant fraction of the total luminosity associated with star formation.

There are excellent reviews on the subject of IRAS galaxies (Soifer, Neugebauer & Houck

1987b), ultra luminous infrared galaxies (ULIRGs, Sanders & Mirabel 1996) and sub-mm SCUBA galaxies (Blain et al 2002) and the reader is referred to them for more details. This subsection summarizes the established properties of these sources as they relate to the CIB.

The range of galaxy luminosities in the mid- to far-IR greatly exceeds that in the UV, optical and NIR. E.g the mid- to far-IR luminosities of IRAS galaxies vary from below a few times 10^{39} erg/sec to over 5×10^{46} erg/sec. Many of the more luminous IRAS galaxies are starbursts. The bulk of the IRAS detected galaxies are late-type spirals, with only a handful belonging to the early (E or S0) type. The shape and slope luminosity function of IRAS galaxies differs from that of the visible band galaxies and is best approximated as two different power-laws at the high and low ends of the galaxy flux distribution (Soifer & Neugebauer 1991). At the bright end of the bolometric luminosity function, the bright mid- to FIR galaxies become the dominant galaxy population in the present-day Universe. The ratio of the FIR to visible galaxy luminosity correlates with 60 to 100 μm color temperature for most galaxies (Soifer et al 1987a,b). Soifer et al (1987), using the Draine & Lee (1984) dust modeling, give a useful approximation for the amount of dust needed to produce a given FIR luminosity:

$$L_{\text{FIR}} = 10^4 \frac{M_{\text{dust}}}{M_{\odot}} \left(\frac{T_{\text{dust}}}{40\text{K}} \right)^5 L_{\odot} \quad (28)$$

This shows that even a tiny amount of dust can make the galaxy very bright in the mid- to far-IR. Zubko, Dwek & Arendt (2004) have developed sophisticated ISM dust models by fitting simultaneously the far-UV to NIR extinctions, the diffuse IR emission and constraining the dust properties from the observed elemental abundances. Assuming that the dust mass-absorption coefficient $\kappa(\lambda) \propto \lambda^{-n_{\text{dust}}}$, the specific flux at wavelength λ received from a galaxy containing M_{dust} a distance d away is given by (Dwek 2004):

$$I_{\nu}(\lambda) = 8 \times 10^3 \frac{M_{\text{dust}}}{M_{\odot}} \left(\frac{d}{1 \text{Mpc}} \right)^{-2} \frac{\kappa(\lambda_0)}{\text{cm}^2 \text{g}^{-1}} \left(\frac{\lambda_0}{\lambda} \right)^{n_{\text{dust}}} \left(\frac{\lambda}{1\mu\text{m}} \right)^{-3} \left[\exp \left(\frac{14387.7}{(\lambda/1\mu\text{m})T_{\text{dust}}} \right) - 1 \right]^{-1} \text{Jy} \quad (29)$$

where λ_0 is some reference wavelength and $n_{\text{dust}} \sim 1$ to 2.

Most IR emitting galaxies can be classified as normal spirals, starbursts or AGNs. Starburst galaxies are especially bright at mid- to far-IR wavelengths and approximately half the galaxies brighter than $L_{\text{FIR}} \simeq 3 \times 10^{10} L_{\odot}$ have star-burst optical spectra (Elston et al 1985). For the ULIRGs their measured star formation rate cannot be maintained for longer than (at most) a Gyr, as at that rate all their ISM will be consumed. The most luminous IRAS galaxies show features of both being a starburst and an AGN. In the less luminous IRAS galaxies their MIR/FIR emission seems to be unrelated to their current SFR. For most IRAS galaxies that are not AGNs, the observed color-color correlations can be accounted by a two-component dust model, where warmer dust is associated with regions of active star formation and the cold component comes from cirrus in the galactic disk (Helou 1986).

One can reconstruct the SED of a typical galaxy in the MIR to FIR range of wavelengths.

Fig. 13 shows such synthetic template: it was constructed accounting for continuum dust emission assuming $T_{\text{dust}} = 35$ K and the free-free emission at long wavelengths. FIR emission lines were scaled proportional to the flux and adopted from: the Galactic IR lines observed by FIRAS (Wright et al 1991), the PAH broad line features at $\lambda \lesssim 12 \mu\text{m}$ were taken from the Dwek et al (1997) Galaxy model of the DIRBE data, and the lines from the ISO Long Wavelength Spectrometer observations of nearby bright IR galaxies by Fischer et al (1999). This SED is in good agreement with the IRAS galaxies average used by Dwek et al (1998), the model of Guiderdoni et al (1998) and with the template of sub-mm emission from Blain et al (2002), where comparison is given with the data from galaxy observations.

The right panel in Fig. 13 plots the K-correction due to this SED (defined as $K_{\text{cor}} \equiv -2.5 \lg[I_{\nu(1+z)}(10\text{pc})/I_{\nu}(10\text{pc})]$) for 100 μm (solid line), 250 μm (dots), 500 μm (dashes), 1000 μm (dashed dotted line) and 2000 μm (dash-dot-dot). One can see the strongly negative K-correction at $\lambda \gtrsim 500 \mu\text{m}$ and high z : galaxy flux should decrease much slower with increasing redshift and it can actually increase with z . This further implies that at sub-mm wavelengths the contribution to the CIB should be more heavily weighted toward high redshift sources.

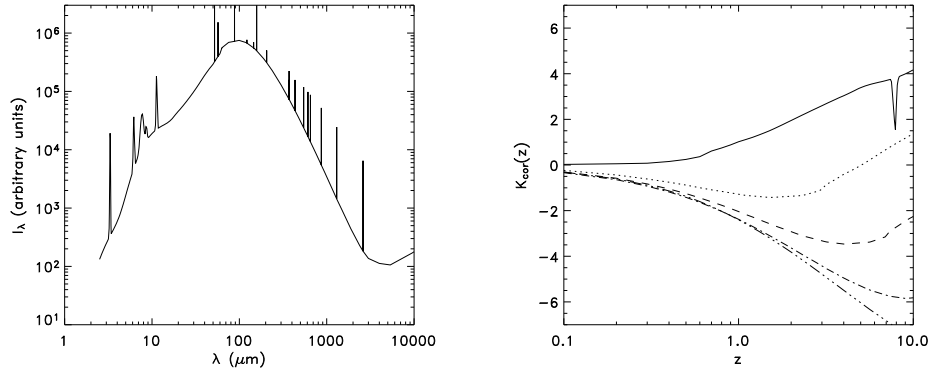


Fig. 13.— **Left:** Typical synthetic sub-mm SED of dusty galaxies including lines from PAHs and ions, atoms and molecules as observed by FIRAS and ISO.
Right: K-correction vs z at various wavelengths: 100 μm (solid line), 250 μm (dots), 500 μm (dashes), 1000 μm (dashed dotted line) and 2000 μm (dash-dot-dot)

Optical follow up of the IRAS catalog shows that on average about 30 % of the bolometric luminosity is emitted in the far-IR via thermal radiation from dust heated by stars (Soifer & Neugebauer 1991) and this number rises to up to 95% for ULIRGs (Sanders & Mirabel 1996). Guiderdoni et al (1997) argue that most galaxies are hidden by dust. The mid- and far-IR number counts indicate that the IR-luminous galaxies evolved more rapidly than their optical counterparts and make a substantial contribution to the star formation at higher z (Elbaz et al 1999). Locally, typical galaxies radiate a little more in the UV to optical bands than in mid-IR to far-IR (Soifer & Neugebauer 1991). But, while luminous IR galaxies contribute a negligible amount to the local rate of star formation, they are major contributors at high z .

Spinoglio et al (1995) assembled a sample of ~ 900 IRAS galaxies out to the $12 \mu\text{m}$ limit of ~ 0.2 Jy and find that the $12 \mu\text{m}$ luminosity is $\propto L_{\text{IR, total}}$ and suggest that their selection by the $L_{12\mu\text{m}}$ is approximately equivalent to that by the total (bolometric) luminosity. They find that the 60 and $25 \mu\text{m}$ luminosities rise more steeply than linear with the bolometric $L_{\text{IR, total}}$ and the opposite is true for optical bands implying that more luminous disk galaxies have more dust shrouded stars. Malkan and Stecker (1998) used these empirical correlations together with assumptions of luminosity evolution to reconstruct the CIB across from near- to far-IR.

Several mid-IR deep surveys have been conducted with ISOCAM, reaching sensitivity levels of $\sim 50 \mu\text{Jy}$ at $15 \mu\text{m}$ (Elbaz et al 1999). Gravitational lensing by known massive clusters was exploited by Metcalfe et al (2003) to go deeper reaching the flux limits of 5 and $18 \mu\text{Jy}$ at 7 and $15 \mu\text{m}$ with ISOCAM (Metcalfe et al 2003). Elbaz et al (2002) demonstrate that MIR luminosities at 6.75 , 12 and $15 \mu\text{m}$ are strongly correlated with the total IR luminosity (8 to $1000 \mu\text{m}$). They infer the redshift distribution of galaxies from the spectroscopically complete galaxy sample in the Hubble Deep Field (North) and find that the correlations hold out to $z \sim 1$. Chary & Elbaz (2001) show that a wide variety of evolutionary models normalized to these correlations and the observed luminosity functions are consistent with the current CIB measurements in the mid- to far-IR. At present about $15\text{--}20\%$ of the bolometric luminosity is emitted in mid- to far-IR, but it is likely that this fraction increases toward early times. Serjeant et al (2001) find good agreement for $90 \mu\text{m}$ galaxies with the local luminosity function from other surveys and evidence for pure luminosity evolution at the rate of $\mathcal{E} \propto (0.98 \pm 0.34) \lg(1+z)$.

The FIRBACK ISO survey (Puget et al 1999) was conducted with the ISOPHOT instrument at $175 \mu\text{m}$ and reached the confusion levels of 45 mJy . It provided a catalog of almost 200 galaxies (at 3-sigma level) down to fluxes $\simeq 180 \text{ mJy}$ (Dole et al 2001). The survey covered four square degrees in three high Galactic latitude regions. The final catalog of 106 sources (4-sigma) between 180 mJy and 2.4 Jy was $> 85\%$ complete. The observed galaxy counts at $170 \mu\text{m}$ require strong evolution at flux levels fainter than 500 mJy . Dole et al (2001) estimate that galaxies out to the flux limit of 135 mJy account for about 5% of the CIB. Analysis of the first Spitzer MIPS observations is consistent with the FIRBACK results (Dole et al 2004).

Significant progress in understanding the sources contributing to the far-IR CIB has been made with the discovery and subsequent studies of the sub-mm galaxies with the SCUBA instrument at the James Clerk Maxwell Telescope.⁷ SCUBA is an array of 37 bolometers at $850 \mu\text{m}$ and 91 at $450 \mu\text{m}$ and can observe at both wavelengths simultaneously with angular resolution of about $15''$; the shorter wavelength is more sensitive to atmospheric conditions. Several hundred SCUBA sources have by now been detected (Blain et al 2002) and they are mostly high- z galaxies. Redshifts of the galaxies have to be determined from optical observations. Because resolution of the SCUBA instrument is relatively low and the galaxies are at high z , and therefore faint in optical bands, redshift determination is difficult. Hughes et al (1998) identified optical starburst counterparts

⁷http://www.jach.hawaii.edu/JACpublic/JCMT/Continuum_observing/SCUBA/index.html

for the sample of five SCUBA sources brighter than 2 mJy, four of which have z between 4 and 5. Scott et al (2000) detected a sample of ten FIRBACK galaxies which are bright at 170 μm also at the SCUBA wavelengths with fluxes $\gtrsim 10$ mJy. Sawicki & Webb (2004) detect another ten 850 μm SCUBA sources brighter than ~ 10 mJy in the general area of the Spitzer First Look Survey. Chapman et al (2003) have obtained spectroscopic redshifts of ten representative sub-mm galaxies, using the VLA to identify the source positions and obtaining the redshifts with the optical spectroscopy from the Keck telescope. They derived a median redshift of 2.4 for the sample and the space densities of $(3.3 \pm 2.3) \times 10^{-6}$, $(6.5 \pm 2.5) \times 10^{-6}$, $(2.4 \pm 1.2) \times 10^{-6}$ Mpc^{-3} at redshift bins $z = [0.5 - 1.2]$, $[1.8 - 2.8]$, $[2.8 - 4]$ respectively. They note that the median redshift range coincides with the peak quasar activity suggesting a close relationship between the two. The space density of the Chapman et al SCUBA sample increases strongly toward higher z suggesting that they make an important component of the SFR at $z > 2$.

Confusion is a major problem for identifying deep galaxies in counts at sub-mm wavelengths. It can be reduced with gravitational lensing by massive clusters which amplifies the flux of galaxies and at the same time increases their apparent separation on the sky (Blain 1997). This has been successfully applied to the fields of known massive clusters to reach flux limits of below 1 mJy at 850 μm (Smail et al 1997, Blain et al 1999, Cowie et al 2002). The cumulative flux from the galaxy counts out to $\simeq 0.5 - 1$ mJy adds up to $0.5 \pm 0.2 \text{ nW m}^{-2} \text{ sr}^{-1}$ accounting for all or most of the CIB at that wavelength. Serjeant et al (2004) account for most of the CIB at 450 μm coming from the SCUBA 8 mJy survey maps of Scott et al (2002). These were combined with a Spitzer identification and integrating the sub-mm fluxes they find that the galaxies contribute most of the measured CIB at 450 μm , but only a small fraction of the CIB at 850 μm .

The surface density of SCUBA galaxies is quite high, $\sim 300 \text{ deg}^{-2}$ and, in principle, one can begin to study their clustering properties. Blain et al (2004) obtained accurate positions for a sample of distant SCUBA galaxies. The sample was followed up with Keck spectroscopy to determine the redshifts of 73 galaxies, constructing a substantially complete ($\sim 70\%$) redshift distribution. They find strong clustering for the sample and, assuming the two-point correlation function $\xi = (r/r_0)^{-\gamma}$ with $\gamma = 1.8$, measure that the SCUBA galaxies at $z \sim 2 - 3$ have a correlation length of $r_0 \simeq (6.9 \pm 2.1)h^{-1}\text{Mpc}$. For comparison the present day blue galaxies have $r_0 = 5.5h^{-1}\text{Mpc}$ (Maddox et al 1990), and the Lyman break galaxies, that predominantly lie at higher z , have clustering length of $r_0 \sim 4h^{-1}\text{Mpc}$ (Porciani & Giavilisco 2002). This should be reflected in larger CIB fluctuations at the sub-mm wavelengths.

6.4. Contribution from quasars/AGNs

A different, from stars, source of energy release is accretion onto massive and supermassive black holes. The latter manifests itself in the emission from AGNs and quasars, the bulk of whose luminosity is produced by accretion onto black holes, not nucleosynthesis. Severgnini (2000) have compared an X-ray sample of the [2–10] KeV and 850 μm SCUBA galaxy sources which resolve

most of the backgrounds in the two bands. They find the ratio of the $850 \mu\text{m}$ to [2–10] KeV fluxes for the sources much smaller than the value observed for the two backgrounds. The [2–10] KeV galaxies brighter than $10^{-15} \text{ erg/cm}^2$ make up $\gtrsim 75\%$ of the X-ray background in this band, but contribute $\lesssim 7\%$ to the sub-mm background. Barger et al (2004) have constructed an optical and NIR catalog of quasars and AGNs from the Chandra Deep Field out to $z \sim 3$. The catalogue currently consists of several hundred galaxies and extends to $m_{\text{AB}} \sim 20.5$ in K band, but in the future could pave a way to direct measurements of the AGN contribution to the NIR CIB levels.

The current thinking is that the contribution of the active galactic nuclei and quasars to the CIB is most likely small. Its precise value depends on bolometric correction, the details of the luminosity function and its evolution at early cosmic times. Madau & Pozzetti (2000) discuss the contribution from these sources to the total EBL. They estimate the total mean mass density of the quasar remnants today to be $\rho_{\text{BH}} \simeq (3 \pm 2) \times 10^6 h M_{\odot} \text{Mpc}^{-3}$ which should have contributed $\sim \frac{c}{4\pi} \epsilon \rho_{\text{BH}} c^2 \langle (1+z)^{-1} \rangle$ by accretion at redshift z to the total bolometric EBL flux. Assuming then that these sources radiated with an average efficiency of $\epsilon \simeq 6\%$ corresponding to standard disk accretion for a Schwarzschild black hole, they argue that, unless dust-obscured accretion on to supermassive black holes results in a much larger efficiency, QSOs peaking at $z \sim 2$, as suggested by observations, are expected to produce no more than 10–20% of the total EBL and a still smaller fraction of that will contribute to the total CIB.

Malkan & Stecker (1998) estimated the levels of the CIB between 2 and $300 \mu\text{m}$ using empirically constructed SED spectra and the observed correlations between the near-IR and mid-IR galaxy luminosities for various galaxy types including Type 1 and 2 Seyfert galaxies. They also concluded that the contribution from Seyferts to the CIB is less than 10%. Lagache et al (2003) discuss the AGN contribution to the CIB from $\simeq 10 \mu\text{m}$ to sub-mm wavelengths and, assuming that the black holes masses which power the AGNs are similar to those measured in the HDF, conclude that the AGN contribution to the CIB is relatively small compared to that of stars.

Elbaz et al (2002) have summed the observed galaxy counts at $15 \mu\text{m}$ from the ISOCAM measurements and obtain the total flux at $2.4 \pm 0.5 \text{ nW m}^{-2} \text{sr}^{-1}$ or just below the upper CIB limits ($\sim 4 - 5 \text{ nW m}^{-2} \text{sr}^{-1}$) discussed above. Of these, they estimate that less than 20 % comes from AGNs at $15 \mu\text{m}$ and less than 10 % at $140 \mu\text{m}$. Matute et al (2004) estimate the luminosity function of AGNs and its evolution from sources in the ELAIS field at $15 \mu\text{m}$ and conclude that their contribution to the CIB at that wavelengths is small ($\sim 2 - 3 \%$).

6.5. Present-day luminosity density

Present day luminosity density is an important normalizing factor in determining the CIB fluxes via eqs. 2,4. It is determined by the galaxy luminosity functions and morphological types. From UV to the near-IR it is dominated by stellar emission and at mid- to far-IR by emission from dust. For the Schechter (1976) luminosity function, $\Phi = \Phi_{*} (L/L_{*})^{-\alpha} \exp(-L/L_{*})$ the luminosity

density, eq. 3, becomes $\mathcal{L}_\nu(0) = L_* \Phi_* \Gamma(\alpha + 2)$. Note that the parameters for the fit are not independent and this parametric form, while very convenient, may not give an accurate measure of the overall luminosity density and its uncertainties.

Because the near-IR CIB is produced by stars and the latter emit most of its energy in the visible bands, any inter-comparison between the near-IR CIB and the present-day galaxy populations must be done over the entire visible to NIR range of wavelengths. Thus in this section we discuss the measurements of the present-day luminosity density from the recent galaxy surveys from UV to NIR and their consistency across the wavelength range.

Early measurements of the luminosity function of galaxies (Broadhurst, Ellis & Shanks 1988, Marzke et al 1994, Loveday et al 1992, Gardner et al 1997) have recently been complemented by much more extensive (and expensive!) surveys in the B band (2dF), visible bands (SDSS) and the near-IR (2MASS) using the latest multi-band and detector technologies.

In the visible, the new measurements from the SDSS data come in five filters from $0.354 \text{ } \mu\text{m}$ to $0.913 \text{ } \mu\text{m}$. Blanton et al (2001) have compiled a substantial catalog of over 10,000 galaxies to the depth of $\sim 21 - 22$ AB magnitudes from SDSS commissioning observations over 140 deg^2 . They computed Petrosian magnitudes over $3''$ apertures arguing that Petrosian magnitudes best reflect the total flux over all the galaxy types. Their first findings gave substantially higher total luminosity densities than earlier measurements. However, a later re-analysis of the SDSS data with a larger catalog (close to 150,000 galaxies) and differently treated evolutionary corrections lead to lower values of $\mathcal{L}_\nu(0)$ in agreement with measurements from the 2dF (Colless et al 2001) and Millennium Galaxy Catalog (Liske et al 2003) surveys in b filters using Kron and isophotal magnitudes.

Kochanek et al (2001) selected over 4,000 galaxies with the median redshift of 0.02 from the 2MASS catalog and measured the luminosity function using isophotal magnitudes $K \leq 11.25$. They also subdivided the sample into early and late type galaxies (using the RC3 catalog) providing measurements of the luminosity function for the two morphologies. Cole et al (2001) have combined the 2MASS and 2dF observations with over 17,000 galaxies with measured redshifts over $\gtrsim 600 \text{ deg}^2$. They computed the luminosity function using (mostly) the Kron magnitudes. The analyzes of both Kochanek et al (2001) and Cole et al (2001) agree within their errors. Huang et al (2003) analyzed a smaller catalog of 1,056 bright ($K < 15$) galaxies with median redshift of 0.14 over $\simeq 8 \text{ deg}^2$ and obtain a significantly higher present-day luminosity density, but claim that the luminosity function they measure evolves significantly with time and, hence, its estimation may be sensitive to proper evolutionary corrections.

The mid- to far-IR measurements of the luminosity function come from IRAS galaxies and ISO surveys. IRAS galaxies are detected most efficiently at $60 \text{ } \mu\text{m}$ in the mid- to far-IR data and this wavelength presents the best band for galaxy identification. Soifer & Neugebauer (1991) used the $60 \text{ } \mu\text{m}$ IRAS Bright Galaxy Sample to derive complete flux-limited samples of galaxies at other IRAS wavelengths. From these samples they derive the luminosity functions at of galaxies

in the local Universe at 12, 25, 60 and 100 μm . ISO observations of the ELAIS (European Large Area ISO Survey) field covered an area of 12 deg² at 15 and 90 μm (Oliver et al (2000) and resulted in the largest ISO catalog (La Franca et al 2004, Rowan-Robinson et al 2004) enabling the measurements of galaxy luminosity function at these wavelengths by Serjeant et al (2001, 2004) and Pozzi et al (2004).

Fig. 14 summarizes the current measurements of the present-day luminosity density from the various surveys. Do they indicate that a substantial flux is missing from the near-IR measurements when normalized to the measurements in the visible bands? Such possibility has been suggested by Wright (2001) using very simplified modeling of galactic SED. Below we discuss this possibility using more realistic galaxy modeling and including a simple treatment of galaxy morphology. With this modeling we show that the data on the luminosity density at various wavelengths are consistent with each other across the entire range from UV to near-IR.

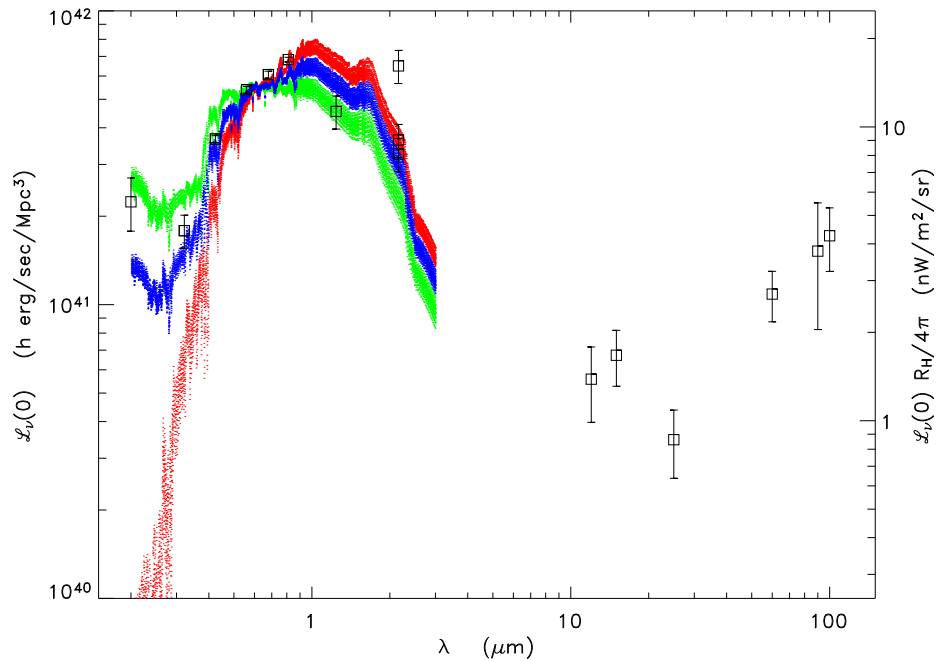


Fig. 14.— Open squares show measurements of the total present-day luminosity density at the various wavelengths. The UV measurements at 0.28 μm is from Sullivan et al (2000). The next five squares in the direction of increasing wavelength correspond to the SDSS measurements from Blanton et al (2001). The near-IR points in K band are taken from Cole et al (2001), Kochanek et al (2001) and the highest point from Huang et al (2003). The measurement in J band at 1.2 μm is from Cole et al (2001). The five mid- to far-IR points are the IRAS measurements of Soifer & Neugebauer (1991) and the 90 μm measurements from the ELAIS field ISO observations (Serjeant et al 2001, 2004). Red sets of lines correspond to the contribution from the early type stellar populations alone with metallicities and ages shown in Fig. 12 as described in the main text, green lines show the same same for late type populations and blue lines show the simple average of the two contributions.

Generating realistic SEDs from stellar evolution models is very important in proper interpretation of the numbers on $\mathcal{L}_\nu(0)$ as Fig. 12 shows. It is interesting to evaluate the total bolometric

flux contained in the luminosity density measurements. Stellar populations contribute directly to emission from UV to near-IR with dust contributions dominating the emissions at longer wavelengths. Integrating the data on the luminosity density from Fig. 14 from UV to 2.2 μm and separately over the IRAS wavelengths we get:

$$\begin{aligned}\mathcal{L}_{\text{bol}}(0.2 - 2\mu\text{m}) &= (9.8 \pm 1.2) \times 10^{41} h \text{ erg/sec/Mpc}^3 \\ \mathcal{L}_{\text{bol}}(12 - 100\mu\text{m}) &= (1.5 \pm 0.3) \times 10^{41} h \text{ erg/sec/Mpc}^3\end{aligned}\quad (30)$$

here we integrated over the near-IR data from Cole et al (2001). Omitting the UV contribution which mostly comes from very young stars would give $\mathcal{L}_{\text{bol}}(0.32 - 2\mu\text{m}) = (8.5 \pm 0.7) \times 10^{41} h \text{ erg/sec/Mpc}^3$. Taking only UV and visible data gives $\mathcal{L}_{\text{bol}}(0.2 - 0.8\mu\text{m}) \simeq (6.4 \pm 0.3) \times 10^{41} h \text{ erg/sec/Mpc}^3$.

In order to do a proper comparison between the data on $\mathcal{L}_\nu(0)$ at visible and NIR bands we divide stellar populations into two types: early (E) and late (L) with the modeling discussed in Sec. 6.2. If each type contains Ω_E , or Ω_L , of the critical density and has stellar populations with mass-to-light ratio of $M/L \equiv \gamma M_\odot/L_\odot$, these populations will produce $\Omega_{E/L}(M_\odot/L_\odot)^{-1}\gamma_{E/L}^{-1}\frac{3H_0^2}{8\pi G}$ leading to:

$$\frac{\Omega_E}{\gamma_E} + \frac{\Omega_L}{\gamma_L} = \frac{\mathcal{L}_{\text{bol}}}{10^{45} h^2 \frac{\text{erg}}{\text{sec Mpc}^3}} \quad (31)$$

If we adopt the average values of $\Omega_E = 2 \times 10^{-3} h^{-1}$ and $\Omega_L = 0.6 \times 10^{-3} h^{-1}$ suggested by Fukugita, Hogan & Peebles (1997) with $\gamma_E = 5$ and $\gamma_L = 1.3$ from the right panel of Fig. 12, we get $\mathcal{L}_{\text{bol,stars}} = 9.1 \times 10^{41} h \text{ erg/sec/Mpc}^3$ in good agreement with eq. 30. (The old SDSS measurements from Blanton et al (2001) would require higher values of $\Omega_{E/L}$, but the latter would still be within the total baryon density parameter Ω_{baryon}). Thus the measurements of the bolometric luminosity density from UV to near-IR suggest that no significant amounts of galaxy fluxes is missing between one wavelength measurement to the next.

Are then the measurements of the luminosity density across the UV to near-IR spectrum consistent with each other and with that expected from realistic stellar populations? In order to see the consistency between the near-IR and visible bands data on $\mathcal{L}_\nu(0)$ we use the SEDs plotted in Fig. 12. We further assume that all the parameters (IMF, SED, Z , etc) are independent of L . The total luminosity density then becomes:

$$f_{\lambda,E} \frac{\Omega_E}{\gamma_E} + f_{\lambda,L} \frac{\Omega_L}{\gamma_L} = \frac{\mathcal{L}_\lambda}{10^{45} h^2 \frac{\text{erg}}{\text{sec Mpc}^3}} \quad (32)$$

Red lines show the least squares fit to eq. 32 for each (Z, t) if only galaxies with the Early type stellar populations were present. This leads to $\Omega_E h^2 \simeq (4.5 - 7) \times 10^{-3}$ for the range of (Z, t) . Green lines show the least squares fit to eq. 32 for each (Z, t) if only galaxies with the Late type stellar populations were present. This leads to $\Omega_L h^2 \sim (1.9 - 2.5) \times 10^{-3}$. These numbers are in broad agreement with the above values on these parameters. It is clear that the luminosity density at visible and UV wavelengths reflects mainly emission from late type populations, whereas in the

near-IR both early type populations can dominate. In principle, equation 32 can be solved for both Ω_E and Ω_L , but the answer will be too reflective of the assumptions made in constructing galactic SEDs to be useful. Instead we prefer fitting the data in Fig. 14 with *a priori* values of Ω_E and Ω_L . The blue lines show an example of simple mean of the green and red lines for each (Z, t) .

In conclusion, we note again that the answers one gets in this way are not unique as the realistic SEDs depends on: 1) galaxy metallicity, Z , and its dependence on other galaxy properties, 2) the details of the IMF, particularly in the poorly measured stellar mass range and its possible dependence on other galaxy properties, 3) galaxy morphology mixes, 4) galaxy luminosity function for each galaxy type, 5) galaxy ages for each morphological type, luminosity/mass etc. If a statistically significant discrepancy between the measurements of $\mathcal{L}_\nu(0)$ is found between the various bands and surveys, it is probably indicative of the variations in any or all of the above points, but we have shown that with realistic (i.e. based on synthetic stellar evolution models) modeling of galactic SEDs the measurements can already be fit reasonably well.

6.6. Deep galaxy counts

The total flux from galaxies measured in deep count surveys gives another measure of the CIB, or more precisely the contribution to the CIB from the known sources. This helps to identify the possible CIB excess and in what cosmological populations and at what times it might arise. The situation from the current set of measurements from NIR to sub-mm bands is discussed below.

6.6.1. Near-IR

In the near-IR the galaxy counts have been measured now to fairly faint limits in J,H,K bands with observations coming from ground and Hubble Space Telescope observations. The integrated flux of the counts saturates at the levels shown in Table 5 (Gardner 1996, Kashlinsky & Odenwald 2000, Cambresy et al 2000, Madau & Pozzetti 2000, Fazio et al 2004). Madau & Pozzetti (2000) show that the contribution from the HDF galaxies to total EBL from visible to near-IR saturates around AB magnitude $m_{AB} \sim 20$ in all bands and discuss that this is unlikely to result from underestimating the abundance of distant sources due to reddening (as their Lyman break shifts into progressively longer wavelength bands) or absorption.

Fig. 15 shows the contributions to the total CIB from galaxies at J,H,K bands. The data come from the compilations summarized in Madau & Pozzetti (2000) and Pozzetti et al (1996, 1998) and the Subaru Deep Field data (Maihara et al 2001); see caption for the figure. The upper panels show dF/dm vs magnitude and the lower panels show the cumulative flux from galaxies brighter than magnitude m . The fluxes saturate at $m_{AB} \sim 20 - 23$. The asymptotic values of the fluxes from ordinary galaxies compared to the observed CIB levels are shown in Fig. 9.

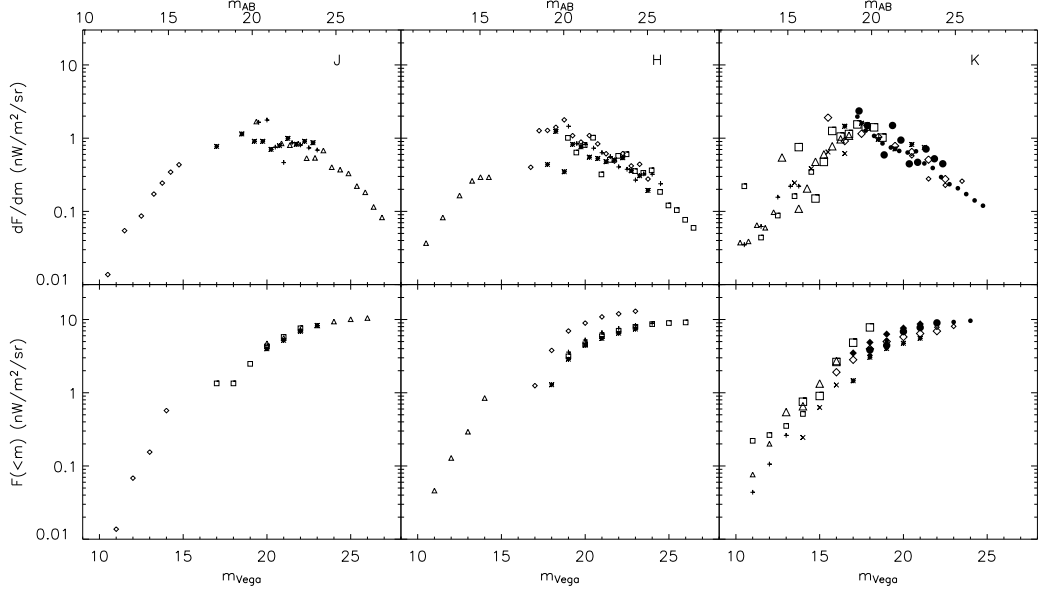


Fig. 15.— Cumulative flux in $\text{nW m}^{-2} \text{sr}^{-1}$ contributed by galaxies from a narrow dm magnitude bin is shown vs the Vega magnitude from galaxies from deep galaxy surveys in J, H, K. The data are as follows:

J band: Crosses from Bershady et al (1998), asterisks from Saracco et al (1999), diamonds from Chester et al (1998) and triangles from Pozzetti et al (1996, 1998) and Madau & Pozzetti (2000).

H band: Crosses are from Yan et al (1998), asterisks and diamonds from Teplitz et al (1998), triangles from Chester et al (1998), and squares from Pozzetti et al (1996, 1998) and Madau & Pozzetti (2000).

K band: crosses are from Chester et al (1998), asterisks from McLeod et al (1995), small open diamonds from Djorgovski et al (1995), small triangles from Mobasher et al (1986), small and large open squares, large triangles and large open diamonds from Gardner et al (1993), \times -signs from Glazebrook et al (1994), filled diamonds from Soifer et al (1994), filled large circles from Pozzetti et al (1996, 1998) and Madau & Pozzetti (2000), and filled small circles from Maihara et al (2001).

ISO galaxy counts at $6.75 \mu\text{m}$ reach $\sim 40 \mu\text{Jy}$ in the HDF (Oliver et al 1997) and Lockman hole regions (Taniguchi et al 1997) and Sato et al (2003) reach sources as faint as $\sim 10 \mu\text{Jy}$ in another region. At these wavelengths the counts have now been complemented by deeper measurements with the Spitzer IRAC instrument.

Fig. 16 shows the contributions to the CIB flux from faint galaxies at 3.6 , 4.5 , 5.8 and $8 \mu\text{m}$ from three recent Spitzer IRAC surveys reported by Fazio et al (2004). The surveys covered 3 independent fields referred to as QSO field (the deepest with ~ 9.2 hours total exposure), the EGS (Extended Groth Strip) field at a higher Galactic latitude and the widest and the shallowest Bootes region survey. They separated stars from galaxies and corrected for incompleteness in the faintest counts (mostly galaxies). At 3.6 and $4.5 \mu\text{m}$ the total flux seems to saturate at the levels of shown in Table 5. At 5.8 and $8 \mu\text{m}$ the saturation of the cumulative flux from observed galaxies is not as clear, although a case can be made that the ceiling of the total flux contribution to the CIB has been reached as well. At any rate we interpret the total fluxes at 5.8 and $8 \mu\text{m}$ as lower limits on the contribution from ordinary galaxies to the CIB and plot them with arrows in Fig. 9.

The numbers from the Spitzer IRAC surveys shown in Table 5 are direct summation of the fluxes from upper panels in Fig. 16. When integrating the counts weighted according to uncertainties, Fazio et al (2004) find total fluxes of 5.4, 3.5, 3.6, and 2.6 $\text{nWm}^{-2}\text{sr}^{-1}$ at 3.6, 4.5, 5.8 and 8 μm respectively.

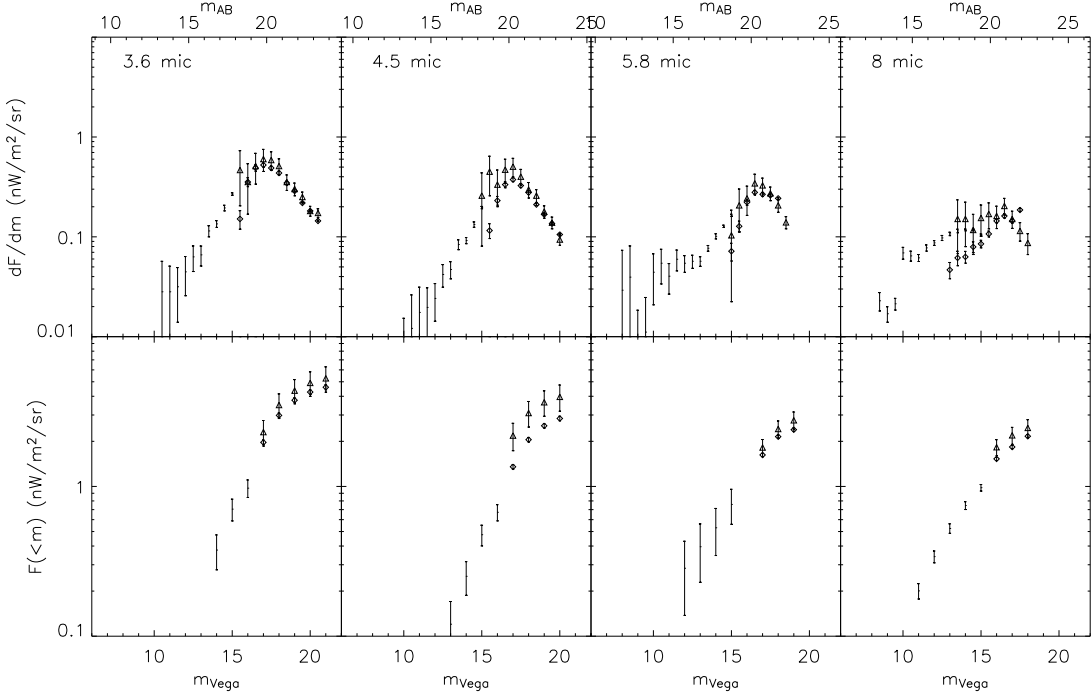


Fig. 16.— Cumulative (bottom set of panels) and differential (top) flux distribution in $\text{nWm}^{-2}\text{sr}^{-1}$ vs the Vega magnitude for galaxies in three different surveys from the Spitzer IRAC galaxy surveys by Fazio et al (2004): dots with errors correspond to their Bootes field, diamonds to their EGS data and triangles to the QSO1700 field observations. AB magnitudes are shown on the upper horizontal axis.

6.6.2. mid-IR

Elbaz et al (2002) used ISOCAM observations of almost 1,000 galaxies at 15 μm to estimate the contribution to the CIB at that wavelength from sources down to 50 μJy . They obtain that these galaxies produce $2.4 \pm 0.5 \text{ nWm}^{-2}\text{sr}^{-1}$ and their contribution may saturate at fluxes $\lesssim 30 - 50 \mu\text{Jy}$.

Spitzer/MIPS 24 μm channel has best mid-IR resolution and its confusion limit corresponds to fainter fluxes. The MIPS FWHM at 24 μm corresponds to 6''. Papovich et al (2004) present the number counts of $\simeq 5 \times 10^4$ sources from the 24 μm Spitzer deep surveys. They show that the counts probe a previously undetected population of very luminous galaxies at high z . The data were obtained in five fields from Spitzer characterization and GTO (Guaranteed Time Observations)

observations. The largest and shallowest of the fields (Bootes) subtended ca. 9 deg² with an exposure of 87 secs per pixel and the smallest and deepest (ELAIS) was ca. 130 arcmin² exposed for just under one hour in each pixel. The counts out to 60 μ m give ~ 2 nWm⁻²sr⁻¹ and Papovich et al (2004) estimate that extrapolating to sources below that limit gives around 3 nWm⁻²sr⁻¹ in total.

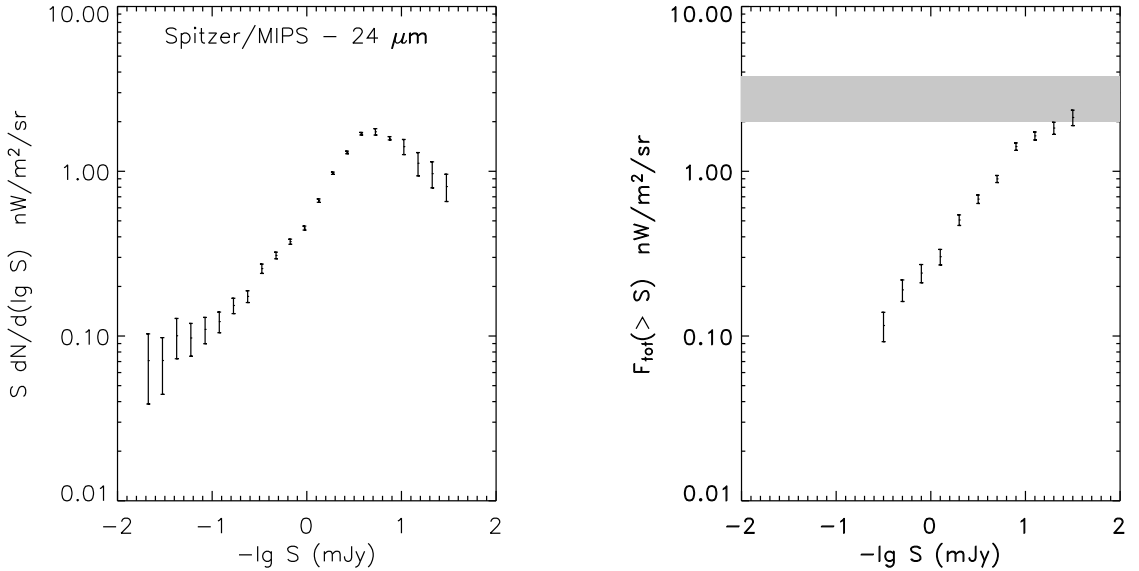


Fig. 17.— **Left:** differential flux distribution in $\text{nWm}^{-2}\text{sr}^{-1}$ from the MIPS counts at 24 μm (Papovich et al 2004) **Right:** cumulative flux contribution as function of the source flux from galaxies shown in the left panel. Shaded area corresponds to the total flux with its uncertainty including the extrapolation from sources fainter than 60 μJy (Papovich et al 2004).

6.6.3. Far-IR and sub-mm

The number counts at mid- and far-IR indicate that the IR-luminous galaxies evolved more rapidly than their optical counterparts and make a substantial contribution to the star formation at higher z (Elbaz et al 1999).

A deep survey (FIRBACK) was performed by ISOPHOT at 170 μm (Lemke et al 1996) out to the depth of 120 mJy where galaxy counts can no longer be fitted with a Euclidean slope. This is confirmed with the MIPS observations of the Chandra Deep Field (Dole et al 2004) which indicate a lower limit on the CIB at 170 μm of 1.4 $\text{nWm}^{-2}\text{sr}^{-1}$ corresponding to about $\sim 10\%$ of the CIB. Dole et al (2004) used early observations with the Spitzer MIPS instrument to measure galaxy counts at 70 and 160 μm down to 15 and 50 mJy respectively. Their counts are consistent with the 60 μm IRAS counts (Lonsdale et al 1990) and the FIRBACK 170 μm survey (Dole et al 2001). From evolutionary modeling they suggest that most of the observed faintest sources lie at $z \sim 0.7$

with a tail out to $z \sim 2$. Integrating the flux from the observed sources leads to the total flux of 0.95 and $1.4 \text{ nWm}^{-2}\text{sr}^{-1}$ at 70 and $160 \mu\text{m}$ respectively. As Fig. 9 shows this corresponds to a small part of the total CIB levels at these wavelengths, so most of the CIB at 70 and $160 \mu\text{m}$ must come from still fainter (and more distant) sources.

The FIR background can be resolved into individual sources with detections by the SCUBA instrument at the James Maxwell Telescope (Smail et al 1997, Blain et al 2002). The total flux at $850 \mu\text{m}$ from the the SCUBA sources is estimated to be $0.5 \pm 0.2 \text{ nWm}^{-2}\text{sr}^{-1}$ (Smail et al 1997).

Serjeant et al (2004) presented statistical detections of galaxies in the Spitzer Early Release Observations through a stacking analysis of their reanalyzed SCUBA 8 mJy survey maps of Scott et al (2002) combined with a Spitzer identification of their positions. Integrating the sub-mm fluxes of the Spitzer populations they find that the $5.8 \mu\text{m}$ galaxies contribute only $0.12 \pm 0.05 \text{ nWm}^{-2}\text{sr}^{-1}$ at $850 \mu\text{m}$, but at the same time contribute $2.4 \pm 0.7 \text{ nWm}^{-2}\text{sr}^{-1}$ at $450 \mu\text{m}$, or almost the entire CIB at that wavelength. This contribution is shown with filled circle at $450 \mu\text{m}$ in Fig. 9.

6.7. CIB fluctuations from clustering of ordinary galaxies

In surveys where the beam is small, galaxies can be resolved and removed down to some limiting magnitude allowing, in principle, to probe the CIB from fainter and typically more distant systems. At $z=1$, the angular scale of $1''$ subtends comoving scale $15h^{-1}\text{Kpc}$, for the WMAP cosmological parameters, so the identified galaxies can be excised almost completely in surveys with arcsec scale resolution. In practice, the precise value of the limiting magnitude depends on the instrument noise levels, foreground emissions, etc.

Small beam also means that the shot-noise component of the fluctuations discussed in Sec. 3.2.2 may be important. The left panel of Fig. 18 plots the shot noise power spectrum (left vertical axis) and the value of σ_{sn} (right vertical axis) given by eqs. 16,15 vs the AB magnitude down to which galaxies have been removed. The right panel shows σ_{sn} vs the wavelength for galaxies fainter than $m_{AB} = 20$ (open circles), 22 (filled circles), and 25 (filled triangles). The shot noise was evaluated from galaxy counts data summarized in Sec. 6.6. In the figure we assumed the beam of $\omega_{\text{beam}} = 2.1 \times 10^{-10} \text{ sr}$ or, in case of a spherical beam, a radius of $\sim 1.6''$. We did not attempt to calculate the (probably substantial) statistical uncertainties in the shot noise components because the various systematic, cosmic variance, etc effects in the different galaxy surveys are difficult to quantify (which would probably make such error bars misleading), but the figure should give a reliable approximation for the magnitude of the expected shot noise.

The left panel of Fig. 19 shows the amplitude of the detected CIB fluctuation at $q^{-1} = 1 \text{ arcsec}$ from the analysis of the deep 2MASS data in J, H, K bands (Kashlinsky et al 2002, Odenwald et al 2003). It is plotted vs the AB magnitude above which galaxies galaxies were clipped out for the three 2MASS bands. Although the present deep galaxy counts data have potentially appreciable uncertainties for evaluating the shot noise amplitude, comparison with Fig. 18 shows that the

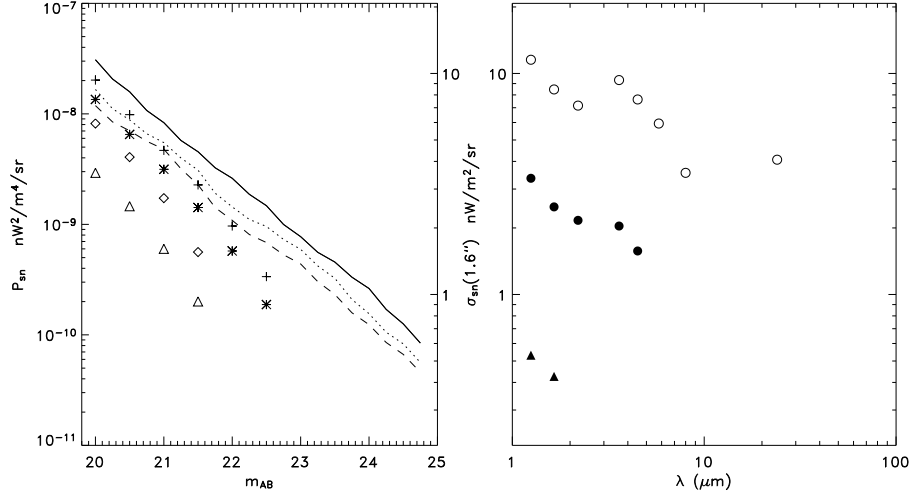


Fig. 18.— **Left:** Shot noise power spectrum (left vertical axis), evaluated according to eq. 16, from galaxies fainter than the AB magnitude shown in the horizontal axis. It was computed for galaxy counts summarized in Sec. 6.6. Left vertical axis shows the corresponding value of σ_{sn} for a beam of $\simeq 1.6''$ in radius. The lines show the shot noise from HDF galaxy counts by Madau & Pozzetti (2000): solid, dotted and dashed lines correspond to J, H and K bands respectively. Symbols show the shot noise from galaxies in the IRAC Spitzer counts data from Fazio et al (2004): plus signs, asterisks, diamonds and triangles correspond 3.6, 4.5, 5.8 and 8 μm respectively. **Right:** σ_{sn} vs λ evaluated from existing deep galaxy counts data. Open circles correspond to galaxies fainter than $m_{\text{AB}} = 20$, filled circles to $m_{\text{AB}} > 22$ and filled triangles to $m_{\text{AB}} > 25$.

detected CIB fluctuations are substantially higher than the shot-noise fluctuation from galaxies remaining in the field. The largest angular scales probed by the analysis were $\pi/q \sim 1.5'$ which at $z=1$ corresponds to $\simeq 1h^{-1}\text{Mpc}$. Hence the data are probing the range of scales where galaxy clustering is in the non-linear regime. The lines show the amplitude for passively evolving galaxies with synthetic spectra from Jimenez & Kashlinsky (1999) for J and K bands. They are normalized to the observations of the galaxy luminosity densities in Fig. 14, the observed power spectrum of galaxy clustering, include the shot-noise component from Fig. 18, and assume no biasing. The high numbers for the near-IR fluctuations are consistent with other findings (Kashlinsky & Odenwald 2000, Matsumoto et al 2000, 2003) after accounting for the beam difference and the fact that in the large-beam DIRBE and IRTS studies no galaxies were removed.

The figure illustrates that the detected CIB anisotropy levels are large compared to simple no-evolution assumptions. They may imply either significant evolution of galaxy populations at early cosmic times, or strong biasing of faint (more distant) galaxy population. The latter would then have to be wavelength dependent because the discrepancy is different in the various bands. Alternatively, Maggiori et al (2002) ascribe the difference to contribution from Population III stars at $z \sim 10 - 20$; this contribution is discussed in the next section.

The slope of the detected power spectrum of the CIB from Kashlinsky et al (2002) depends on the clipping magnitude cutoff as shown in the right panel of Fig. 19. If progressively fainter galaxies

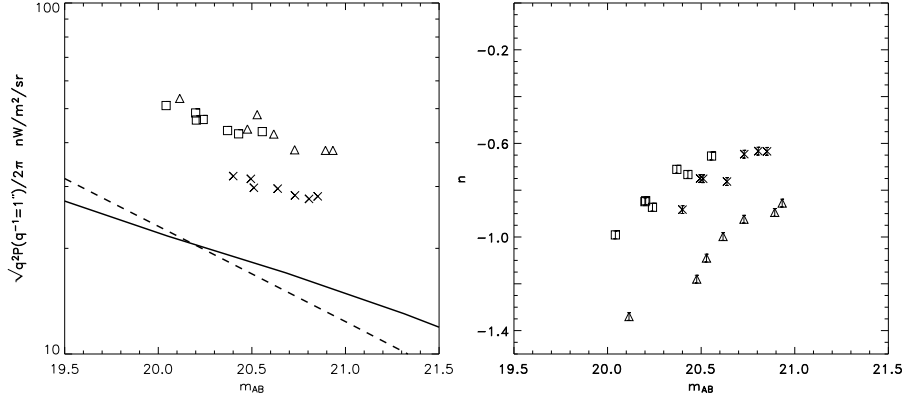


Fig. 19.— **Left:** Amplitude of the RMS CIB flux fluctuation at $q^{-1} = 1$ arcsec from Fig. 11 vs AB clipping magnitude beyond which galaxies were excised from the field. Open triangles, open squares and crosses correspond to the 2MASS J,H,K bands respectively. Dashed and solid lines show the fluctuation from passively evolving galaxies, including the shot-noise component, for J and K bands respectively. **Right:** Power law index n for the CIB power spectrum $P(q) \propto q^n$ from the deep 2MASS data shown in Fig. 11 is plotted vs the limiting clipping magnitude. Same symbol notation as in the left panel.

are removed the slope of the power spectrum flattens. This is consistent with fainter galaxies being at higher z when the clustering pattern was less evolved and the slope reflects evolution of galaxy clustering with time. The slope of this dependence is similar in all three bands. The power spectrum of the present-day galaxy clustering on non-linear scales has the spectral index $n \simeq -1.3$ (Groth & Peebles 1977, Maddox et al 1990), so it would appear that the deep 2MASS J band patch with the lowest m_{cut} probes galaxies out to smaller z . In CDM models the non-linear power spectrum of galaxy clustering evolves toward steeper slope (higher $|n|$) at low z consistent with the trend in Fig. 19b.

6.8. Cumulative flux from galaxy counts vs CIB measurements

At many IR wavelengths the counts from ordinary galaxies are deep enough to make a 'reasonable' guess about their total contribution to the CIB. This would indicate whether other sources of radiation existed that produced the observed CIB flux and its fluctuations. Table 5 summarizes the total fluxes observed directly by the deepest currently available galaxy populations and one can compare them with the CIB measurements summarized in Fig. 9.

At mid-IR there are no direct CIB measurements to compare, but indirect upper limits are close to the lower limits from the counts so probably no surprises are expected. At far-IR most of the CIB has been resolved at 450 and 850 μm with the flux from the observed counts not yet saturating. At NIR the counts from the observed 'ordinary' galaxy populations saturate at levels a factor of $\sim 2 - 3$ lower than the claimed levels of the mean CIB measurements and the fluctuations analysis. Furthermore, the CIB fluctuations results from the deep 2MASS data suggest that the

Table 5. Integrated CIB flux from observed NIR galaxy counts

λ	Flux (nWm $^{-2}$ sr $^{-1}$)	Comments ^a
1.25 μm ¹	9.71 $^{+3.00}_{-1.90}$	Saturates at $m_{\text{AB}} \gtrsim 24 - 25$
1.65 μm ¹	9.02 $^{+2.62}_{-1.68}$	Saturates at $m_{\text{AB}} \gtrsim 24 - 25$
2.2 μm ¹	7.92 $^{+2.04}_{-1.21}$	Saturates at $m_{\text{AB}} \gtrsim 22 - 23$
3.6 μm ²	5.27 \pm 1.02	Saturates at $m_{\text{AB}} \gtrsim 22 - 23$
4.5 μm ²	3.95 \pm 0.77	Saturates at $m_{\text{AB}} \gtrsim 22 - 23$
5.8 μm ²	$\gtrsim 2.73 \pm 0.22$	Possibly saturates at $m_{\text{AB}} \gtrsim 22 - 23$, but data too uncertain. ^b
8 μm ²	$\gtrsim 2.46 \pm 0.21$	Possibly saturates at $m_{\text{AB}} \gtrsim 22 - 23$, but data too uncertain. ^b
1.25 $\mu\text{m} \leq \lambda \leq 8 \mu\text{m}$	11.4 \pm 4.6	NIR (bolometric) flux
1.25 $\mu\text{m} \leq \lambda \leq 4.5 \mu\text{m}$	9.7 \pm 3.2	—
15 μm ³	2.4 \pm 0.5	Saturates at $S \lesssim 0.05 \text{ mJy}$. ^b
24 μm ⁴	2.7 $^{+1.1}_{-0.7}$	Saturates at $S \lesssim 0.05 \text{ mJy}$. ^b
70 μm ⁵	> 0.95	Does not saturate out to $S \gtrsim 15 \text{ mJy}$. ^c
170 μm ⁵	> 1.4	Does not saturate out to $S \gtrsim 180 \text{ mJy}$. ^c
450 μm ⁶	2.4 \pm 0.7	Sub-mm fluxes of Spitzer sources at 24 μm account for most of the CIB
850 μm ⁷	0.5 \pm 0.2	Sources out to $S \simeq 0.5 - 1 \text{ mJy}$ account for most of the CIB

Note. — References: ¹ Madau & Pozzetti (2000), ² Fazio et al (2004), ³ Elbaz et al (2002), ⁴ Papovich et al (2004), ⁵ Dole et al (2004), ⁶ Serjeant et al (2004), ⁷ Blain et al (1999)

^a Saturation point is defined as the magnitude where $\frac{1}{F(<m)} \frac{dF}{dm} \leq 0.2$

^b CIB not measured directly at that wavelength

^c Counts are not measured to sufficiently faint limits.

excess arises in galaxy populations with $m_{AB} \gtrsim 21$ and likely comes from early times.

Fig. 20 plots the NIR CIB excess left over after galaxy counts contributions from Table 5 are subtracted from the observed CIB levels shown in Fig. 9. The last point is plotted at $4 \mu\text{m}$, where IRTS data are still available and galaxy counts were extrapolated to this wavelengths using the numbers in Table 5. Integrating over the points in the figure leads to the total bolometric flux for the near-IR CIB excess between 1 and $4 \mu\text{m}$ of $29.4 \pm 13.0 \text{ nW m}^{-2} \text{sr}^{-1}$. Ignoring the last point (open circle) in the figures leads to $26.4 \pm 12.2 \text{ nW m}^{-2} \text{sr}^{-1}$.

Zodiacal light at these wavelengths would come from reflected Solar emission and observations suggest a slope $\propto \lambda^{-2}$ (Kelsall et al 1998 and Fig. 4). Assuming that zodiacal light errors are proportional to the zodiacal flux, the excess may be attributable to the residual zodi emission if the points at 1.25 and $4 \mu\text{m}$ can be discarded. Comparison with the zodiacal light surface brightness shown in Fig. 4 suggests that in this case, the relative errors in the zodiacal emission modeling would have to have amplitude of $\gtrsim 40\text{--}50\%$ (see Kelsall et al 1998 and Fig. 4) at the near-IR bands. They would also have to be the same in all the different CIB measurements with different instruments and different zodiacal models used. Galactic cirrus emission would at these wavelengths contribute emission with a much smaller and a roughly flat SED (Leinert et al 1998).

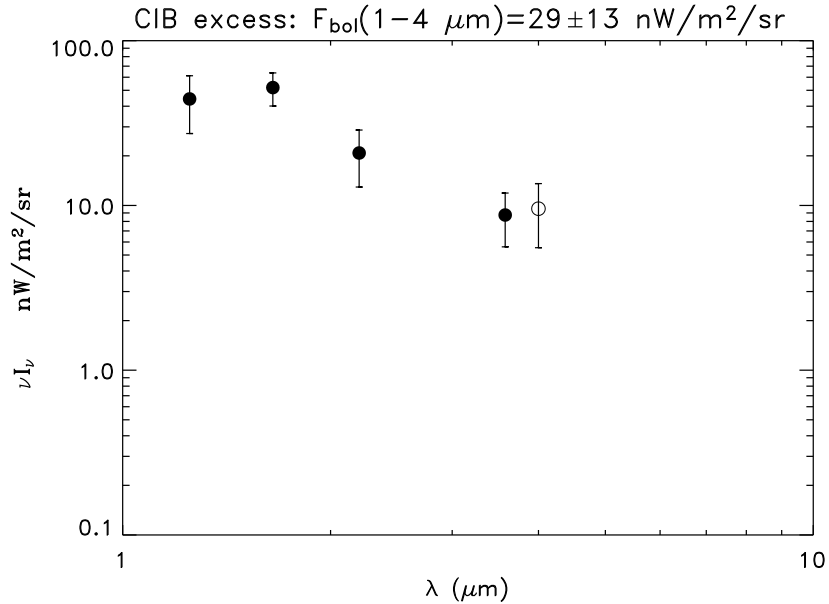


Fig. 20.— CIB excess at near-IR: filled circles correspond to CIB measurements minus the cumulative flux from the observed galaxy populations. As discussed in the text, the various measurements are consistent, but for the purposes of this plot, the CIB mean levels were taken from Cambresy et al (2001) at J band, and from the IRTS measurements at 1.63 to $4 \mu\text{m}$. Filled circles show wavelengths where galaxy counts can be summed directly. Open circle corresponds to extrapolation of the observed fluxes from galaxy counts given in Table 5 to $\lambda = 4 \mu\text{m}$, the maximal wavelengths of the IRTS measurements.

7. Population III

The epoch of the first stars, when Population III stars formed, is now emerging as the next cosmological frontier. It is not clear what these stars' properties were, when they formed or how long their era lasted before leading to the stars and galaxies we see today. On the other hand, if the excess near-IR CIB is real, as many independent measurements suggest, it may well be attributable to emissions by these stars and would make the CIB and its structure a unique probe directly into the epoch and efficiency of Population III formation and evolution. This would provide a powerful application of the CIB-related science to one of the most outstanding remaining questions in the standard cosmological picture.

Recent measurements of quasar spectra reveal the Gunn-Peterson trough at $\lambda_{\text{rest}} \leq 1216\text{\AA}$ at $z \gtrsim 6 - 7$ indicating the location of the reionization epoch (Becker et al 2001, Djorgovski et al 2001). These quasars already show the presence of metals suggesting that the first metal free stars had to form at still earlier epochs and enrich the IGM by $z \sim 7$. At epochs corresponding to $z \gtrsim 7$ the Universe had to contain significant amounts of neutral hydrogen leading to absorption of all radiation at wavelengths shorter than the Lyman limit. Interestingly, the J band filter probes wavelengths longer than the Lyman limit at $z \lesssim 14$ and the K band at $z \lesssim 20$, so much of the near-IR CIB can probe the Population III era even if reionization has not yet occurred.

7.1. What were the first stars?

Population III stars are the first stars to form in the metal-free Universe and so far remained an entirely hypothetical (and theoretical) class of objects since introduced by Rees in the late seventies (Rees 1980 and references cited therein). Much of what can be attributed to consequences of that early and possibly brief era depends on the the mass Population III stars had and we start this section with a brief discussion of the theoretical spectrum of possibilities and the current ideas.

Should the first stars have been different from modern day stellar objects? We know from observations that star formation takes places in gas clouds much more massive than $M_{\text{Chandra}} = (\frac{\hbar c}{G m_p^2})^{3/2} m_p \simeq 1.44 M_{\odot}$, a mass-scale of a typical self-gravitating object supported by nuclear fusion, and must be caused by gravitational collapse (stellar material is much more dense than the clouds in which they form) and fragmentation (stars are much smaller in mass than the parental clouds). Thus the gravitational collapse processes must lead to final fragments that are just in the right mass range to support nuclear burning.

Hoyle (1953) provided a plausible and elegant answer to this that became known as “opacity limited fragmentation theory”. It goes as follows: the cooling time is much shorter in galactic mass gas clouds than the dynamical collapse time and the ratio of the two decreases with increasing gas density (Rees & Ostriker 1977). Gravitational collapse thus proceeds isothermally leading to a decrease in the Jeans mass inside the cloud, $M_{\text{Jeans}} \propto T^{3/2} \rho^{-1/2}$. The cloud becomes susceptible

to fragmentation into masses of $\sim M_{\text{Jeans}}$, which themselves collapse and fragment into smaller pieces. This process continues until the density increases enough so that the optical depth across the fragment is sufficiently high to trap the radiation released by the collapse. This requires $\tau \propto \kappa \rho^{2/3} M^{1/3}$ of order unity (for absorption; for scattering this happens at higher τ). For clouds of solar metallicity the collapse proceeds at $T \sim 10\text{K}$ and fragmentation stops at $\sim 0.01M_{\odot}$ (Low & Lynden-Bell 1977, Silk 1977). For metal free gas clouds the collapse proceeds at higher T ($\gtrsim 10^4\text{K}$ in the absence of hydrogen molecules, Dalgarno & McCray 1972). Thus the early thinking in the pre-CDM era was that the first stars would have to be much more massive. On the other hand, Rees (1976) has shown, from very general arguments of maximal cooling efficiency, that the minimal mass is roughly independent of T and is $M_{\text{min}} \simeq M_{\text{Ch}}(k_B T / m_p c^2)^{1/4}$. I.e. in metal free gas the cooling is very inefficient so T is high, but at the same time - because opacity is generated by the same coolants - τ is smaller and the fragmentation stops at higher densities and smaller M_{Jeans} .

However, a consensus based on recent numerical investigations within the framework of the Λ CDM models is now emerging that fragmentation of the first collapsing clouds at redshifts $z_* \sim 10 - 30$ was very inefficient and that the first metal-free stars after all were very massive objects with mass $\gtrsim 100M_{\odot}$ ((Abel et al 2002; Bromm et al 1999), see recent review by Bromm & Larson 2004). Such stars would form in small mini-halos and live only a few million years, much less than the age of the Universe ($\simeq 2 \times 10^8$ years at $z = 20$), making their direct detection still more difficult. On the other hand the net radiation produced by these massive stars could give substantial contributions to the total diffuse background light ((Rees 1978)) and since their light is red-shifted much of that contribution will be today in the infrared bands ((Bond et al 1986)). This could make them significant contributors to the near-IR CIB.

Such massive, metal-free stars will be dominated by radiation pressure and would radiate close to the Eddington limit: $L \simeq L_{\text{Edd}} = \frac{4\pi G m_p c}{\sigma_T} M \simeq 1.3 \times 10^{38} M/M_{\odot}$ erg/sec, where σ_T is the cross section due to electron (Thompson) scattering. The energy spectrum for emission from these stars will be quite featureless and close to that of a black body at $T \sim 10^{4.8-5}\text{K}$ (Schaerer 2003, Tumlinson et al 2003). Unlike their metal rich counterparts Population III stars are not expected to have significant mass-loss during their lifetime (Baraffe et al 2001). If sufficiently massive ($\gtrsim 240M_{\odot}$, Bond et al 1984, Heger et al 2003) such stars would also avoid SN explosions and collapse directly to black holes in which case their numbers can significantly exceed that required to produce the metallicities observed in Population II stars. The lifetime of these stars will be independent of mass: $t_L \simeq \epsilon M c^2 / L \simeq 3 \times 10^6$ years, where $\epsilon = 0.007$ is the efficiency of the hydrogen burning. These numbers are in good agreement with detailed computations (e.g. Schaerer 2002).

From the WMAP large-scale polarization measurements (Kogut et al 2003) it is known that the Universe's optical depth to recombination is $\tau \simeq 0.2$ requiring the re-ionization to occur by $z_* \simeq 20$. Numerical calculations suggest that when a Population III star forms it is surrounded by a gaseous nebula from the gas of the host halo which was not incorporated into the stars (Bromm et al 1999). The nebula and the IGM would remain neutral in the absence of Population III. In general, the resultant SED would thus be made up of three components: 1) direct stellar emission not absorbed

by Lyman continuum; 2) Lyman emission of the absorbed part of stellar SED, 3) free-free emission from the IGM. Consequently, Santos et al (2002) consider two extremes for the reprocessing of the ionizing radiation from Population III: 1) Each Population III star is surrounded by a dense nebula with all the reprocessing of ionizing radiation taking place there, and 2) the nebula is optically thin to the ionizing photons and all the reprocessing takes place in the IGM. Fig. 21 shows the SED from Santos et al (2002) produced by a $1000 M_{\odot}$ metal-free star for the two extreme cases of photon propagation. Superimposed are also the J and K filters redshifted to $z = 20$ and 10.

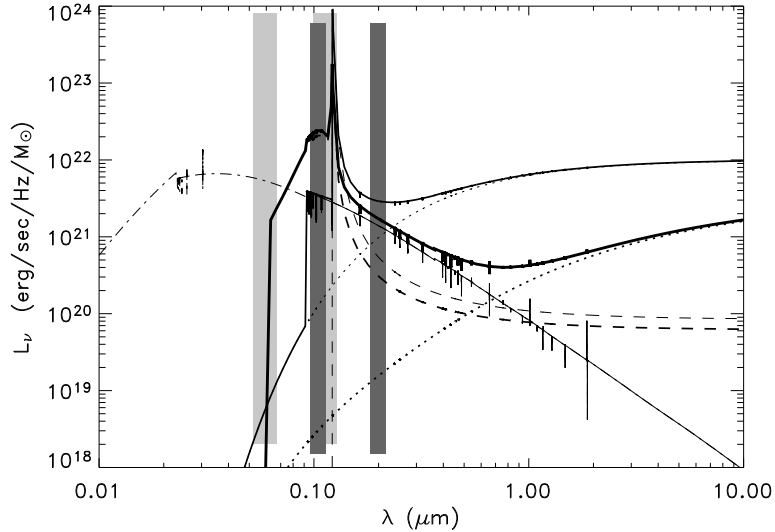


Fig. 21.— An example of the Population III SED produced by a $1000 M_{\odot}$ metals-free star from Santos et al (2002). Light and dark shaded area show the range probed respectively by the J and K band DIRBE filter at $z = 20$ and 10. Dashed-dotted line shows the spectrum of a $300 M_{\odot}$ metal free star; thin solid line shows the part of that SED longward of the Lyman limit. Dotted lines show the free-free emission from the surrounding medium and dashed lines show the nebulae emission; thick and thin lines of each type correspond to the two extremes photon propagation considered by Santos et al (2002). Thick solid lines correspond to the total SED produced by the Population III emission in the two extreme cases.

There are several intuitive reasons why Population III produce significant both CIB levels and fluctuations:

- Each unit mass of Population III (if made of massive stars) emits $\gtrsim 10^5$ more light than normal stars.
- A higher fraction of the total luminosity would be redshifted into the NIR bands from hot objects at these redshifts than from $z \sim 2 - 3$. E.g. the K band redshifted to $z \simeq 20$ corresponds to rest wavelength of 1000 Å, roughly the Lyman limit wavelength.
- Massive stars (assuming Population III were indeed massive stars) radiate with a higher mean radiative efficiency, $\epsilon = 0.007$, than the present day stellar populations.
- Because their era was presumably brief, Population III epochs contain less projected volume

than the ordinary galaxy populations spanning the epochs of Population I and I stars. Hence, the larger relative fluctuations.

- Biasing is higher for Population III because they form out of rarer regions which leads to the amplified correlations.

7.2. Isotropic component of CIB

It was noted by several authors that the near-IR CIB signals such as e.g. detected in the 2MASS long integration data (Kashlinsky et al 2003) may come from the Population III stars (Magliocchetti, Salvaterra & Ferrara 2003, Santos, Bromm & Kamionkowski 2002, Salvaterra & Ferrara 2003, Kashlinsky et al 1999, Cooray et al 2004, Kashlinsky et al 2004). The argument can be shown to be (almost) model-independent provided Population III stars were indeed very massive.

Our discussion in Sections 7.2 through 7.4 follows Kashlinsky et al (2004):

For a flat Universe the co-moving volume per unit solid angle contained in the cosmic time interval dt is $dV = c(1+z)^{-1}d_L^2 dt$, where d_L is the luminosity distance. Each Population III star will produce flux $Lb_{\nu'}(1+z)/4\pi d_L^2$, where b_{ν} is the fraction of the total energy spectrum emitted per unit frequency and $\nu' = \nu(1+z)$ is the rest-frame frequency. (The Population III SED is normalized so that $\int b_{\nu} d\nu = 1$). The co-moving mass density in these stars is $\int Mn(M, t)dM = \Omega_{\text{baryon}} \frac{3H_0^2}{8\pi G} f_*$, where f_* is the fraction of the total baryonic mass in the Universe locked in Population III stars at time t . The net flux per unit frequency from a population of such stars with mass function $n(M)dM$ is given by:

$$\frac{d}{dt}I_{\nu} = \frac{\int Ln(M, t)dM}{4\pi d_L^2} (1+z) \langle b_{\nu'} \rangle \frac{dV}{dt} = \frac{c}{4\pi} \langle b_{\nu'} \rangle \langle \frac{L}{M} \rangle f_* \rho_{\text{baryonic}} \quad (33)$$

Here $\langle b_{\nu} \rangle \equiv \int Ln(M, t)b_{\nu} dM / \int Ln(M, t)dM$ denotes the mean Population III SED averaged over their initial mass function and $\langle \frac{L}{M} \rangle \equiv \int Ln(M, t)dM / \int Mn(M, t)dM$. For Gaussian density field $f_* \sim 5 \times 10^{-2} - 3 \times 10^{-3}$ if on average Population III formed in 2–3 sigma regions (see later). Provided that $L/M = \text{constant}$, this result does not depend on the details of the initial mass function of Population III stars (cf. Fig. 5 of Salvaterra & Ferrara 2003). (Note that for the present day stellar populations their mass-to-light ratio depends strongly on stellar mass and $\langle \frac{L}{M} \rangle$ is much smaller than the Population III value of $4\pi G m_p c / \sigma_T \simeq 3.3 \times 10^4 L_{\odot} / M_{\odot}$ leading to substantially smaller net fluxes). Assuming no significant mass loss (Baraffe et al 2001) during their lifetime t_L for Population III stars, these stars will produce CIB of amplitude:

$$\nu I_{\nu} = \frac{3}{8\pi} \frac{1}{4\pi R_H^2} \frac{c^5}{G} \epsilon \Omega_{\text{baryon}} \frac{1}{t_L} \int f_* \langle \nu' b_{\nu'} \rangle \frac{dt}{1+z} \quad (34)$$

Note that in eq. 34, c^5/G is the maximal luminosity that can be achieved by gravitational processes. It enters there because ultimately the nuclear burning of stars is caused by gravity

as they evolve in gravitational equilibrium with the (radiation) pressure. Eq. 34, has a simple meaning illustrating its relative model-independence: the cumulative bolometric flux produced is $L_{\max} = c^5/G \simeq 10^{26} L_{\odot}$ distributed over the surface of the Hubble radius, $4\pi R_H^2$, times the model dependent, but more-or-less understood, dimensionless factors. The spectral distribution of the produced diffuse background will be determined by $\langle \bar{b}_{\nu} \rangle \equiv \int f_{*}(1+z)^{-1} b_{\nu} dt / \int f_{*}(1+z)^{-1} dt$ i.e. the mean SED averaged over the Population III era redshifts. The value of $L_{\max}/4\pi R_H^2$ is $\simeq 3 \times 10^8$ nW/m²/sr so even with small values of $\Omega_{\text{baryon}}, \epsilon, f_{*}$, the net flux from Population III stars could be indeed substantial.

The first stars had to form in the rare regions of the density field that reached the turn-around over-density while the bulk of the matter was still in linear regime (density contrast < 1). They would then turn-around and, if certain conditions are met, collapse and form the first generation of stars. For Gaussian density field, as is the case with the CDM models, this would specify the value of f_{*} at each time. It is perhaps a bit unexpected that the WMAP polarization measurements indicated that first stars started forming at $z_{*} = 20_{-9}^{+10}$, but the most straightforward explanation is that the earliest stars formed out of very high peaks of the density field leading to smaller f_{*} .

Once they turn around and begin to collapse the primordial clouds will quickly heat up to their virial temperature, T_{vir} , and only efficient cooling will enable isothermal collapse when gas pressure is smaller than gravity (or $T < T_{\text{vir}}$). The details of what determines collapse and formation of Population III stars are not yet clear, but molecular cooling seems critical in the initial stages of metal-free collapse. In general H_2 cooling is effective at $T \gtrsim 400$ K (Santos et al 2002), but some simulations suggest rotational H_2 cooling can effectively dissipate binding energy of the cloud only if $T > 2000$ K (Miralda-Escude 2003). The numbers that follow have thus been evaluated for $T_{\text{vir}} = 400$ K and 2000 K. The relation between comoving scale r , the mass contained by that radius and the virial temperature at the onset of the collapse is:

$$M = 3.6 \times 10^{11} \frac{\Omega}{0.3} \left(\frac{r}{1h^{-1}\text{Mpc}} \right)^3 h^{-1} M_{\odot} ; \quad T_{\text{vir}} = 36 \left(\frac{\Omega}{0.3} \right)^{1/3} \left(\frac{M}{M_{\odot}} \right)^{2/3} (1+z) \text{ K} \quad (35)$$

In the spherical linear approximation, the mass that at some early epoch, z_i , had density contrast ($\delta_{\text{col}} = 1.68$ times the growth factor between z_i and z) will collapse at redshift z . For Gaussian density field, the regions that collapse correspond to $\eta = \delta_{\text{col}} / [\langle \delta_M^2 \rangle]^{1/2} > 1$ standard deviations the value of $f_{*} \simeq \text{erfc}(\eta/\sqrt{2})$. The value of the RMS density contrast, $[\langle \delta_M^2 \rangle]^{1/2}$ at redshift z can be evaluated given the power spectrum of the assumed model (Λ CDM) normalized to large-scale CMB data and can be estimated from Fig. 3 and eqs. 35. Population III stars had to form out of $\eta \sim 2 - 3$ sigma rare fluctuations which for Gaussian distribution correspond to f_{*} varying between $\sim 5 \times 10^{-2}$ and $\sim 3 \times 10^{-3}$; departures from spherical symmetry would accelerate the collapse thereby decreasing η and increasing f_{*} . Because η is a decreasing function of decreasing z , and f_{*} is a (rapidly) increasing function of decreasing η , the average \bar{f}_{*} will be dominated by the late times of Population III evolution.

Fig. 22 shows the total bolometric flux evaluated according to eq. 34 evaluated for Λ CDM

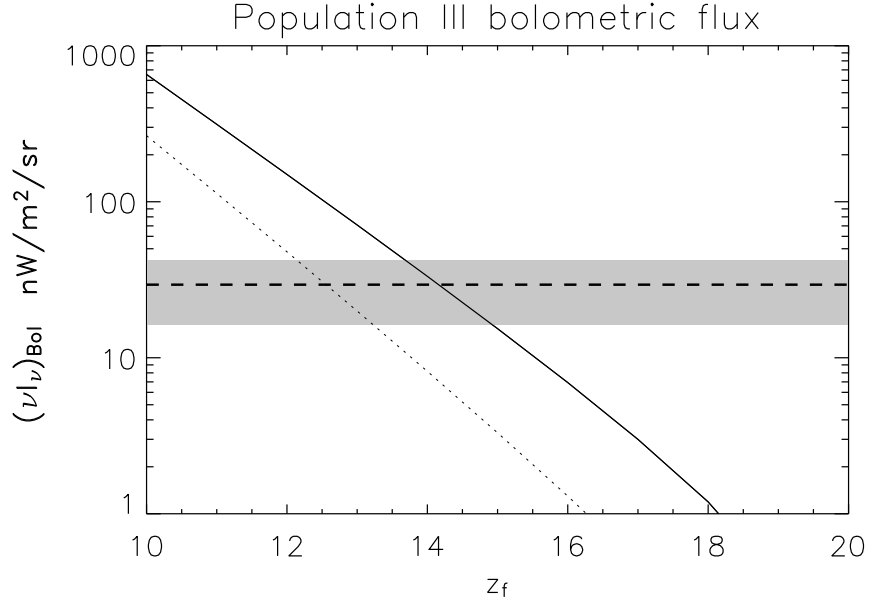


Fig. 22.— Bolometric flux produced from the Population III era lasting until the redshift z_f shown along the horizontal axis. Solid line assumes Population III stars form in collapsing regions with $T_{\text{vir}} = 400$ K and dashed line corresponds to $T_{\text{vir}} = 2000$ K. Shaded area shows the bolometric flux of the CIB excess at near-IR evaluated from Fig. 20 with its uncertainty.

model for $T_{\text{vir}} = 400$ K (solid line) and $T_{\text{vir}} = 2000$ K plotted vs the redshift marking the end of the putative Population III era, z_f . The lines in the figure assume that efficiency of Population III formation is regulated only by parameter f_* . The prediction for the total bolometric flux produced by Population III is fairly robust. On the other hand, the way it is distributed among the various bands or its energy spectrum depends on the details of how Lyman- α ionizing photons are absorbed and re-emitted along the line-of-sight. Santos et al (2002) model the redistribution of the total flux produced from the Population III era and produce good fits to the observed near-IR CIB at J and K bands. Clearly, in order to account for the near-IR CIB excess measured at $1-4 \mu\text{m}$, the diffuse bolometric flux from Population III stars must exceed the observed excess; any additional flux will then have to be redistributed to different wavelengths. This can be achieved if the Population III stars were massive and their era lasted at least until $z_f \sim 15$. Interestingly, the existence of the CIB excess at J band suggests that if this excess originated from the Population III era, the latter should have extended to $z \lesssim 14$.

This discussion suggests that Population III era could have produced CIB at levels comparable to those in Fig. 20, but it could also have produced substantially lower (or higher) fluxes, while the measurements of the CIB mean levels can be significantly affected by the systematics and be mistaken for the various residual errors. On the other hand, as is shown below, Population III stars, whose emission arises at epochs when the spatial spectrum of galaxy clustering is not yet evolved, should have produced a unique and measurable signature via the CIB fluctuations. It is

that signature, both its spectrum in the angular and energy frequency domain, that could provide the ultimate insight into the Population III epochs (Cooray et al 2004, Kashlinsky et al 2004).

7.3. Contribution to anisotropies in CIB

In order to evaluate the amplitude and spectrum of the CIB from Population III era we start with the density field of the Λ CDM model. For reference, a 1 arcminute angular scale subtends comoving scale $\simeq 1.5h^{-1}\text{Mpc}$ between $z = 6$ and $z = 15$ for WMAP cosmological parameters and equation of state with $w = -1$. As Fig. 3 shows, on sub-arcminute scales the density field is in quasi-linear to non-linear regime (density contrast $\gtrsim 0.2$) for the Λ CDM model. There the spectrum due to clustering evolution was modified significantly over that of the linear Λ CDM spectrum, and the fluctuations amplitude has increased from its primordial value especially since the effective spectral index on these scales for Λ CDM model was $n \lesssim -2$.

At $z = 20$ the Universe is $\sim 2 \times 10^8$ years old which is much larger than the age of the individual Population III stars, $t_L \sim 3 \times 10^6$ years. If Population III era lasted for only one generation forming at z_* , the CIB fluctuations will be $\delta_{\text{CIB}} \sim \sqrt{\pi}\Delta(qd_A^{-1}; z)|_{z_*}$, where $\Delta(k)$ is given by eq. 12. In what follows we define t_* as the time-length of the period in which Population III stars were the dominant luminosity sources in the Universe.

Several points are worth noting about eq. 11 when applied to Population III era: 1) For given amplitude of the mean CIB levels from Population III, the value of $\Delta(k)$ is inversely proportional to $\sqrt{t_*}$ and thus measures the duration of the Population III era. The density perturbations grow with decreasing z , thus most of the contribution to the integral in eq. 10 comes from the low end of z over some range of b_ν . At some wavelengths the overall dependence on t_* wins out at some (shortest NIR) wavelengths and the longer the Population III phase, the smaller are the relative fluctuations of the CIB from them. 2) In the Harrison-Zeldovich regime of the power spectrum, $P_3 \propto k$, one would have $\delta_{\text{CIB}} \propto q^{1.5}$. 3) The transition to the Harrison-Zeldovich regime occurs in the linear regime at all relevant redshifts and happens at the co-moving scale equal to the horizon scale at the matter-radiation equality. All this would allow probing of the Population III era, its duration, and the primordial power spectrum at high redshifts on scales that are currently not probed well. Interestingly, short duration of the Population III will lead to smaller CIB flux, but larger relative fluctuations and vice versa.

In addition to the small angular scale increase due to non-linear gravitational evolution, the fluctuations in the clustering distribution of Population III systems will be amplified because, within the framework of the Λ CDM model these systems had to form out of rare peaks of the primordial density field (Kaiser 1984, Jensen & Szalay 1986, Politzer & Wise 1996, Kashlinsky 1987, 1991, 1998). This leads to biased (enhanced) 2-point correlation function of the Population III regions, ξ_b over that of the underlying density field, $\xi(r) = \frac{1}{2\pi^2} \int P_{\Lambda\text{CDM}}(k)k^2 j_0(kr)dk$. In the Λ CDM model the Population III stars at $z \sim 10 - 20$ will form in regions having $\eta > 1$. In this limit the biasing

factor given by eq. 29 of Kashlinsky (1998) reduces to check:

$$\xi_b = \frac{1}{2} \left[\exp \left(\frac{\eta^4}{\delta_{\text{col}}^2} \xi \right) - 1 \right] \quad (36)$$

In the limit of $\xi \rightarrow 0$ this reduces to the more familiar form of $\xi_b(r) \simeq \frac{\eta^4}{2\delta_{\text{col}}^2} \xi(r)$. We adopt eq. 36 in evaluating the numbers below.

There will also be shot-noise fluctuations due to individual Population III systems entering the beam. The relative magnitude of these fluctuations will be $N_{\text{beam}}^{-1/2}$, where N_{beam} is the number of the Population III systems within the beam. This component may be important at very small angular scales, where $N_{\text{beam}} \sim 1$, and will contribute to the power spectrum: $P_{\text{SN}} = \frac{1}{n_2}$, where $n_2 = c \int n_* d_L^2 (1+z)^{-1} dt$ is the projected angular number density of Population III systems. The detection of the shot-noise component in the CIB power spectrum at small angular scales will give a direct measure of both the duration of the Population III era and constrain the makeup and masses of the Population III systems. Calculations show that unless the Population III era was very short, the shot noise correction to the CIB would be small on scales greater than a few arcseconds (Kashlinsky et al 2004).

Because of the Lyman absorption by the surrounding matter prior to reionization, essentially all the flux emitted by Population III stars at rest wavelength less than 912 Å will be absorbed by the Lyman continuum absorption in the surrounding medium (Gunn & Peterson 1965, Yoshii & Peterson 1994, Haiman 2002, Santos 2004) and the contribution to the CIB will be cut-off at $\lambda < 912(1+z_f)$ Å. At longer wavelengths the flux, including emission from the nebulae around each star, will propagate without significant attenuation. Population III stars emit as black bodies at $\log T \simeq 4.8 - 5$ (Schaerer 2002) and the Lyman limit at $z \sim 20$ is shifted to $\sim 2\mu\text{m}$ at $z = 0$. The 2MASS J band filter contains emission out to $1.4 \mu\text{m}$ and represents the shortest wavelength where excess in the CIB over that from ordinary galaxies has been measured (Kashlinsky & Odenwald 2000, Cambresy et al 2001, Kashlinsky et al 2002, Odenwald et al 2003). If the measured excesses in CIB fluctuations and isotropic component at J band are indeed attributable to Population III, their era must have lasted until $z \lesssim 14$.

Fig. 23 shows the resultant CIB fluctuations from Population III stars from 1.25 to $8 \mu\text{m}$. The fluctuations are normalized to reproduce the CIB excess at $2.2 \mu\text{m}$ of $10 \text{ nW m}^{-2} \text{sr}^{-1}$. All Population III stars were assumed to start forming at $z = 20$, but differently colored lines correspond to different values of z_f , the redshift of the end of Population III era. Because of the Lyman continuum absorption there would be no appreciable CIB fluctuations at J band if $z_f \lesssim 14$ (no blue lines) and the contribution at J band will come from $z \sim 13$, rather than $z = 20$. Taken at face value, the presence of excess CIB fluctuations in J band indicates that the Population III stars were possibly the dominant sources of luminosity until $z_f \lesssim 14$.

7.4. Can CIB anisotropies from Population III be measured?

Both DIRBE and 2MASS data indicate CIB anisotropies at amplitudes larger than the contribution from ordinary galaxy populations (Kashlinsky & Odenwald 2000, Kashlinsky et al 2002, Odenwald et al 2003) and are consistent with significant contributions due to Population III. However, because the measured signal contains contributions from remaining galaxies (all galaxies for DIRBE and $K \geq 19$ galaxies for 2MASS), it is difficult to isolate the contribution from the Population III stars.

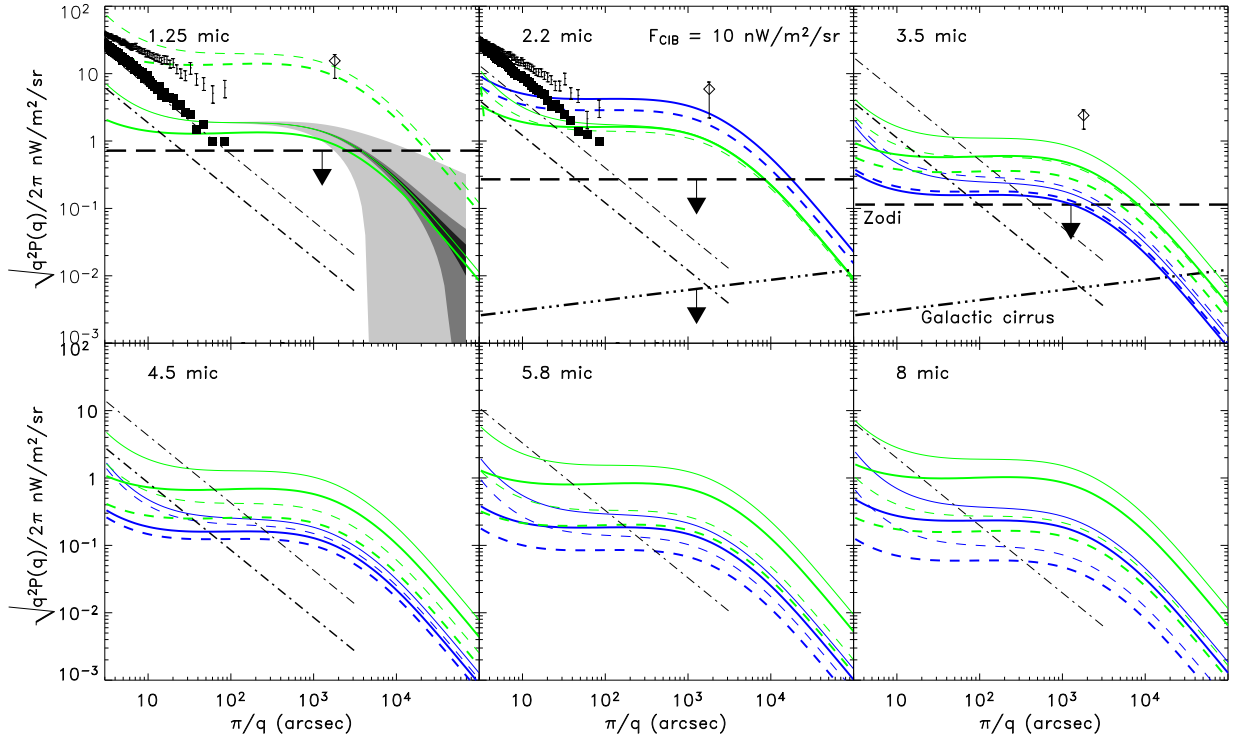


Fig. 23.— CIB fluctuations, $\sqrt{q^2 P_2/2\pi}$, from Population III stars forming at $z_* = 20$ are shown with colored lines. Blue and green lines correspond to Population III era ending at $z_f = 15$ and 10 respectively. Thick and thin colored lines correspond to the two extremes of Population III SED modeling after Santos et al (2002) and shown in Fig. 21. Solid and dashed colored lines correspond Population III forming in haloes with $T_{\text{vir}} \geq 400\text{K}$ and $T_{\text{vir}} \geq 2000\text{K}$. Filled squares at 1.25 and 2.2 μm show residual atmospheric fluctuations from ground based 2MASS measurements after 1 hour of exposure from Odenwald et al (2003). Thick long dashes are adopted from Kashlinsky et al (2004) and denote the upper limit on zodiacal light fluctuations from (Ábrahám et al 1997) scaled to the corresponding band. Thick dashed-triple-dotted line denotes cirrus fluctuations: these are upper limits at 2.2 micron and an estimate from (Kiss et al 2003) at 3.5 micron. Dot-dashed lines correspond to shot noise from galaxies fainter than AB magnitude = 22 (thickest), and $m_{\text{AB}} = 20$ (thin). Diamonds with error bars show the CIB fluctuations at $\sim 0.7^\circ$ from the COBE DIRBE fluctuations analysis (Kashlinsky & Odenwald 2000). Note that because of the large DIRBE beam, these results include contribution from all galaxies as well as other sources such as Population III. The K band CIB fluctuation from deep integration 2MASS data is shown at the largest scale accessible to those data with \times ; the 2MASS data shown in the figure were taken for the patches for which galaxies were removed brighter than $K \simeq 19$ (Kashlinsky, Odenwald et al 2002, Odenwald, Kashlinsky et al 2003). The cosmic variance 1-sigma uncertainty is shown with shaded regions for 1.25 μm . The darkest shade corresponds to a total of 1,000 deg^2 observed, and the lighter shade corresponds to a total of 100 deg^2 .

Population III stars, if massive, should have left a unique and measurable signature in the near-IR CIB anisotropies over angular scales from ~ 1 arcminute to several degrees as Fig. 23 shows. Detection of these fluctuations depends on the identification and removal of various foreground emission (and noise) contributions: atmosphere (for ground-based measurements), zodiacal light from the Solar system, Galactic cirrus emission, and instrument noise.

Kashlinsky et al (2004) discuss observability of the Population III CIB fluctuations vs the confusion arising from the various foregrounds. The confusion may arise from 1) Galactic cirrus emission, 2) galaxies with ordinary stellar populations not removed from the data, 3) zodiacal light fluctuation, and 4) atmospheric fluctuations from ground measurements. They estimated the contributions from the various foregrounds to the fluctuations from 1 to $3.5 \mu\text{m}$. The numbers from their discussion are plotted in the top panels of Fig. 23.

Below is brief discussion of the various contaminants when searching for the CIB fluctuations from the Population III era:

- *Atmosphere*: Filled squares in Fig. 23 show the residual atmospheric fluctuations at 1.25 and $2.2 \mu\text{m}$ on sub-arcminute scales after one hour of integration from one of the deep 2MASS fields measurements (Odenwald, Kashlinsky et al 2003). Atmospheric gradients become important on larger angular scales ($\gtrsim 0.05 - 0.1^\circ$) and their effects can be highly variable on a wide range of time scales (e.g. Adams & Skrutskie 1995, <http://pegasus.phast.umass.edu/adams/airglowpage.html>) making detection of arcminute and degree scale CIB fluctuations difficult in ground based observations. Yet these problems can be completely avoided with space-based experiments.

- *Ordinary galaxies* must be eliminated to sufficiently faint levels so that the remaining fluctuations in their cumulative emission are sufficiently small. The dashed-dotted lines in Fig. 23 show the shot-noise fluctuations estimated from the observed deep counts from 1 to $8 \mu\text{m}$. Thin lines correspond to galaxies brighter than $m_{\text{AB}} = 20$ identified and removed and thick lines when the same is possible out to $m_{\text{AB}} = 22$. One can see that ideally one would have to identify galaxies out to $m_{\text{AB}} \gtrsim 23 - 24$ in order to measure the CIB fluctuations from Population III era across the entire range of scales.

- *Zodiacal light* emission from interplanetary dust (IPD) is the brightest foreground at most IR wavelengths over most of the sky. There are some structures in this emission associated with particular asteroid families, comets, and an earth-resonant ring, but these structures tend to be confined to low ecliptic latitudes or otherwise localized. The main IPD cloud is generally modeled with a smooth density distribution. Observationally, intensity fluctuations of the main IPD cloud have been limited to $< 0.2\%$ at $25 \mu\text{m}$ (Ábrahám et al 1997). Extrapolating this limit to other DIRBE wavelengths using the observed mean high-latitude zodiacal light spectrum from COBE DIRBE (Kelsall et al 1998), Kashlinsky, Arendt et al (2004) arrive at the limits shown in Figure 23. Because the Earth is moving with respect to (orbiting within) the IPD cloud, the zodiacal light varies over time. Likewise, any zodiacal light fluctuations will not remain fixed in celestial coordinates. Therefore repeated observations of a field on timescales of weeks to months should be

able to distinguish and reject any zodiacal light fluctuations from the invariant Galactic and CIB fluctuations. The upper limit on zodiacal light fluctuations can be evaluated also at the bottom panels of Fig. 23 using extrapolations of the DIRBE- measured zodiacal light spectrum from Fig. 4. The zodiacal light is expected to be very smooth at all the near-IR bands.

- *Galactic cirrus.* Intensity fluctuations of the Galactic foregrounds are perhaps the most difficult to distinguish from those of the CIB. Stellar emission may exhibit structure from binaries, clusters and associations, and from large scale tidal streams ripped from past and present dwarf galaxy satellites of the Milky Way. At long IR wavelengths, stellar emission is minimized by virtue of being far out on the Rayleigh–Jeans tail of the stellar spectrum (apart from certain rare classes of dusty stars). At near-IR wavelengths stellar emission is important, but with sufficient sensitivity and angular resolution most Galactic stellar emission, and related structure, can be resolved and removed. IR emission from the ISM (cirrus) is intrinsically diffuse and cannot be resolved. Cirrus emission is known to extend to wavelengths as short as $3 \mu\text{m}$ (Arendt et al 1998). Statistically, the structure of the cirrus emission can be modeled with power-law distributions. Using the mean cirrus spectrum, measurements made for the cirrus fluctuations in the far-IR with ISO (Kiss et al 2003) were scaled all the way to $3.5 \mu\text{m}$ by Kashlinsky, Arendt et al (2004), providing the estimated fluctuation contribution from cirrus that is shown in Figure 23. The extrapolation to shorter wavelengths is highly uncertain, because cirrus (diffuse ISM) emission has not been detected at these wavelengths, and the effects of extinction may become more significant than those of emission, but cirrus contribution is generally expected to be several orders of magnitude lower than the CIB fluctuations (Arendt et al 1998). We do not show the expected cirrus fluctuations at the wavelengths corresponding to the bottom panels of Fig. 23 as the simple extrapolations of the cirrus SED from Fig. 4 may be inadequate due to the presence of PAH emission at these wavelengths.

Figure 23 shows that CIB fluctuations from Population III would be the dominant source of diffuse light fluctuations on arcminute and degree scales even if Population III stars epoch was briefer, and their diffuse flux smaller, than the current CIB numbers suggest. Their angular power spectrum should be very different from other sources of diffuse emission and its measurement thus presents a way to actually discover Population III and measure the duration of their era and their spatial distribution. The latter would provide direct information on primordial power spectrum on scales and at epochs that are not easily attainable by conventional surveys. This measurement would be imperative to make and is feasible with the present day space technology.

The previous discussion suggests that CIB fluctuations from the Population III era are observable, but because of the large-scale atmospheric gradients, space observations are required for detection. The following is needed:

- 1) In order to make certain that the signal is not contaminated by distant ordinary galaxies with normal stellar populations, one would need to conduct a deep enough survey in order to identify and eliminate ordinary galaxies from the field. In practice, as Fig. 9 indicates, going to $m_{\text{AB}} \simeq 24$ would be sufficient.

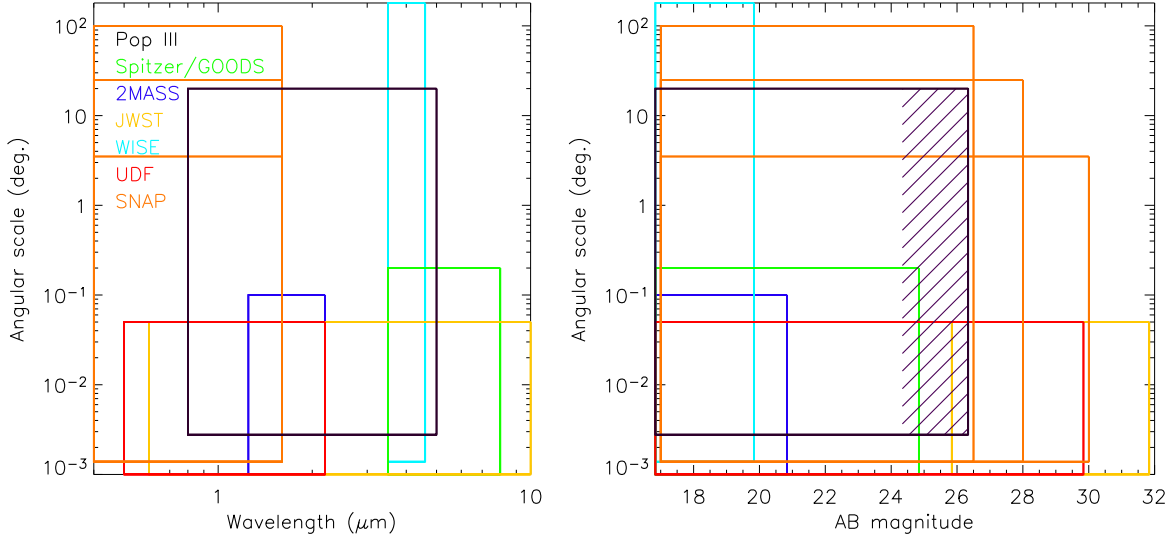


Fig. 24.— Black rectangular box shows the regions of the parameters required for a space mission to measure the CIB anisotropies from Population III. Cross-hatched region in the right panel displays the magnitude range where Population III stars are expected to dominate CIB anisotropies. Other colors correspond to the currently existing datasets or planned NASA missions which can be utilized for this purpose: red is the Hubble Deep Field from HST (<http://www.stsci.edu/ftp/science/hdf/hdf.html>), dark blue is for the deep 2MASS data (15; 20), green is the NASA’s *Spitzer* GOODS project (<http://www.stsci.edu/ftp/science/goods/>), light blue corresponds to the planned NASA WISE MIDEX mission (<http://www.astro.ucla.edu/~wright/WISE>), yellow corresponds to the field-of-view of the NASA James Webb Space Telescope planned for the end of the decade (<http://jwst.gsfc.nasa.gov>) and orange color to the three surveys planned by SNAP (<http://snap.lbl.gov>).

2) A direct signature of Population III signal is that there should be a Gunn-Peterson Lyman-break feature in the spectral energy distribution of the CIB fluctuations, i.e. at wavelengths $\leq 912(1+z_f)^{-1}$ Å. That spectral drop would provide an indication of the epoch corresponding to the end of the Population III era. At longer wavelengths the spectral energy distribution of the CIB fluctuations would probe the history of energy emission and its re-distribution by the concurrent IGM. At wavelengths $\gtrsim 10\mu\text{m}$ zodiacal light fluctuations may become dominant. Hence one would want $0.9\mu\text{m} \lesssim \lambda \lesssim 5 - 10\mu\text{m}$.

3) On angular scales from a few arcminutes to $\sim 10^\circ$ Population III would produce CIB anisotropies with a distinct and measurable angular spectrum, but its measurement will be limited by the cosmic or sampling variance. Calculations show that for reliable results on scales up to θ one would need to covers area a few times larger (Kashlinsky et al 2004). Shaded regions in the upper left panel of Fig. 23 show that in order to get reliable results on scales up to $\theta \gtrsim 1^\circ$ one would need to observe areas of $\gtrsim 10^\circ$ across.

Fig. 24 shows the parameters a space-based survey should have in order to probe Population III CIB anisotropies and compares it with the currently planned space missions. The left panel shows the projection on the (angular scale)–wavelength plane; the right panel shows the projection onto the (angular scale)–sensitivity plane. Clearly, such a Population III experiment needs to have

a wide field-of-view (FOV) and at the same time have good angular resolution (preferably up to a few arcseconds). The sensitivity requirements were taken to reach the ability to identify and eliminate from the data ordinary galaxies that at all the near-IR wavelengths contribute $\sigma_{\text{sn}} \lesssim 1 \text{ nWm}^{-2}\text{sr}^{-1}$; Fig. 18 shows that this is reachable at $m_{\text{AB}} \gtrsim 24$ which with modern technologies and a $\sim 0.5 \text{ m}$ mirror is achievable from space in $\sim 1 \text{ hr}$ integrations. None of the currently planned surveys cover perfectly the required range of parameters, although a combination of various missions instruments may do a part of the job. Cooray et al (2004) propose a rocket experiment similar to an earlier experiment by Xu et al (2002) with an FOV of a few degrees and $\sim \text{arcmin}$ resolution, whereas Kashlinsky et al (2004) argue for a dedicated space mission based on the existing detector technologies.

8. Snapshot of the future

It is important to resolve as much of the CIB as possible into individual contributors and isolate the contributions to the total mean flux and anisotropies by the cosmic epoch. It is also important to isolate the epochs from which luminous sources contribute to the part of the CIB which remains unresolvable by contemporary instruments and techniques. Significant progress in these directions is expected to happen with the current (Spitzer) and planned space missions which should cover larger scales, have better angular resolution and go deeper across the entire range of the IR spectrum. In this section we give a brief overview of the IR missions and their potential for CIB studies.

Spitzer

The Spitzer telescope (initially known as SIRTF - Space InfraRed Space Facility) has been launched aboard a Boeing Delta II rocket in August 2003. The telescope carries three instruments: InfraRed Array Camera (IRAC), Multiband Imaging Photometer (MIPS) and InfraRed Spectrograph (IRS). IRAC is a four-channel camera that provides simultaneous $5.12' \times 5.12'$ images. The pixel scale is $1.2''$ in all IRAC bands. The Multiband Imaging Photometer for SIRTF (MIPS) is designed to provide very deep imaging and mapping at 24, 70, and $160 \mu\text{m}$. In integrations of 2000 seconds, it reaches $5-\sigma$ detection limits at these wavelengths of 0.2, 0.5, and 8 mJy, respectively. The pixel scale is $2.4''$ at $24 \mu\text{m}$, $4.5''$ at $70 \mu\text{m}$ and $15''$ at $160 \mu\text{m}$.

On the observational side the following surveys have already been approved by the Spitzer Legacy⁸ and Director's Discretionary⁹ programs:

⁸<http://ssc.spitzer.caltech.edu/legacy/>

⁹<http://ssc.spitzer.caltech.edu/fls/>

- **First Look Survey:** The extragalactic component of the First Look Survey (FLS) is intended to reach the 1-sigma sensitivities of $\simeq 10\mu\text{J}$ with IRAC and 1 to 27 mJy with MIPS over a 4 sq. deg. and a 1 sq. deg. field. A smaller 0.25 sq. deg. region will be covered with 10 times the nominal integration time. Although the survey is very shallow, the $160\ \mu\text{m}$ data are already expected to be confusion limited even for this shallow survey.
- **SWIRE:** The SWIRE project (Lonsdale et al 2004) will cover 7 fields between 5 and 15 sq. deg. in size with sensitivities that are several times better than the FLS. A stated goal of the SWIRE project is to investigate galaxy formation in the $0.5 < z < 2.5$ range.
- **GOODS:** The GOODS project ¹⁰ will observe 300 square arcmin divided into two fields: HDF North and Chandra Deep Field South. Mean exposure time per position is 25 hours per band with IRAC. At $24\ \mu\text{m}$, MIPS will obtain 10 hour exposures, if on orbit experience shows that this will be a distinct advantage over planned Guaranteed Time Observations (GTO). MIPS GTO proposals for these regions at 70 and $160\ \mu\text{m}$ are sufficiently deep, that the GOODS project will not duplicate these observations. If it will prove useful, the GOODS observations will also include an ultra-deep field in the HDF-N region with up to 100 hours of integration. The GOODS team intends to use the resolved galaxy counts, which should include L^* galaxies to redshifts to $z = 5$, to establish the best lower limits on the $3.6 - 24\ \mu\text{m}$ mean CIB.

On the data analysis side of the long term programs, the National Science Foundation has approved:

- **LIBRA**, or Looking for Infrared Background Radiation Anisotropies, ¹¹ is an NSF-supported 5 year project to measure CIB anisotropies from early epochs. The integrated light of all galaxies in the deepest counts to date fails to match the observed mean level of the CIB, indicating a significant high-redshift contribution to the CIB. The project will use the Spitzer and deep 2MASS data at $1 - 160\ \mu\text{m}$ to measure the spatial fluctuations of this residual high- z portion of the CIB. Analysis of these spatial fluctuations will provide information on the luminosity of the early universe, and on the developing structure of galaxies and clusters of galaxies at early epochs.

Astro-F

Japan's Astro-F or the Infrared Imaging Surveyor (IRIS) is an infrared astronomy mission scheduled for launch in 2005 into a sun-synchronous polar orbit. IRIS employs a 70 cm telescope cooled to 6 K using liquid helium. ASTRO-F is designed for advanced surveys with two observation modes. The first is a general survey, one rotation in one orbital period, which is used for the all sky survey. The second is a pointing mode for imaging and spectroscopic observations of a limited

¹⁰<http://www.stsci.edu/science/goods>

¹¹<http://haiti.gsfc.nasa.gov/kashlinsky/LIBRA>

region of the sky. Two focal-plane instruments are installed. One is Far-Infrared Surveyor (FIS) and the other is Infrared Camera (IRC). The FIS is a photometer optimized for all-sky survey with far-infrared arrays, and is expected to produce catalogs of infrared sources with much better sensitivity and higher angular resolution than the IRAS. The FIS can be operated as an imager or a Fourier-transform spectrometer in the pointing mode. The IRC is a three-channel camera that covers the wavelength bands from $2 \mu\text{m}$ to $25 \mu\text{m}$, and has the capability to perform low-resolution spectroscopy with prisms/grisms on filter wheels. The field of view of the IRC is 10 arcmin and the spatial resolution is approximately 2 arcsec. Large format arrays are used to attain the deep survey with wide field and high angular resolution. IRC observations are carried out only in pointing mode.

The detection limits will be 1 - 100 μJy in the near-mid infrared and 10-100 mJy in the far infrared. It is planned to conduct a large area (~ 4 square degree) survey at the K and L bands for CIB studies.

WISE

WISE (Wide-field Infrared Survey Explorer)¹² has been selected as NASA's next Medium-Class Explorer (MIDEX) mission with a tentative launch date in 2008. It will have four bands at 3.5, 4.6, 12 and $23 \mu\text{m}$ with $\simeq 3''$ pixels. During its 6 month mission WISE satellite will provide an all-sky coverage about 1,000 more sensitive than IRAS. It should detect ULIRGs out to $z \sim 3$ and bright L_* IR galaxies out to $z \sim 1$.

Herschel and Planck

The European Space Agency's Herschel Space Observatory¹³ (formerly called Far Infrared and Submillimetre Telescope, or FIRST), with an anticipated launch in 2007, will be the first space observatory covering the full far infrared and sub-millimeter waveband, and its passively cooled telescope will have a 3.5 meter diameter mirror. It will be located at L2 and will provide photometry and spectroscopy in the 57 to $670 \mu\text{m}$ range (Pilbratt 2004). The Observatory will have 3 instruments: The Photodetector Array Camera and Spectrometer (PACS), the Spectral and Photometric Imaging REceiver (SPIRE) instrument, and the Heterodyne Instrument for the Far Infrared (HIFI) instrument. SPIRE is made of two sub-instruments: a three-band imaging photometer operating at 250, 360 and $520 \mu\text{m}$, and an imaging Fourier Transform Spectrometer (FTS) covering 200-670 μm . The field of view of the photometer will be $4' \times 8'$, observed simultaneously in the three spectral bands. An internal beam steering mirror allows spatial modulation

¹²<http://wise.ssl.berkeley.edu/>

¹³<http://astro.esa.int/herschel/>

of the telescope beam and will be used to jiggle the field of view in order to produce fully-sampled images. Observations can also be made by scanning the telescope without chopping. In addition to pointed imaging and spectroscopy of distant galaxies, it is planned that the telescope will conduct deep confusion limited surveys of $\gtrsim 100$ deg 2 of the sky.

Planck satellite ¹⁴ is designed mainly for CMB measurements and will be launched together with Herschel. Its High Frequency Instrument (HFI) has bands at 350, 550, 850 and 1380 μm with resolution of 10 to 5 arcminutes and will be useful for CIB studies. Its all sky survey will probably be too shallow to constrain galaxy evolution, but will give good measurements of the bright end of galaxy counts. With its scanning strategy Planck will survey some high Galactic latitude areas much deeper (a factor ~ 3 in flux) and they could be useful for studies of the far-IR to sub-mm CIB fluctuations at arcminute to degree angular scales.

JWST

Successor to the Hubble Space Telescope, the James Webb Space Telescope ¹⁵ is a large, infrared-optimized space telescope scheduled for launch in August, 2011 (Sabelhaus & Decker 2004). JWST will have a large mirror, 6.5 meters in diameter. It will reside in an L2 Lissajous orbit. It will have two instruments of direct relevance to CIB science: the NIR camera (NIRCAM) and the MIR Instrument (MIRI). The NIRCAM will cover wavelengths from 0.6 to 5 μm with 0.03 arcsec/pixel resolution from 0.6 to 2.3 μm and 0.064 arcsec/pixel at 2.3 to 5 μm . The MIRI will provide the JWST with imaging and spectroscopy at wavelengths from 5 through 27 microns with ~ 0.2 arcsec/pixel. The FOV will be $\simeq 1.5' \times 1.5'$. The telescope will be able to detect Lyman break galaxies out to $z \gtrsim 10$ and supernovae out to $z \gtrsim 20$ (Gardner et al 2004). Its science goals in cosmology will be to identify the end of dark ages and the assembly of galaxies at observer bands from visible to mid-IR.

SNAP

The SuperNovae Acceleration Probe (SNAP), or the Joint Dark Energy Mission, ¹⁶ is planned as a combined DOE and NASA space mission designed to probe the equation-of-state of the Universe with high z supernovae out to $z \sim 2$ (Aldering et al 2004). It is scheduled tentatively for launch early in the next decade. SNAP will cover wavelengths from visible to 1.7 μm and will be useful for NIR CIB studies. Panoramic, wide and deep surveys are currently planned to cover up to $\sim 10^4$, 1000 and 15 deg 2 and will go to AB magnitudes of $\sim 26.5, 28$ and 30 respectively. Fig. 24

¹⁴<http://www.rssd.esa.int/Planck>

¹⁵<http://www.jwst.nasa.gov>

¹⁶<http://snap.lbl.gov>

shows that these SNAP surveys at the longest SNAP wavebands should be very useful in uncovering the potential high- z contribution to the CIB fluctuations at $\lesssim 1.5 \mu\text{m}$ including from Population III.

SCUBA-2, SOFIA, ALMA

SCUBA-2¹⁷ will replace the current SCUBA on the James Clerk Maxwell Telescope in 2006. It will have a total of $\sim 10,000$ bolometers and offer simultaneous imaging of a 50 arcmin^2 FOV at 450 and $850 \mu\text{m}$ mapping the sky up to 1,000 times faster than the current SCUBA array (Audley et al 2004).

The Stratospheric Observatory for Infrared Astronomy (SOFIA)¹⁸ is under development by NASA, and is expected to have its initial science operations in early 2007. This observatory, with its 2.5 m telescope, operates at 41,000 to 45,000 feet aboard a Boeing 747 aircraft, providing access to much of the far-IR spectrum. It will provide complementary capabilities to the Spitzer Space Telescope, permitting higher spatial resolution, and hence lower confusion limits at far infrared wavelengths. The High Angular Resolution Widefield Camera (HAWC) provides imaging capability at 50, 90, 160, and $215 \mu\text{m}$. Surveys are planned to detect high redshift galaxies (D. A. Harper, private communication). The instrument will reach the confusion limit in about 40 hours, so such observations will be carried out over very limited areas. The instrument will be useful to follow up observations of high redshift sources detected by Spitzer or other surveys.

The Atacama Large Millimeter Array (ALMA)¹⁹ in Chile is planned as a synthesis radio telescope built in international collaboration between North America and Europe which will operate at millimeter and sub-mm wavelengths. It will reach resolution of $\lesssim 1''$ over fields of several square arcmin.

SAFIR, SPIRIT, SPECS

Planned for the end of the next decade these prospective NASA missions will achieve both high angular resolution (arcsecond to sub-arcsecond) and high sensitivity ($\sim \mu\text{Jy}$) necessary to resolve and characterize most of the sources comprising the cosmic infrared background at far-IR and sub-mm wavelengths.

¹⁷<http://www.jach.hawaii.edu/JACpublic/JCMT/scuba/scuba2/>

¹⁸<http://sofia.arc.nasa.gov/Sofia/>

¹⁹<http://alma.nrao.edu> and <http://www.eso.org/projects/alma/>

Recommended by the National Academy of Sciences Decadal Review ²⁰ SAFIR ²¹ stands for a Single Aperture Far-Infrared observatory (Lester et al 2004). It is a large cryogenic space telescope scheduled for launch around 2015 to 2020. The SAFIR telescope will operate between 20 μm and 1 mm and will be cooled to about 5 K. The combination of large mirror size and cold temperature will make SAFIR significantly more sensitive than the Spitzer and Herschel instruments with sensitivity limited only by the irreducible noise of photons in the astrophysical backgrounds.

In the Community Plan for Far-IR/Submillimeter Space Astronomy ²² it is envisaged that SAFIR will be followed by a kilometer baseline FIR interferometer designed to provide both wide field-of-view imaging and spectroscopy. This interferometer is widely known as the Sub-millimeter Probe of the Evolution of Cosmic Structure (SPECS). SAFIR and SPECS were selected for study under the ROSS/Vision Mission study program, and the Space Infrared Interferometer Telescope (SPIRIT), a science pathfinder for SPECS, was selected for study under the NASA ROSS Origins Science mission concept study program. These will be the first instruments that would achieve sub-arcsecond resolution at FIR/sub-mm wavelengths and provide the μJy -level sensitivity over a field-of-view of $\sim 1 \text{ arcmin}^2$ (Leisawitz 2004). All three observatories, in addition to high sensitivity and resolution, will have spectral resolution of the order of $R \sim 1000$.

9. Concluding remarks

Cosmic Infrared Background presents a complementary, and sometimes the only, way to detect cumulative emission from galaxies at all cosmic times, including from objects inaccessible to current or future telescopic studies. Thanks to better detector sensitivities and new measurement techniques it is now possible to identify and remove foreground emissions at IR wavelengths and begin to measure the CIB. Because of the difficulties in identifying the mean level of the CIB in the presence of strong foreground emissions, it is often useful to attempt to measure the CIB fluctuations spectrum. The latter also allows to isolate the contributions to the CIB from progressively fainter galaxies and, on average, earlier cosmic epochs from surveys with $\sim \text{arcsec}$ angular resolution.

We have reviewed how mean levels of the CIB and, both the amplitude and the angular spectrum of, its anisotropies relate to the properties of the underlying galaxy populations. The various foreground contributions and the latest measurements of the mean CIB and its fluctuations were summarized from the near-IR to sub-mm. There are mutually consistent detections of the

²⁰Astronomy and Astrophysics in the New Millennium 2001, National Research Council
<http://www.nap.edu/books/0309070317/html/>

²¹<http://safir.jpl.nasa.gov/>

²²in Proceedings “New Concepts for Far-Infrared/Submillimeter Space Astronomy”, eds. D.J. Benford and D. Leisawitz (Washington, DC: NASA), NASA CP-2003-212233, pp. XV-XXV (2003)

mean levels and fluctuations of the CIB in the near-IR, low upper limits in the mid-IR and detections of the mean CIB in the far-IR longward of $100 \mu\text{m}$.

There are two broad classes of contributors to the CIB: from 'ordinary' (metal rich) stellar populations and from objects from the Population III era. The data on the present-day galaxy luminosity density present an important normalization point for interpretation of the CIB measurements. We showed that by constructing realistic SEDs for the stellar component one can get a fair agreements between the different luminosity density measurements at various wavelengths. This implies that it is unlikely that significant flux is unaccounted for in galaxy measurements at different bands and with different instruments and methods, and the results are consistent with the independently derived measurements of the present-day stellar density parameter, Ω_* . The same holds true at longer wavelengths where emission from dust is the dominant contributor.

Total flux from observed ordinary galaxy populations gives a lower limit on their contribution to the CIB and can be estimated from a variety of galaxy counts data from the near-IR to sub-mm bands. We summarized such estimates based on various most recent measurements and conclude that 1) at far-IR wavelengths the observed background is most likely accounted for by the observed galaxy populations, which are probably located at $z \gtrsim 1 - 2$; 2) at mid-IR wavelengths the total fluxes saturate at levels which are just below the best current upper limits on the CIB and probably account for at least a large fraction of the CIB; 3) at near-IR wavelengths the total contributions from the observed galaxy population saturate at levels significantly lower than the claimed detections of the CIB mean levels and anisotropies. The latter detections, if taken at face value, would indicate substantial contributions from much earlier epochs than probed by the observed faintest galaxy populations.

A plausible candidate to explain the excess in the near-IR CIB would be emissions from Population III era objects. Their expected contributions should have left a unique and observable signature in the spectrum of the CIB anisotropies if Population III were massive stars as is currently expected. The contributions from the various foreground emissions are such that this signature can, and should be, observed with future space-based instruments and properly tuned observations.

Finally, the current (Spitzer) and planned space missions and new instruments in the IR and sub-mm are expected to bring a wealth of high quality observational data. This data can and, no doubt, will be used for further progress in the CIB studies and in identifying the history of light emission from collapsed objects in the early Universe.

Acknowledgments

I am grateful to my collaborators on the CIB-related topics who have contributed much to the results discussed in this review. In alphabetical order they are: Rick Arendt, Roc Cutri, Jon Gardner, Mike Hauser, Raul Jimenez, John Mather, Harvey Moseley, Sten Odenwald, Mike Skrutskie. In addition to them, over the years I have benefited from many useful discussions and

correspondence with Dominic Benford, Eli Dwek, Dale Fixsen, Tom Kelsall, Alex Kutyrev, Toshio Matsumoto, Bernard Pagel. I am grateful to the following people who have supplied some of the data shown in the figures above: Rick Arendt (IRAC galaxy counts), Dale Fixsen (FIRAS spectral response), Tom Jarrett (2MASS star counts), Drs. Iwamuro and Maihara (Subaru deep counts), Dr Toshio Matsumoto (IRTS results), Lucia Pozzetti and Piero Madau (HDF galaxy counts), Mike Santos and Mark Kamionkowski (Population III SED spectra). I thank David Leisawitz for fruitful discussions on the future sub-mm space missions and Alan Sweigart on mysteries of stellar evolution. Finally, I am grateful to Rick Arendt for careful reading of and comments on the various drafts of this manuscript, to Dale Fixsen for likewise stimulating comments on the manuscript, and to the Editor, Marc Kamionkowski, for patience and encouragement in this, what turned out to be a longer-than-planned, project. I acknowledge useful comments from an anonymous referee. This work was supported by the National Science Foundation grant No. AST-0406587.

REFERENCES

Abbott, L.F. & Wise, M.B. 1984, Ap.J.,282, L47

Abel, T. et al 2002, Science, 295, 93

Ábrahám, P., Leinert, Ch., & Lemke, D. 1997, A&A, 382, 702-705

Adams, J. & Skrutskie, M. 1995, preprint, <http://pegasus.phast.umass.edu/adams/air.ps>

Aldering, G. et al 2004, PASP, submitted. astro-ph/0405232

Arendt, R. et al 1998, Ap.J.,508,74

Arendt, R.G. & Dwek, E. 2003, Ap.J., 585,305

Arimoto, N. & Yoshii, Y. 1987, A & A, 173, 23

Audley, M.D. et al 2004, astro-ph/0410439

Bahcall, J. & Soneira, R. 1983, Ap.J.Suppl., 44,73

Baldry, I. & Glazebrook, K. 2003, Ap.J., 593, 258

Baraffe, I., Heger, A. & Woosley, S.E. 2001, Ap.J.,550,890

Barger, A. J., et al 2004, A.J., 126, 632

Baugh, C. M., Cole, S., Frenk, C. & Lacey, C, 1998, Ap.J.,498,504

Becker, R. H. et al 2001, A.J., 122, 2850

Beichman, C.A. 1997, in “Diffuse Infrared Radiation and the IRTS”, eds. Okuda, H., Matsumoto, T. and Roellig, T., p.82.

Beichman, C. & Helou, G. 1991, Ap.J., 370, L1

Bennett, C. L. et al 2003, Ap.J. Suppl., 148, 1

Bershady, M., Lowenthal, J., Koo, D. 1998, Ap.J., 505, 50

Bernstein, R., Freedman, W.L., & Madore, B.F. 2002, Ap.J., 571, 56

Bernstein, R., Freedman, W.L., & Madore, B.F. 2002, Ap.J., 571, 107

Blain, A. 1997, MNRAS, 290, 553

Blain, A., Kneib, J.-P., Ivison, R.J., & Smail, I. 1999, Ap.J., 512, L87

Blain, A., Smail, I., Ivison, R.J., Kneib, J.-P. & Frayer, D. T. 2002, Physics Reports, 369, 111

Blain, A., Chapman, S.C., Smail, I., & Ivison, R.J. 2004, Ap.J., 611, 725

Blanton, M. et al 2001, A.J., 121, 2358

Blanton, M. et al 2003, Ap.J., 592, 819

Boggess, N. et al et al 1992, Ap.J., 397, 420

Bond, J.R., Arnett, W.D. & Carr, B.J. 1984, Ap.J., 280, 825

Bond, J.R., Carr, B.J. & Hogan, C. Ap.J., 1986, 306, 428

Booulander, F. et al et al 1996, A & A, 312, 256

Bouwens, R.J., et al. 2004, Ap.J. Letters, 616, L79

Bremer, M.N., et al 2004, Ap.J., 615, L1

Broadhurst, T., Ellis, R.S., & Shanks, T. 1988, MNRAS, 235, 827

Bromm, V. et al 1999, Ap.J., 527, L5

Bromm, V. & Larson, R. 2004, Ann. Rev. A. A., in press. astro-ph/0311019

Bruzual, G. 1983, Ap.J. Suppl., 53, 497

Bruzual, G. & Charlot, S. 1993, Ap.J., 405, 538

Burigana, C. & Popa, L. 1998, A & A, 334, 420

Cambresy, L., Reach, W. T., Beichman, C. A., & Jarrett, T. H. 2001, Ap.J., 555, 563

Carr, B.J., Bond, J.R., & Arnett, W.D. 1984, Ap.J., 277, 445

Cassali, M.M. & Hawarden, T.G. 1992, JCMT-UKIRT Newslett., 4, 33

Chapman, S. C., Blain, A. W., Ivison, R.J., & Smail, I. 2003, Nature, 422,695

Chary, R. & Elbaz, D. 2001, Ap.J., 556, 562

Chester, T., Jarrett, T., Schneider, S., Skrutskie, M., & Huchra, J. 1998, BAAS, 192.5511

Cohen, M. 1997, in “Diffuse Infrared Radiation and the IRTS”, eds. Okuda, H., Matsumoto, T. and Roellig, T., p.61.

Cole, S. et al 2001, MNRAS, 326, 255

Colless, M. et al 2001, MNRAS, 328, 1039

Cooray, A., Bock, J., Keating, B., Lange, A. & Matsumoto, T. 2004, 606, 611

Cowie, L., Songaila, A., Hu, E., & Cohen, J.G. 1996, A.J., 112,839

Cowie, L., Barger, A. & Kneib, J-P. 2002, A.J., 123, 2197

Cutri, R. et al 2003, VizieR Online Data Catalog, 2246,0
(<http://vizier.u-strasbg.fr/viz-bin/VizieR?-source=II/2460>)

Dalgarno, A. & McCray, R.A. 1972, Ann. Rev. A. A., 10, 375

Davis, M. & Peebles, J.E. 1983, Ap.J., 267, 465

Dickinson, M. et al 2004, Ap.J., 600, L99

Djorgovski, S. & Davis, M. 1987, Ap.J., 299, 15

Djorgovski, S. et al 1995, Ap.J., 438, L13

Djorgovski, S., Castro, S., Stern, D. & Mahabal, A. 2001, Ap.J., 560, L5

Dole, H. et al 2001, A&A, 372, 364

Dole, H. et al 2004, Ap.J. Suppl., 154, 87

Dole, H. et al 2004, Ap.J. Suppl., 154, 93

Draine, B. & Lee, H. M. 1984, Ap.J., 285, 89

Dwek, E. 2004, 2004, Ap.J., 607, 848

Dwek, E. et al 1997, Ap.J., 475, 565

Dwek, E. et al 1998, Ap.J., 508, 106

Dwek, E. & Arendt, R. 1998, Ap.J., 508, L9

Dwek, E. & Slavin, J. 1994, Ap.J.,436, 696

Eftstathiou, G., Sutherland, W.J. & Maddox, S.J., 1990, Nature, 348, 705

Eisenhardt, P. et al 2004, Ap. J. Suppl., 154, 48

Elbaz, D. et al. 1999, A&A, 351, L37

Elbaz, D. et al. 2002, A & A, 384, 848

Elias, J.H. 1978, A.J., 83, 791

Elston, R., Cornell, M. E. & Lebofsky, M. 1985, A985, Ap.J., 296,106

Faber, S.M. & Gallagher, J.S. 1979, ARAA, 17, 135

Faber, S.M. et al 1989, Ap.J.Suppl.,69,763

Fall, S. M., Charlot, S. & Pei, Y. 1996, Ap.J., 464, L43

Fazio, G. G. et al 2004, Ap.J.Suppl., 154, 10

Finkbeiner, D.P., Davis, M. & Schlegel, D.J. 2000, Ap.J.,544,81

Fioc, M. & Rocca-Volmerange, B. 1997, A&A, 326, 950

Fischer, J. et al 1999, Ap & Sp Sci, 266,91

Fixsen, D. et al 1994, Ap.J., 420,457

Fixsen, D. et al 1996, Ap.J., 473, 576

Fixsen, D. et al 1998, Ap.J., 508,123

Fixsen, D. J., Moseley, S. H., Arendt, R. 2000, Ap.J. Suppl., 128, 651

Fixsen, D. & Dwek, E. 2002, Ap.J., 578, 1009

Fixsen, D. & Mather, J. 2002, Ap.J., 581, 817

Franceschini, A., Toffolatti, L., Mazzei, P., Danese, L., & de Zotti, G. 1991, A & A Suppl., 89, 285

Franceschini, A., Aussel, H., Cesarsky, C. J., Elbaz, D., & Fadda, D. 2001, A & A, 378, 1

Fukugita, M., Hogan, C.J., & Peebles, P.J.E. 1998,Ap.J.,503,518

Gardner, J. P., Cowie, L. L., & Wainscoat, R. 1993, Ap.J., 415, L9.

Gardner, J.P. 1996,in “Unveiling the cosmic infrared background”, ed. E. Dwek, p. 127

Gardner, J.P. et al 1997, Ap.J.,480, L99

Gardner, J.P. et al 2004, SPIE, in Proc. "Optical, Infrared and Millimeter Space Telescopes", vol. 5487, ed. Mather, J. p. 564

Gautier, T.N., Boulanger,F., Perault, M., & Puget, J.L. 1992, A.J., 103,1313

Giavalisco, M. 2002, ARAA, 40,579

Gorjian, V., Wright, E.L., & Chary, R.R. 2001,Ap.J.,536,550

Groth, E.J. & Peebles, P.J.E. 1977, Ap.J., 217, 385

Guiderdoni, B. et al 1997, Nature, 390, 257

Guiderdoni, B., Hivon, E., Bouchet, F., & Maffei, B. 1998, MNRAS, 295, 877

Gunn, J. E. & Peterson, B. A. 1965, Ap.J., 142, 1633

Hacking, P. & Soifer, B. 1991, Ap.J., 367, L49

Haiman, Z. 2002, Ap.J., 576, L1

Haiman, Z. & Knox, L. 2000, Ap.J.,530, 124

Haiman, Z. & Loeb, A. 1997, Ap.J., 490, 571

Hamilton, A. J. S., Mathews, A., Kumar, P., & Lu, E. 1991, Ap.J., 374, L1

Hamman, F. & Ferland, G. 1999, ARAA, 37, 487

Hartmann, D. & Burton, W.B. 1997, "An Atlas of Galactic Neutral Hydrogen Emission", Cambridge University Press.

Hauser, M. & Dwek, E. 2001, Ann Rev A A, 39, 249

Hauser, M. et al 1998, Ap.J.,508,25

Heger, A. et al 2003, Ap.J., 591, 288

Helou, G. 1986, Ap.J., 311, L33

Hoyle, F. 1953, Ap.J., 118, 513.

Huang, J.-S.; Glazebrook, K.; Cowie, L. L.; Tinney, C. 2001, Ap.J., 584, 203

Hughes, D. et al 1998, Nature, 394, 241

Ingalls, J.G. et al 2004, Ap.J. Suppl., 154, 281

Jensen, L. & Szalay, A., 1986, Ap.J.,305,L5

Jimenez, R. & Kashlinsky, A. 1999, Ap.J.,511,16

Kaiser, N. 1984, Ap.J.,284,L9

Kashlinsky, A. 1982,MNRAS, 200, 585

Kashlinsky, A. 1987, Ap.J.,317,19

Kashlinsky, A. 1992, Ap.J., 399, L1

Kashlinsky, A. 1998, Ap.J.,492,1

Kashlinsky, A., Mather, J.C., Odenwald, S. & Hauser, M. 1996, Ap.J.,470,681

Kashlinsky, A., Mather, J.C., Odenwald, S. 1999, preprint

Kashlinsky, A. & Odenwald, S. 2000a, Ap.J.,528,74

Kashlinsky, A. & Odenwald, S. 2000b, Science,289,246

Kashlinsky, A., Odenwald, S., Mather, J.C., Skrutskie, M. & Cutri, R. 2002, Ap.J.,579,L53

Kashlinsky, A., Arendt, R., Gardner, J.P., Mather, J. & Moseley, S.H. 2004, Ap.J., 608, 1

Kauffmann, G., White, S.D.M. & Guiderdoni, B. 1993,MNRAS, 264, 201

Kawara, K. et al 2004, A & A, 413, 843

Kelsall, T. et al 1998, Ap.J., 508,44

Kennicutt, R. C., Tamblyn, P. & Condgon, C. W. 1994, Ap.J., 435, 22

Kennicutt, R. C. 1998, Ap.J., 498, 541

Kennicutt, R. C. 1998, ARAA, 36, 189

Kiss, Cs., Ábrahám, P., Klaas, U., Lemke, D., Héraudeau, Ph., del Burgo, C., Herbstmeier, U. 2003, A&A, 399, 177-185

Kneib, J.-P., Ellis, R. S., Santos, M. R. & Richard, J. 2004, Ap.J., 607, 697

Knox, L., Cooray, A., Eisenstein, D., & Haiman, Z. 2001, Ap.J., 550,7

Kochanek , C. et al 2001, Ap.J.,560,566

Kogut, A. et al 2003, Ap.J.Suppl.,148,161

La Franca, F. et al, 2004, A.J., 127, 3075

Lagache, G. & Puget, J.-L. 2000, A & A, 355,17

Lagache, G., Dole, H. & Puget, J.-L. 2002, MNRAS, 338, 555

Leinert, Ch. et al 1998, A & A Suppl., 1998, 127,1

Leisawitz, D. 2004, Adv. Sp. Res., 34, 631

Lester, D. et al 2004, SPIE, in Proc. "Optical, Infrared and Millimeter Space Telescopes", vol. 5487, ed. Mather, J. p. 1507

Lilly, S., LeFevre, O., Hammer, F. & Crampton, D. 1996, Ap.J., 460, L1

Lemke, D. et al 1996, A&A,315, L64

Liske, J. et al 2003, MNRAS,344, 307

Lonsdale, C., Hacking, P.B., Conrow, T.P., & Rowan-Robinson, M. 1990, Ap.J., 358, 60

Lonsdale, C. 1996, in "Unveiling the cosmic infrared background", ed. E. Dwek, p. 147

Lonsdale, C. et al 2004, Ap.J. Suppl., 154, 54

Loveday, J., Peterson, B. A., Efstathiou, G. & Maddox, S.J. 1992, Ap.J., 390, 338

Low, C. & Lynden-Bell, D. 1976,MNRAS, 176, 367

Madau, P. et al 1996, MNRAS, 283, 1388

Madau, P., Pozzetti, L. & Dickinson, M. 1998, Ap.J., 498, 106

Madau, P. & Pozzetti, L. 2000,MNRAS,312,L9

Maddox, S, Efstathiou, G., Sutherland, W. & Lovdeay, J. 1990, MNRAS, 242, 43P

Magliochetti, M., Salvaterra, R., Ferrara, A. 2003, MNRAS,342,L25

Maihara, T. et al 2001, PASJ, 53, 25

Malkan, M.A. & Stecker, F.W. 1998, Ap.J., 496, 13

Marleau, F. et al 2004, Ap. J. Suppl., 154, 66

Marzke, R.O., Geller, M.J., Huchra, J.P., & Corwin, H.G., 1994, A.J., 108,437

Mather, J.C., Fixsen, D. & Shafer, R.A. 1993, Proc. SPIE, 2019, 168

Mattila, K. 2003, Ap.J.,591,119

Matsumoto, T., Akiba, M., & Murakami, H. 1988, Ap.J., 332, 575

Matsumoto, T. et al 2000,in "ISO surveys of a dusty Universe", eds. Lemke, D. et al. p.96

Matsumoto, T. et al 2003, Ap.J., submitted, astro-ph/0411593

Matute, I. et al 2002, MNRAS, 332, L11

McLeod, B. A., Bernstein, G. M., Rieke, M. J., Tollestrup, E. V., & Fazio, G. G. 1995, Ap.J.Supp., 96, 117

Metcalfe, L. et al 2003, A & A, 407, 791

Minezaki, T. et al. 1998, A.J., **115**, 229.

Miralda-Escude, J. 2003, Science, 300, 1904

Mobasher, B., Ellis, R. S., & Sharples, R. M. 1986, MNRAS, 223, 11

Murakami, H. et al 1996, PASJ, 48, L41

Noda, M. et al 1992, Ap.J., 391, 456

Noda, M. et al 1994, Ap.J., 428, 363

Odenwald, S., Kashlinsky, A., Mather, J.C., Skrutskie, M. & Cutri, R. 2003, Ap.J., 583, 535

Oke, J.B. & Gunn, J. 1983, Ap.J., 266, 713

Oliver, S. et al 1997, MNRAS, 289, 471

Oliver, S. et al 1997, MNRAS, 316, 749

Oliver, S. et al 2004, Ap.J. Suppl., 154, 30

Pahre, M., Djorgovski, S., & de Carvalho 1998, A.J., 116, 1606

Pahre, M., Djorgovski, S., & de Carvalho 1998, A.J., 116, 1591

Papovich, C. et al 2004, Ap.J. Suppl., 154, 70

Partridge, R. B. & Peebles, P.J.E. 1968, Ap.J., 148, 377

Peacock, J.A. & Dodds, S.J., 1996, MNRAS, 280, L19

Peebles, P.J.E. 1980, *The large scale structure of the Universe*, Princeton University Press

Peebles, P.J.E. & Wilkinson, D.T. 1968, Phys.Rev., 174, 2168

Pello, R., Schaefer, D., Richard, J., Le Borgne, J.-F., & Kneib, J.-P. 2004, A & A, 416, L35

Percival, W.J. et al 2002, MNRAS, 337, 1068

Persson, S.E., Murphy, D.C., Krzeminski, W., Roth, M. & Rieke, M.J. 1998, A.J., 116, 2475

Pettini, M., Smith, L.J., King, D.L., & Hunstead, R.W., 1997, Ap.J., 486, 665

Pilbratt, G.L. 2004, SPIE, in Proc. "Optical, Infrared and Millimeter Space Telescopes", vol. 5487, ed. Mather, J. p. 401

Politzer, H.D. & Wise, M.B. 1984, Ap.J., 285, L1

Porciani, C. & Giavalisco, M. 2002, Ap.J., 565, 24

Pozzetti, L., Bruzual, A.G. & Zamorani, G. 1996, MNRAS, 281, 953

Pozzetti, L., Madau, P., Zamorani, G., Ferguson, H.C. & Bruzual, A.G. 1998, MNRAS, 298, 1133

Pozzi, F. et al 2004, Ap.J., in press, astro-ph/0403242

Press, W. & Schechter, P. 1974, Ap.J., 187, 425

Puget, J.-L. et al 1996, A & A, 308, L5

Puget, J.-L. et al 1999, A & A, 345, 29

Reach, W.T. et al 1995, Nature, 374, 521

Rees, M.J. 1976, MNRAS, 176, 483

Rees, M.J. 1978, Nature, 275, 35

Rees, 1980, Physics Scripta, 21, 614

Rees, M.J. & Ostriker, J.P. 1977, MNRAS, 179, 541

Renault, C., et al 2001, A&A, 371, 771

Rowan-Robinson, M. et al 1997, MNRAS, 289, 490

Rowan-Robinson, M. et al 2004, 351, 1290

Sabelhaus, P.A. & Decker, J. E. 2004, SPIE, in Proc. "Optical, Infrared and Millimeter Space Telescopes", vol. 5487, ed. Mather, J. p. 550

Salpeter, E. 1953, Ap.J., 121, 161

Salvaterra, R. & Ferrara, A. 2003, MNRAS, 339, 973

Sanders, D. B. & Mirabel, I. F. 1996, ARA&A, 34, 749

Santos, M.R., Bromm, V., Kamionkowski, M. 2002, MNRAS, 336, 1082

Santos, M. 2004, MNRAS, 349, 1137

Saracco, P., D'Odorico, S., Moorwood, A., Buzzoni, A., Cuby, J.-G., & Lidman, C. 1998, A&A, 349, 751

Sato, Y. et al 2003, A & A, 405, 833

Sawicki, M. & Webb, T.M.A. 2004, Ap.J., in press, astro-ph/0402454

Scalo, J.M. 1986, Fund. Cosm Phys., 11, 1

Scaramella, R., Vettolani, G. & Zamorani, G. 1991, Ap.J., 376, L1

Schaerer, D. 2002, Aston. Astrophys., 382, 28

Schechter, P. 1976, 203, 297

Schlegel, D.J., Finkbeiner, D.P. & Davis, M. 1998, Ap.J., 500, 525

Scott, D. et al 2000, A & A, 3357, L5

Scott, S.E. et al 2002, MNRAS, 331, 817

Serjeant, S. et al 2001, MNRAS, 322, 262

Serjeant, S. et al 2004, Ap.J. Suppl., 154, 118

Serjeant, S. et al 2004b, MNRAS, in press, astro-ph/0401289

Severgnini, P. et al 2000, A & A 360, 457

Silk, J. 1977, Ap.J., 214, 152

Silk, J. 1996, in “Unveiling the cosmic infrared background”, ed. E. Dwek, p. 139

Smail, I., Ivison, R.J., & Blain, A. 1997, Ap.J., 490, L5

Smail, I., Ivison, R.J., Blain, A. & Kneib, J-P. 2002, MNRAS, 331, 495

Soifer, B.T. et al 1986, Ap.J., 303, L41

Soifer, B.T. et al 1987a, Ap.J., 320, 238

Soifer, B.T., Neugebauer, G., & Houck, J. R. 1987b, ARA&A., 25, 187

Soifer, B.T. & Neugebauer, G. 1991, A.J., 101, 354

Soifer, B. et al 1994, Ap. J., 420, L1

Sommerville, R., Primack, J. & Faber, S. 1999, MNRAS, 320, 504

Spinoglio, L. et al 1995, Ap.J., 453, 616

Stanev, T. & Franceschini, A. 1998, Ap.J., 494, L159

Stanway, E.R. et al 2004, Ap.J., 607,704

Stark, A. et al 1992, Ap.J.Suppl., 79,77

Stecker, F.W., de Jager, O.C., & Salamon, M.H. 1992, Ap.J.,390, L49

Stecker, F.W., & de Jager, O.C. 1993, Ap.J.,415, L71

Steidel, C., Giavilisco, M., Pettini, M., Dickinson, M. & Adelberger, K. 1996, Ap.J., 462, L17

Sugiyama, N. 1995, Ap.J. Supl., 100, 281

Sullivan, M. et al 2000, MNRAS, 312,442

Sweigart, A., Greggio, L. & Renzini, A. 1990, Ap.J., 364, 527

Taniguchi, Y. et al 1997, A & A, 328, L9

Tegmark, M. et al 2004, Phys. Rev. D, 69, 103501

Teplitz, H., Gardner, J. P., Malumuth, E., & Heap, S. 1998, Ap.J., 507, L17

Tinsley, B.A. 1976, in 6th Advanced Course of the Swiss Society of Astronomy and Astrophysics, eds. L. Martinet & M. Mayor, Saas Fee , 1976

Tinsley, B. 1980, Fund. Cosmic Physics, 5, 287

Toomre, A. & Toomre, J. 1972, Ap.J., 178, 623

Totani, T., Yoshii, Y. & Sato, K. 1997, Ap.J., 483, L75

Totani, T. et al 2001,Ap.J.,559,592

Treu, T., Stiavelli, M., Casertano, S., Moller, P., & Bertin, G. 2002, Ap.J., 564, L13

Tumlinson, J., Shull, J.M., & Venkatesan, A. 2003,Ap.J.,584,608

Tully, B. & Fisher, J.R. 1977, A & A, 54,661

van der Wel, A., Franx, M., van Dokkum, P.G., & Rix, H.-P. 2004, Ap.J., 601, L5

van Dokkum, P.G., Franx, M., Kelson, D. & Illingwoarth, G. 2001, Ap.J., 553, L39

Wainscoat, R.J., Cohen, M., Volk, K., Walker, H.J., & Schwartz, D.E. 1992, Ap.J.Suppl.,83,111

Walter, F. et al 2004, Ap.J., Ap.J., 615, L17

Willick, J.A. 2000, in Proceedings of the XXXVth Rencontres de Moriond: Energy Densities in the Universe

Wright, E.L. et al 1991, Ap.J., 381, 200

Wright, E.L. 1998, BAAS, 29, 1354

Wright, E.L. & Reese, E.D. 2000, Ap.J., 545, 43

Wright, E.L. 2000, Ap.J., 553, 538

Wright, E.L. 2001, Ap.J., 556, L17

Wright, E.L. 2003, astro-ph/0306058

Wuyts, S., van Dokkum, P.G., Kelson, D., Franx, M., & Illingworth, G. 2004, Ap.J., 605, 677

Xu, J. et al 2002, Ap.J., 580, 653

Yan, L., McCarthy, P., Storrie-Lombardi, L., & Weymann, R. 1998, Ap.J., 503, L19

Yoshii, Y. & Peterson, B. 1994, Ap.J., 436, 551

Yoshii, Y. & Takahara 1988, Ap.J., 326, 1

Zubko, V., Dwek, E. & Arendt, R. 2004, Ap. J. Suppl. Ser., 152, 211